Plant Communications
Research Article

CellPress
Partner Journal

The chromosome-level reference genome assembly for *Panax notoginseng* and insights into ginsenoside biosynthesis

Zhouqian Jiang[1], Lichan Tu[1,2], Weifei Yang[3], Yifeng Zhang[1,2], Tianyuan Hu[1], Baowei Ma[1], Yun Lu[1], Xiuming Cui[4], Jie Gao[1], Xiaoyi Wu[1], Yuru Tong[2], Jiawei Zhou[1], Yadi Song[1], Yuan Liu[1], Nan Liu[1], Luqi Huang[5,*] and Wei Gao[1,2,6,*]

[1]School of Traditional Chinese Medicine, Capital Medical University, Beijing, China

[2]School of Pharmaceutical Sciences, Capital Medical University, Beijing, China

[3]Annoroad Gene Technology, Beijing, China

[4]Faculty of Life Science and Technology, Kunming University of Science and Technology, Kunming, China

[5]State Key Laboratory Breeding Base of Dao-di Herbs, National Resource Center for Chinese Materia Medica, China Academy of Chinese Medical Sciences, Beijing, China

[6]Advanced Innovation Center for Human Brain Protection, Capital Medical University, Beijing, China

***Correspondence: Luqi Huang (huangluqi01@126.com), Wei Gao (weigao@ccmu.edu.cn)**

https://doi.org/10.1016/j.xplc.2020.100113

ABSTRACT

***Panax notoginseng*, a perennial herb of the genus *Panax* in the family Araliaceae, has played an important role in clinical treatment in China for thousands of years because of its extensive pharmacological effects. Here, we report a high-quality reference genome of *P. notoginseng*, with a genome size up to 2.66 Gb and a contig N50 of 1.12 Mb, produced with third-generation PacBio sequencing technology. This is the first chromosome-level genome assembly for the genus *Panax*. Through genome evolution analysis, we explored phylogenetic and whole-genome duplication events and examined their impact on saponin biosynthesis. We performed a detailed transcriptional analysis of *P. notoginseng* and explored gene-level mechanisms that regulate the formation of characteristic tubercles. Next, we studied the biosynthesis and regulation of saponins at temporal and spatial levels. We combined multi-omics data to identify genes that encode key enzymes in the *P. notoginseng* terpenoid biosynthetic pathway. Finally, we identified five glycosyltransferase genes whose products catalyzed the formation of different ginsenosides in *P. notoginseng*. The genetic information obtained in this study provides a resource for further exploration of the growth characteristics, cultivation, breeding, and saponin biosynthesis of *P. notoginseng*.**

Key words: chromosome-level, genome, ginsenoside, *P. notoginseng*, regulation, transcriptome

Jiang Z., Tu L., Yang W., Zhang Y., Hu T., Ma B., Lu Y., Cui X., Gao J., Wu X., Tong Y., Zhou J., Song Y., Liu Y., Liu N., Huang L., and Gao W. (2021). The chromosome-level reference genome assembly for *Panax notoginseng* and insights into ginsenoside biosynthesis. Plant Comm. **2**, 100113.

INTRODUCTION

The Chinese medicine Sanchi is prepared from the dried root and rhizome of *Panax notoginseng* (Burk.) F. H. Chen, a perennial herb that belongs to the Araliaceae ginseng species (Briskin, 2000; Ng, 2006). Generally, Sanchi is collected and washed before *P. notoginseng* flowers bloom in autumn and is obtained by separating the main root and rhizome after drying (Wang et al., 2016). *P. notoginseng* has a long history of use in China for eliminating congestion and hemostasis and reducing swelling and pain. The brilliant work of the Ming Dynasty, Compendium of Materia Medica (A.D. 1552–1578), already described *P. notoginseng*. The medicinal value of *P. notoginseng* arises from the chemical ingredients it contains. To date, the chemical components isolated from *P. notoginseng* include mainly saponins, flavones, sugars, volatile oils, and amino acids (Jia et al., 2019). Among these, saponin compounds are the main chemical constituents and are also recognized as the main active ingredients (Xiong et al., 2019). Modern medical research has shown that saponins from *P. notoginseng* improve

Published by the Plant Communications Shanghai Editorial Office in association with Cell Press, an imprint of Elsevier Inc., on behalf of CSPB and CEMPS, CAS.

myocardial ischemia (Zhang et al., 2017b), protect the liver (Zhong et al., 2019), defend against cardiovascular disease (Chan et al., 2002), lower blood pressure (Pan et al., 2012), and improve arteriosclerosis (Min et al., 2008); they also have antithrombotic (Dang et al., 2015) and anticancer activities. As a rare and valuable medicinal material in China, *P. notoginseng* is also used in various prescriptions, such as capsules, injections, and powders. It is in widespread use, with total annual output values exceeding 70 billion RMB (Gui et al., 2013; Cui et al., 2014).

To date, the principal means of obtaining saponins has been to extract and isolate them from the original plants; however, the plant saponin content is low, and this process has a low extraction efficiency and is not environmentally friendly. Therefore, reconstruction of the saponin biosynthetic pathway for heterologous production is an alternative method for obtaining these valuable resources. At present, over 80 tetracyclic triterpenoid saponins have been identified (Xu et al., 2019) from the roots, stems, leaves, flowers, and fruits of *P. notoginseng*, and these saponins can be divided into protopanaxadiol (PPD) and protopanaxatriol (PPT) based on a hydroxyl substitution at the C-6 position of the molecular structure. The biosynthetic pathway of saponins in *P. notoginseng* is divided into four main stages. First, the direct precursors isopentenyl allyl diphosphate (IPP) and dimethylallyl diphosphate (DMAPP) are synthesized by the mevalonate and 2-methyl-D-erythritol-4-phosphate pathways (Deng et al., 2017). Second, isopentenyl transferase and terpene synthases (Niu et al., 2014) catalyze the synthesis of 2,3-oxidosqualene from IPP and DMAPP (Jiang et al., 2017). Third, 2,3-oxidosqualene undergoes cyclization and hydroxylation (Han et al., 2011, 2012) to form the core structures PPD and PPT (Luo et al., 2011; Lu et al., 2018). Finally, the formation of various saponins is catalyzed by a number of glycosyltransferases (GTs) (Yu et al., 2019). The genetic and functional diversity of GTs gives rise to a variety of structurally diverse saponins.

To explore the biosynthetic pathway of ginsenosides, the genome of *P. notoginseng* has been explored and information mined (Zhang et al., 2017a; Chen et al., 2017). However, because of sequencing technology limitations, existing genomic information generated from second-generation short-read sequencing is insufficient (Shen et al., 2018; Zhao et al., 2019). Here, we present a high-quality *P. notoginseng* genome obtained using a combination of Illumina, PacBio, and Hi-C (high-throughput chromosome conformation capture) technologies; this is also the first chromosome-level genome of the genus *Panax*. Using comparative genomics, we explored the evolution and whole-genome duplication (WGD) events of *P. notoginseng*. We performed detailed transcriptional analysis and explored gene-level regulatory mechanisms that control the formation of characteristic tubercles, the biosynthesis of saponins at temporal and spatial levels, and the regulation of transcription factors. Combined with genomic analysis, we screened a series of UDP-dependent GT (UGT) candidate genes, five of which were identified as having catalytic functions. Our study provides genetic information for further comprehensive analysis of the saponin biosynthetic pathway and the evolution of the ginseng genus, and also describes useful techniques for the breeding of *P. notoginseng*.

RESULTS

Genome sequencing, assembly, and annotation

According to the *K*-mer distribution analysis (K = 31), the estimated size of the *P. notoginseng* genome ($2n = 2x = 24$ chromosomes) is 2.38 Gb, and the heterozygosity and repeat contents are 0.58% and 69.05%, respectively (Supplemental Figure 1 and Supplemental Table 1). We combined Illumina, PacBio, and Hi-C technologies to sequence and assemble a high-quality, chromosome-level *P. notoginseng* reference genome. A total of 240.22 Gb of Illumina reads, 284.07 Gb of PacBio long reads, and 340.83 Gb of Hi-C data were generated, resulting in ~325.23× coverage of the *P. notoginseng* genome (Supplemental Table 2). The final assembled genome was 2.66 Gb in size and consisted of 219 scaffolds, with a scaffold N50 of 216.47 Mb and a contig N50 of 1.12 Mb (Figure 1 and Table 1). The assembled sequence was then anchored onto 12 pseudochromosomes with lengths of 176.58–295.55 Mb. The total length of the pseudochromosomes accounted for 99.89% of the genome sequences, with a scaffold L50 number of 6 (Supplemental Figure 2; Supplemental Table 3). The genome of *P. notoginseng* had a GC content of 34.45% (Supplemental Table 4).

To test the coverage of the *P. notoginseng* genome, the short reads generated from Illumina sequencing were mapped, and 99.82% of these reads could be mapped to the scaffolds with 97.97% overall coverage (Supplemental Table 5). The completeness of the genome assembly was evaluated using BUSCO (Benchmarking Universal Single-Copy Orthologs) (Simao et al., 2015). Based on BUSCO analysis, 96.6% of plant sets were identified as complete (2049 out of 2121 BUSCOs) (Supplemental Table 6). All analyses suggested a high quality of the *P. notoginseng* genome assembly.

Based on a combination of homology-based and *de novo* approaches, 85.85% of the assembled *P. notoginseng* genome (Supplemental Table 7) consisted of repetitive elements; among them, long terminal repeat (LTR) retrotransposons accounted for the largest proportion and made up 58.88% of the genome (Supplemental Table 8; Supplemental Figure 3A and 3B). Compared with the published reference genome version, there were more predictions of repetitive sequences, a phenomenon that also occurs in other highly repetitive genomes (Xia et al., 2017, 2020; Wei et al., 2018; Zhang et al., 2020a). We compared the predicted repeat sequences with the RepBase database and calculated the degree of difference between them, from which LTR retrotransposons broke out at approximately 8% and an unknown outbreak happened earlier at approximately 5% (Supplemental Figure 3C).

An integrated strategy of *de novo predictions, homology-based searches, and RNA sequencing* was used to predict the protein-coding genes of the *P. notoginseng* genome. A total of 37 606 genes were annotated, with an average length of 5059.63 bp and an average exon number per gene of 5.21 (Supplemental Table 9; Supplemental Figure 4). The number of genes was similar to the numbers reported in two articles about the *P. notoginseng* genome published in 2017 (34 369 and 36 790), but other values, such as the average gene length and the average number of exons per gene, have been updated

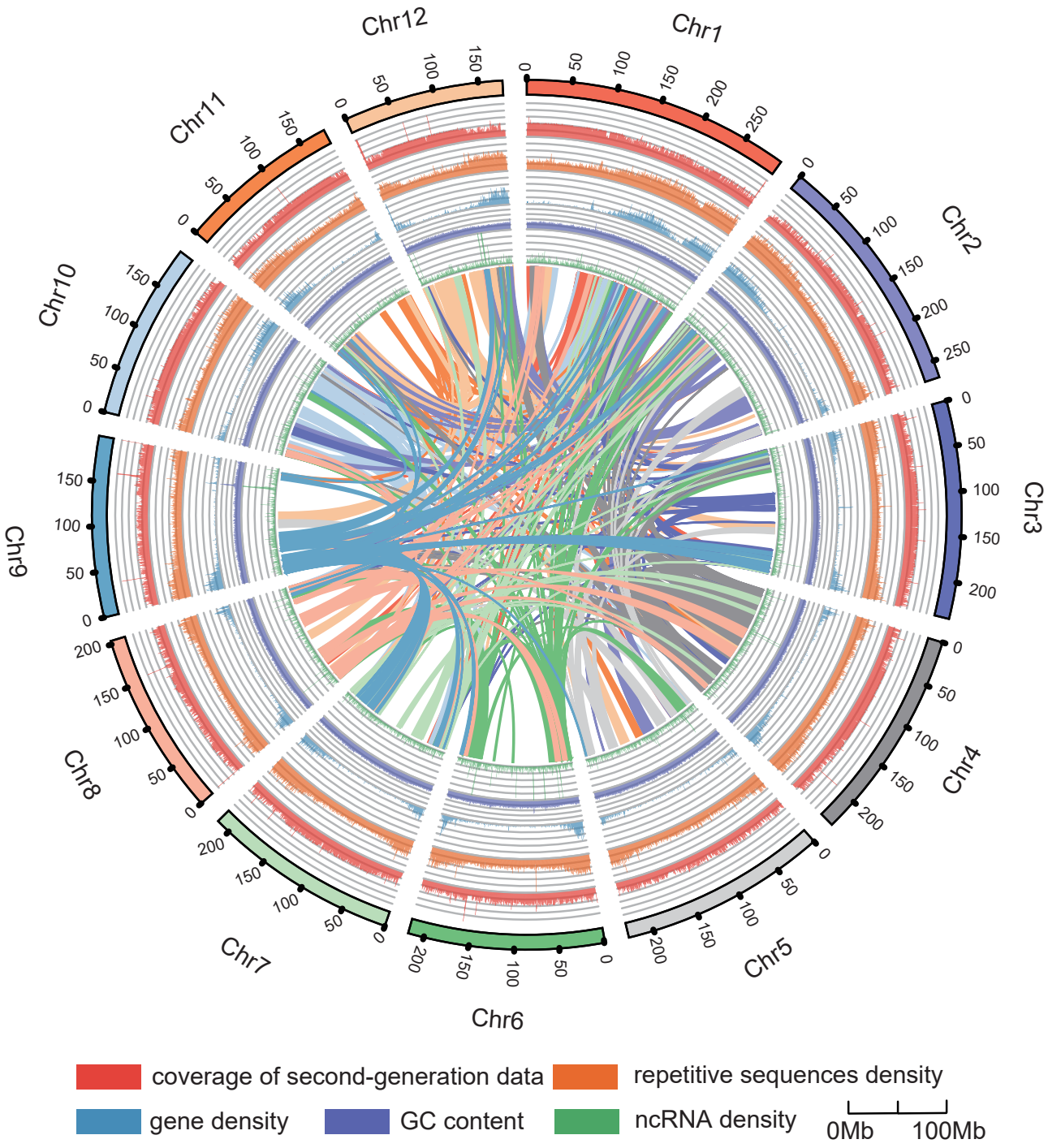

Figure 1. Genome assembly characterization and chromosome locations of *P. notoginseng*.
Landscape of the *P. notoginseng* genome: from outside to inside, chromosome number and length, coverage of second-generation data, density of repetitive sequences, gene density, GC content, noncoding RNA density, and genomic synteny.

(Supplemental Table 10). Compared with another Araliaceae plant, *Panax ginseng* C.A. Mey (59 352 genes) (Kim et al., 2018), *P. notoginseng* has a smaller number of genes, which may be related to the subsequent duplication event of *P. ginseng* after the divergence of the two plants. Among the annotated *P. notoginseng* genes, 36 154 (~96.14%) were functionally classified by BLASTing against various functional databases (Supplemental Table 11). We further annotated noncoding RNA genes, obtaining 14 430 microRNA genes, 1513 transfer RNA (tRNA) genes, 314 ribosomal (rRNA) genes, and 272 small nuclear (snRNA) genes (Supplemental Table 12).

Items	PN201908CCMU	2017pub-1	2017pub-2
Total length of contigs (Gb)	2.66	1.85	2.39
Contig N50	1.12 Mb	13.16 kb	16 kb
Longest contig (bp)	13.35 Mb	120.91 kb	199.81 kb
Scaffold N50	216.47 Mb	157.81 kb	96 kb
Longest scaffold (bp)	295.55 Mb	1.19 Mb	834.33 kb
GC content (%)	34.45	34.85	28.65
Number of genes	37 606	34 369	36 790
Average gene length (bp)	5059.63	2705	3307.48
BUSCO (%)	96.6	N	82.4
Average CDS length (bp)	1202.85	957	942.43
Average exon length (bp)	231.00	251.39	211.92
Average exon number per gene	5.21	3.8	4.45
Average intron length (bp)	917.71	622.64	686.08
Percentage of repeat sequences (%)	85.85	61.31	75.94
Percentage of LTR-RTs (%)	58.88	57.41	66.72
Reference	This study	(Zhang et al., 2017a)	(Chen et al., 2017)

Table 1. Summary of the final genome assembly of *P. notoginseng* and comparison with published genomes.

Genome evolution and expansion and contraction of gene families

We compared our *P. notoginseng* assembly with sequenced genomes from seven other plants: *P. ginseng*, *Daucus carota* from Apiales, four dicot species (*Arabidopsis thaliana*, *Vitis vinifera*, *Capsicum annuum* L., and *Glycyrrhiza uralensis*), and a monocot, *Oryza sativa*. Based on gene family clustering analysis, 30 874 *P. notoginseng* genes (82.28%) clustered into 15 655 gene families (Supplemental Table 13 and Supplemental Figure 5), which included 7264 gene families shared by all 8 species and 1059 families specific to *P. notoginseng* (Supplemental Figure 6). Gene ontology (GO) and KEGG enrichment analysis of these *P. notoginseng*-specific gene families showed that they were mainly involved in a series of biological activities, e.g., mature ribosome assembly, cytosolic part, small-molecule binding, and RNA transport (Supplemental Table 14; Supplemental Figure 7).

We selected 458 single-copy gene families among the 8 species to construct phylogenetic trees. As expected, *P. notoginseng* clustered with another Araliaceae species, *P. ginseng*, and these two species were most closely related to the Apiales family (Figure 2A). We estimated that *P. notoginseng* and *P. ginseng* diverged from the Apiaceae approximately 62.0 million years ago (mya), and *P. notoginseng* and *P. ginseng* diverged around 4.2 mya. These results show that the relationship between *P. notoginseng* and *P. ginseng* is very close, consistent with their very similar morphologies and secondary metabolites.

We compared expanded and contracted gene families in the 8 plant species with their most recent common ancestor. In total, 989 gene families were expanded in *P. notoginseng*, and 1823 gene families were contracted (Supplemental Figure 8). Compared with *P. ginseng* (6449), the number of expanded gene families in *P. notoginseng* was significantly smaller, perhaps because *P. ginseng* has experienced one more WGD event than *P. notoginseng*. We performed GO and KEGG enrichment analysis on expanded and contracted gene families in the *P. notoginseng* genome. The functions of the expanded gene families were mainly enriched in GO terms such as transposition, fatty acid biosynthetic process, respiratory chain, and catalytic activity (Supplemental Figure 9; Supplemental Table 15). The functions of the contracted gene families were mainly enriched in GO terms such as protein phosphorylation, protein modification process, β-glucan biosynthetic process, 1,3-β-D-glucan synthase complex, and purine nucleotide binding (Supplemental Table 16). 1,3-β-D-Glucan is reported to be involved in plant defense against fungi (Lee et al., 2006; Schober et al., 2009), and contraction in associated gene families may be related to the susceptibility of *P. notoginseng to* fungal pathogens and may explain why it readily develops root rot.

Analysis of WGD and its contribution to terpenoid biosynthesis

To study the WGD events that occurred during the evolution of *P. notoginseng*, we first analyzed the 4-fold synonymous third-codon transversion rate (4DTv) (Figure 2B) of syntenic gene pairs (Jaillon et al., 2007). There were two peaks in the 4DTv distribution at approximately 0.16 and 0.50 for all syntenic gene pairs in the *P. notoginseng* genome. The first peak at approximately 0.50 corresponded to the core eudicot γ triplication event, and the second peak at approximately 0.16 revealed that *P. notoginseng* underwent another WGD event after diverging from *V. vinifera* and *D. carota*. By comparing the *P. notoginseng* genome with the *V. vinifera* genome, we found that 65% of *P. notoginseng* gene models were located in syntenic blocks that corresponded to single *V. vinifera* regions. Meanwhile, 42% of the *V. vinifera* gene models in syntenic blocks had two orthologous regions, and 22% had one orthologous region (Supplemental Figure 10). The results of a genome collinearity analysis between *V. vinifera* and

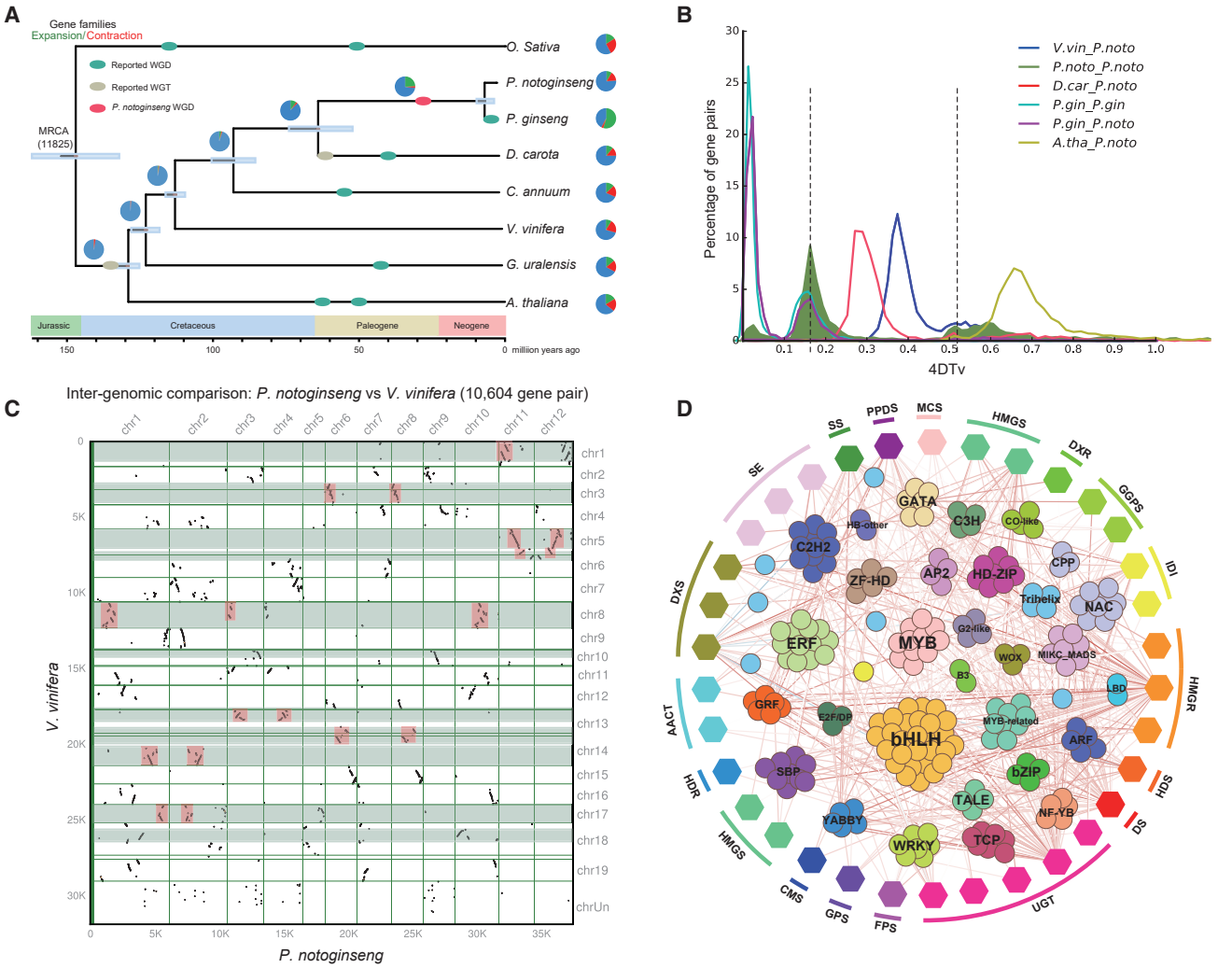

Figure 2. Genome evolution and transcription factor regulation analysis of *P. notoginseng*.

(A) Inferred phylogenetic tree with 458 single-copy genes from eight plant species. Gene family expansions are indicated in green, and gene family contractions are indicated in red. The timings of WGD and whole-genome triplications (WGT) are superimposed on the tree. Divergence times are estimated by maximum likelihood (PAML).

(B) Distribution diagram of 4DTv values. The dark green-filled part indicates the 4DTv analysis inside *P. notoginseng*, and the peaks marked by the dotted line indicate where the two WGD events of *P. notoginseng* occurred.

(C) Syntenic dot plots show a 2:1 chromosomal relationship between the *P. notoginseng* genome and the *V. vinifera* genome. The area in the pink box on each horizontal line represents the collinear block between the two genomes.

(D) Correlation analysis of transcription factors with pathway genes. Pathway genes are represented by hexagons and transcription factors by circles. The line indicates the nature of the correlation: red for a positive correlation and blue for a negative correlation. The darker the color, the higher the correlation.

P. notoginseng indicated that the WGD event occurred in the *P. notoginseng* genome and that there was a 1:2 syntenic relationship between *P. notoginseng* and *V. vinifera* (Figure 2C and Supplemental Figure 11). Based on the distribution of K_s (Supplemental Figure 12) and 4DTv analysis, we calculated that the WGD event occurred approximately 29.6 mya in the ancestor of *P. notoginseng*. Compared with *P. notoginseng*, *P. ginseng* experienced one additional WGD event (Kim et al., 2018), and this recent event occurred approximately 1.85 mya after divergence from *P. notoginseng*. The timing of the WGD events was similar to the results of an evolutionary analysis of the *P. ginseng* genome (28 and 2.2 mya), confirming the accuracy of the present results (Kim et al., 2018).

Through homologous alignment and a Pfam database search, we identified gene families that were potentially involved in terpenoid biosynthesis in the eight species (Supplemental Table 17). The copy numbers of some gene families in the *P. notoginseng* genome were significantly greater than those in other plant genomes; these included families such as *DXS*, *MCS*, *HDS*, *HDR*, and *SQE*. We also observed that the average copy number of most key enzyme genes in *P. ginseng* was approximately twice that in *P. notoginseng* (Supplemental Figures 13 and 14). We next performed K_a/K_s analysis of these pathway genes to calculate the duplication times of their gene pairs in the *P. notoginseng* genome. The gene pair duplication times were concentrated around the time of the WGD event of

P. notoginseng (Supplemental Figure 15; Supplemental Table 18), indicating that they may have arisen from the WGD event.

Transcriptome analysis and transcriptional regulation of saponin biosynthesis

To further explore the genetic information in *P. notoginseng*, we performed detailed transcriptome sequencing of *P. notoginseng* plants on the basis of the high-quality genome. Samples for transcriptome sequencing were obtained from 1- to 4-year-old *P. notoginseng* plants that were subdivided into root, stem, leaf, flower, rhizome, fibril, periderm, phloem, and tubercle (Supplemental Figures 16 and 17). Data processing (Supplemental Figures 18 and 19; Supplemental Table 19) and related transcriptome analyses, such as alternative splicing event analysis (Supplemental Figure 20; Supplemental Table 20) (Laloum et al., 2018), new transcription prediction (Dassanayake et al., 2009), single-nucleotide polymorphism analysis (Supplemental Figure 21; Supplemental Table 21) (Sarkar and Maranas, 2020), analysis of gene expression levels (Supplemental Figures 22 and 23), and identification of differentially expressed genes (DEGs) (Supplemental Figure 24; Supplemental Table 22), are detailed in the Supplemental materials.

We further analyzed the regulation of transcription factors in *P. notoginseng*. A total of 2150 transcription factors from 57 different families (Supplemental Table 23) were identified; we then used correlation analysis to map the gene regulation network (Figure 2D) between terpenoid biosynthetic pathway genes and transcription factors. The transcription factor families that were highly correlated with pathway genes included mainly bHLH (Deng et al., 2020), ERF (Zhang et al., 2020b; Paul et al., 2020), MYB (Li et al., 2020), WRKY (Villano et al., 2020), NAC (Jin et al., 2020), and C2H2 transcription factors (Han et al., 2020), as well as other families that play an important role in plant growth and development, stress resistance, and secondary metabolism.

Based on the expression levels of pathway genes (Supplemental Table 24), we explored the secondary metabolism of saponins in *P. notoginseng* plants at the temporal and spatial levels. At the temporal level, we compared the expression patterns of 29 genes from the saponin biosynthesis pathway in the same tissues of 1- to 4-year-old plants. In most tissues, highly expressed genes were concentrated in 3- or 4-year-old tissues, but in the stems, highly expressed genes were mainly concentrated in 1- to 2-year-old tissues (Figure 3). In addition, through comparative transcriptome analysis, we identified 7792 DEGs that were highly expressed in 3- to 4-year-old plants but poorly expressed in plants of other ages. At the spatial level, we compared gene expression patterns in different tissues of same-aged plants. Except in 1-year-old plants, most of the pathway genes were specifically expressed in flowers, and a few were highly expressed in rhizomes and roots (Supplemental Figure 25).

Analyzing key enzyme genes involved in ginsenoside biosynthesis

The biosynthesis of *P. notoginseng* saponins is attributed to the activity of a series of key enzyme genes, among which the largest and most diverse gene families are the CYP450s and the UGTs. Phylogenetic analysis of CYP450s showed that more genes were enriched in the CYP71, CYP72, CYP76, CYP716, and CYP94 superfamilies (Supplemental Figure 26; Supplemental Table 25). Most of the genes in these superfamilies are involved in the oxidative stress response (Heitz et al., 2012) and in the biosynthesis of triterpenes (Carelli et al., 2011; Fukushima et al., 2011; Han et al., 2011), sterols, indole alkaloids (Irmler et al., 2000; Collu et al., 2001; Nafisi et al., 2007), geraniol iridoid (Höfer et al., 2013), and so forth.

Most of the saponin compounds in *P. notoginseng* are triterpene glycosides that contain sugar groups, indicating that UGT genes play a vital role in the modification of these saponins. Phylogenetic analysis of 158 UGT genes showed that most were classified into subfamilies, such as UGT73 (Lim et al., 2002, 2003), UGT71 (Song et al., 2016), UGT94 (Itkin et al., 2016; Ono et al., 2010), UGT91 (Shibuya et al., 2010), UGT85, and UGT74 (Figure 4A; Supplemental Table 26). The UGTs encoded by genes in these subfamilies have been reported to catalyze the glycosylation of flavonoids, isoflavones (Modolo et al., 2007), diterpenes, triterpenes, benzoate, lignans (Grubb et al., 2014; Tanaka et al., 2014; Dai et al., 2015), and other compounds.

We used UGTs involved in terpene biosynthesis as queries (Wang et al., 2015; Wei et al., 2015; Yan et al., 2014) to search for homologous UGT candidate genes in the *P. notoginseng* genome and designed primers for cloning (Supplemental Table 27). We ultimately cloned the full lengths of 32 UGT genes (Supplemental Figure 27) and named them *PnUGT1–PnUGT32*. Then, by expressing their proteins in *Escherichia coli*, we determined that five of them (*PnUGT1–5*) had catalytic functions in the biosynthesis of ginsenosides. We used an *E. coli*-expressed empty vector as the negative control (Supplemental Figure 28). Using PPT and F1 (Monoglycoside; PPT-C20-glucosyl) as substrates, the crude enzyme of gene *PnUGT3* could add a glucosyl group at the C6 position to produce Rh1 (Monoglycoside; PPT-C6-glucosyl) and Rg1 (Diglycoside; PPT-C6-glucosyl, C20-glycosyl), respectively (Figure 4B and Supplemental Figure 29). Its functions are therefore consistent with the functions of UGTPg1 and UGTPg101 from *P. ginseng* (Wei et al., 2015; Yan et al., 2014), but this is a new gene cloned for the first time in *P. notoginseng*. Using PPD and PPT as substrates, the crude enzyme of gene *PnUGT1* could add a glucosyl group at the C20 position to produce CK (Monoglycoside; PPD-C20-glucosyl) and F1 (Monoglycoside; PPT-C20-glucosyl), consistent with the functions of UGTPg100 and UGTPg101 from *P. ginseng* (Wei et al., 2015). In addition, PnUGT1 could catalyze the production of ginsenoside F2 (Diglycoside; PPD-C3-glucosyl, C20-glycosyl) from Rh2 (Monoglycoside; PPD-C3-glucosyl) (Figure 4B and Supplemental Figure 30), which is the first reported new function in *P. notoginseng*. The crude enzyme of gene *PnUGT5* could catalyze the production of Rh2 from PPD, and crude enzymes of genes *PnUGT2* and *PnUGT4* could then extend the sugar chain and generate Rg3 (Monoglycoside; PPD-C3-glucosyl-glucosyl) from Rh2 (Figure 4B and Supplemental Figure 31), consistent with the functions of UGTPg45 and UGTPg29 from *P. ginseng* (Wang et al., 2015). In addition, the last four genes have also been experimentally shown to perform catalytic functions in *Saccharomyces cerevisiae* (Wang et al., 2020).

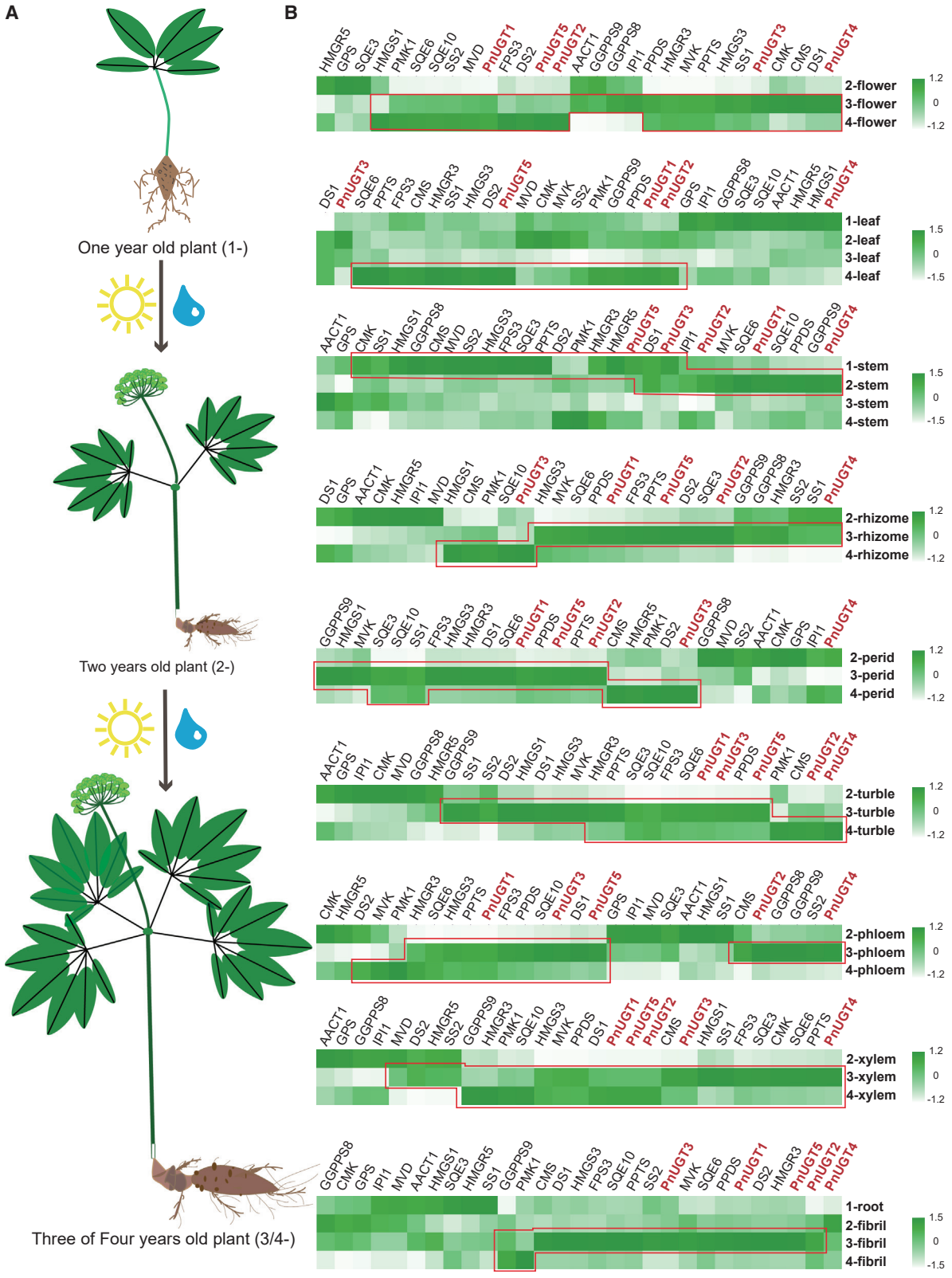

Figure 3. Temporal expression profile of key enzyme genes in the saponin biosynthesis pathway.

(A) A brief view of the morphological changes in *P. notoginseng* as the years of growth increase during the cultivation process.

(B) Temporal expression heatmap of terpenoid biosynthetic pathway genes in *P. notoginseng*. Taking the leaf's heatmap as an example, the Arabic numerals in the label indicate the years of growth; for example, 2-leaf indicates that the sample is the leaf of a 2-year-old *P. notoginseng* plant.

(legend continued on next page)

Besides the more common ginsenoside compounds mentioned above, there are many unique saponins in *P. notoginseng*, such as notoginsenoside R1, notoginsenoside R2, notoginsenoside R4, and notoginsenoside Fc, which have better water solubility and good pharmacological activities (Supplemental Figure 32). To screen out more UGT genes, we conducted weighted gene co-expression network analysis (WGCNA) and expression profile consistency analysis. Through WGCNA, we constructed a correlation network between all genes annotated as UGT in the *P. notoginseng* genome and identified 7 gene modules with strong correlation, including 29 pathway genes and 139 UGT genes (Figure 4C and Supplemental Figure 33). Among them, *PnUGT2* was included in the blue module, and *PnUGT1* and *PnUGT5* were included in the green module. We further analyzed the annotation information and GO enrichment of these candidate UGT genes and found that most were enriched in GO terms such as GO:0008152 (metabolic process) or GO:0071555 (cell wall organization) and had different transferase activities (Supplemental Table 28). We then compared the expression patterns of genes in the terpene biosynthesis pathway and identified UGT genes with similar expression patterns. By comparing the expression levels in each transcriptome sample, the expression patterns of key enzyme genes could be divided into three categories (Figure 5): most were highly expressed in flowers, some were highly expressed in roots (each part), and a small number were most highly expressed in leaves (Supplemental Figure 34). A total of 35 UGT genes that were highly expressed and clustered with the pathway genes were screened from the correlation evolution tree (Supplemental Figure 35; Supplemental Table 29). Combining the results of the two analyses above, we identified candidate UGT genes that may be involved in the notoginsenoside biosynthetic pathway, although the specific functions of the encoded enzymes have yet to be experimentally verified.

DISCUSSION

P. notoginseng, one of the most widely used Chinese medicinal plants from the family Araliaceae, is renowned in China and worldwide for its good efficacy. The main active ingredients in *P. notoginseng* are saponins, including higher contents of ginsenoside Rg1, ginsenoside Rb1, and notoginsenoside R1 (Su et al., 2016; Duan et al., 2017; Zhang et al., 2018, 2019), and other active compounds, such as ginsenoside Rd, ginsenoside Rg3, ginsenoside Re (Xie et al., 2020), notoginsenoside R2, and notoginsenoside Fc (Liu et al., 2018). The biosynthesis of saponins in *P. notoginseng* has attracted extensive attention from researchers, and some key enzyme genes, such as *HMGR*, *AACT*, *SS*, *PMK*, *MVK*, *IDI*, and *CYP450*, have been identified. However, the complete biosynthetic pathways of unique notoginsenosides have not yet been resolved, and further research and exploration are needed.

Gene mining of high-quality genomic and transcriptomic data can provide resources for further exploration of plant growth and secondary metabolism mechanisms (Tu et al., 2020). As early as 2017, two *P. notoginseng* reference genomes were published (Zhang et al., 2017a; Chen et al., 2017); however, the quality of these genomes was insufficient because of the limited sequencing capacity at that time. We therefore performed whole-genome sequencing of *P. notoginseng* from Genuine Producing Areas based on third-generation PacBio sequencing technology and used Hi-C technology to construct a high-quality, chromosome-level genome. The assembled genome was 2.66 Gb in size, with a scaffold N50 of 216.47 Mb and a contig N50 of 1.12 Mb. In addition to the depth or accuracy of gene sequencing, this reference genome was greatly improved compared with previous genomes and was resolved to the chromosome level, which can more intuitively reveal the gene distribution and overall genomic landscape.

In addition to *P. notoginseng*, other plants belonging to Araliaceae are used as medicines, including the well-known plants *P. ginseng*, *Panax quinquefolius* L., and *Panax zingiberensis* C.Y. Wu et K.M. Feng. Based on chemotaxonomy, plants of *Panax* L. can be divided into two groups. The chemical composition of the first group mainly comprises dammarane-type tetracyclic triterpenes, and there are obvious similarities in plant morphology, including a short and erect rhizome and a carrot-like fleshy root. In terms of geographical distribution, plants in this group show a characteristic narrow and intermittent distribution, which has been observed in an ancient group of *Panax* plants. Representative plants include *P. notoginseng*, *P. ginseng*, *P. quinquefolius*, and others. The saponins of the second group are mainly oleanane-type pentacyclic triterpenes, and their plant morphology includes a long and creeping rhizome and an undeveloped fleshy root. They are distributed over a wide and continuous geographical area and may represent an evolutionary group of *Panax* plants. Representative plants from this group include *P. zingiberensis* C.Y. Wu et K.M. Feng, *P. stipuleanatus* H.T. Tsai et K.M. Feng, *Panax japonicus* (T. Nees) C.A. Mey. and *Panax japonicus* C.A. Mey. var. major (Burk.) C.Y. Wu et K.M. Feng, and others. Based on cytotaxonomy analysis, we found that *Panax* plants had different ploidy types. For example, *P. notoginseng* and *P. japonicus* are diploid, and *P. ginseng* and *P. quinquefolius* are tetraploid, further indicating that *P. notoginseng* is in a relatively primitive evolutionary position among *Panax* plants. By comparing genomes, we found that after diverging from carrots, an independent WGD event occurred in *P. notoginseng*. We then studied the distribution of K_a/K_s values of key enzyme gene pairs in the saponin biosynthesis pathway and found that the WGD event may have contributed to the generation of these gene pairs, directing the metabolic flux toward the production of saponins. Based on the locations of coding genes on the chromosomes, we also found two sets of gene cluster duplication. Notably, upstream HDR, SS, and SE genes and downstream CYP450 and UGT genes that are known to be involved in ginsenoside biosynthesis are close to each other in the *P. notoginseng* genome (Supplemental Figure 36). The gene cluster also contains some UGT and transcription factor genes identified in this study, which are likely to participate in

Based on the gene expression levels, the pattern of expression change for any one gene can be observed after the data in each column are standardized. The area marked by the red box indicates high gene expression levels. Each heatmap has its own color scale: the higher the expression, the greener the color.

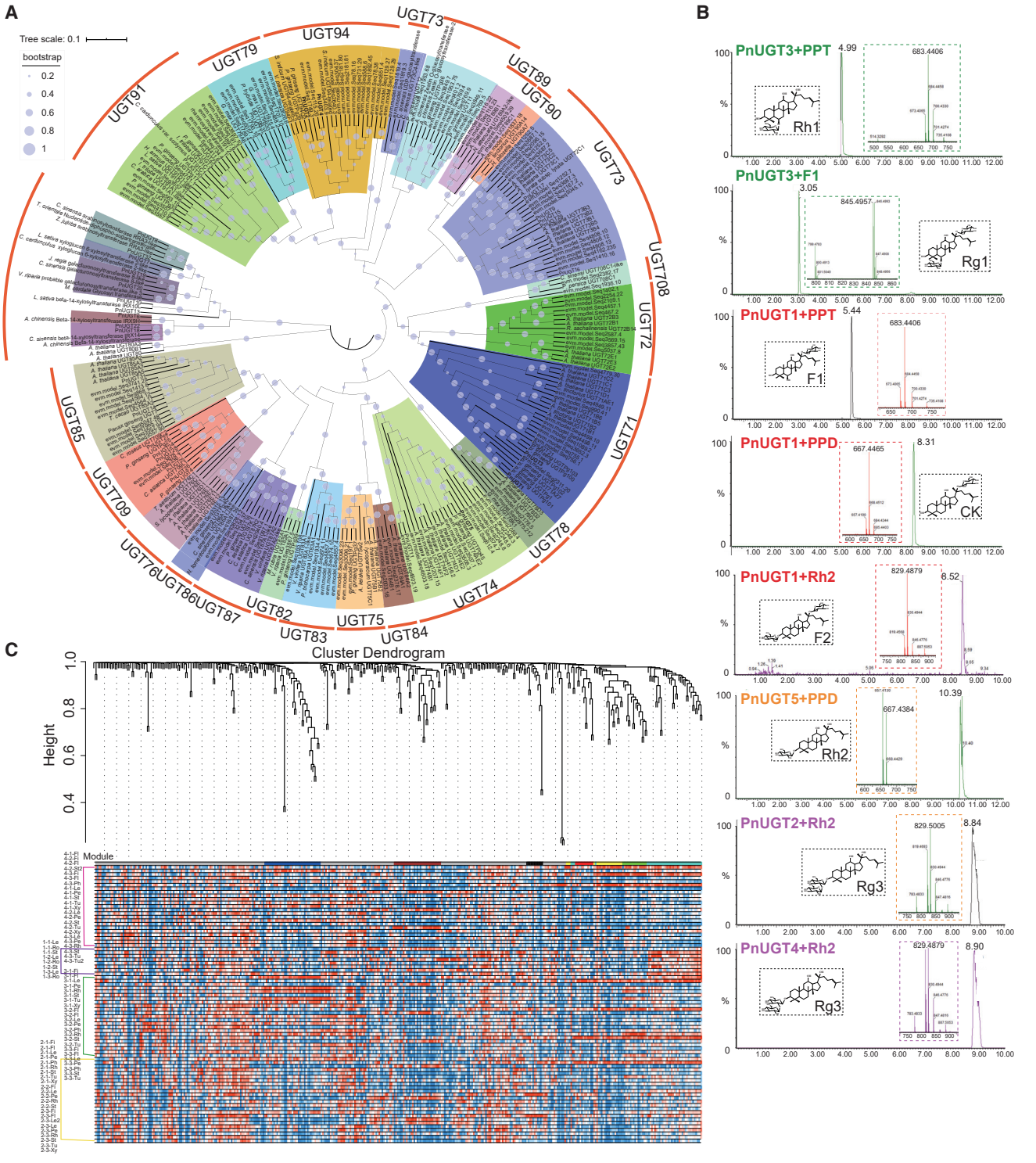

Figure 4. Screening for candidate UGT genes and functional verification of five UGT genes.

(A) Phylogenetic analysis of UGT genes. The UGT gene families clustered into one clade are represented by different colors. The bootstrap value associated with each branch is represented by a light-purple circle: the larger the radius, the greater the bootstrap value.

(B) UPLC/Q-TOF analysis of five functional UGT genes. In catalytic reactions, PnUGT3 uses PPT and F1 as substrates, PnUGT1 uses PPD, PPT, and Rh2 as substrates, PnUGT5 uses PPD as a substrate, and PnUGT2 and PnUGT4 use Rh2 as a substrate to generate corresponding ginsenoside compounds. The chemical structures and characteristic mass spectrum peaks of products from each reaction are displayed in the dashed box of each track.

(C) WGCNA analysis of UGT genes.

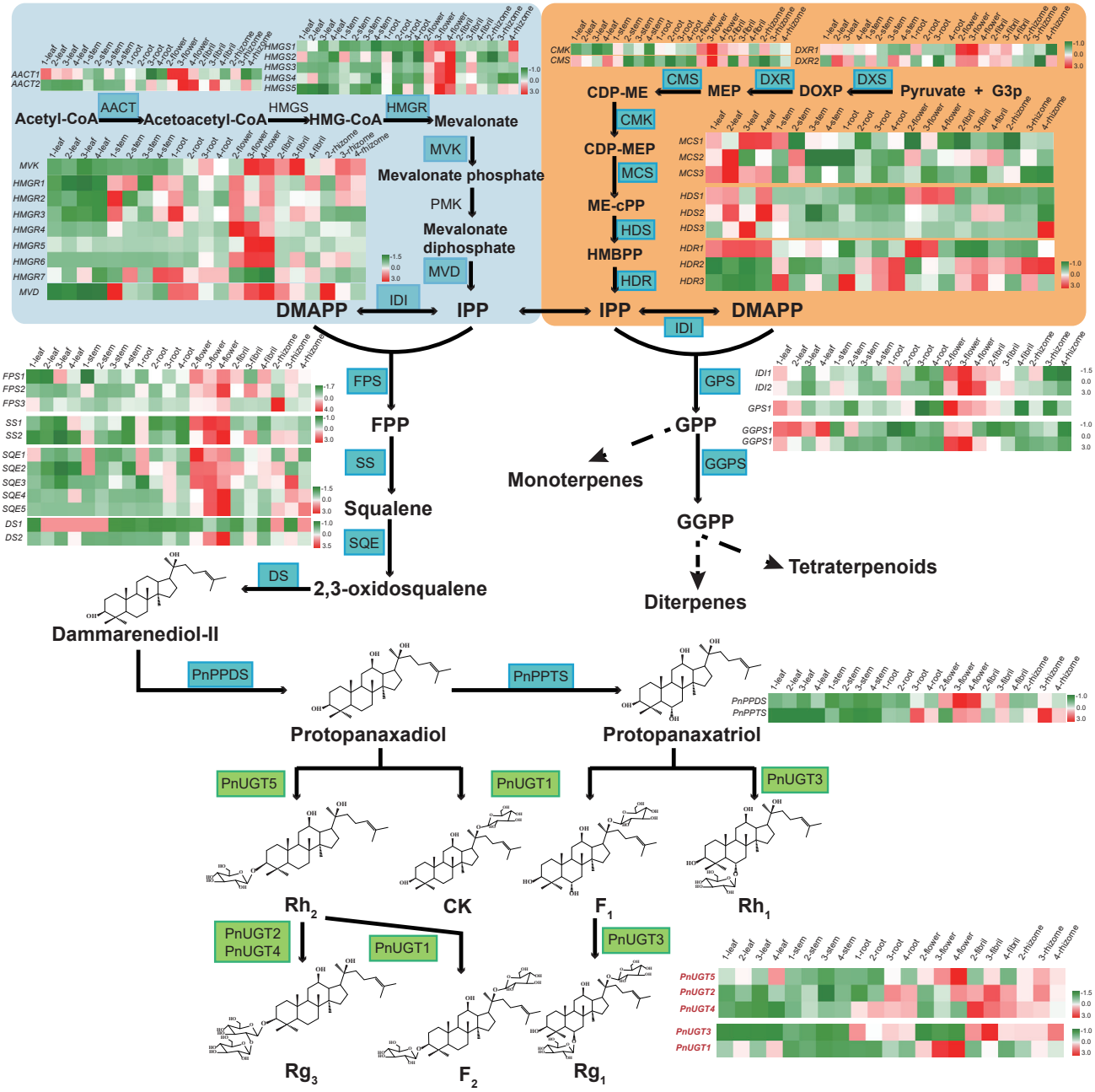

Figure 5. Overview of the saponin biosynthetic pathway in *P. notoginseng* and expression profiles of key enzyme genes.
The genes in the green box are the UGT genes identified in this study.

the biosynthesis and regulation of saponins. Compared with *P. notoginseng*, *P. ginseng* experienced one additional WGD event, which was manifested in the larger genome size, more expanded gene families, and multiple copies of key enzyme genes. In summary, we analyzed and explored the genetic information of *P. notoginseng*, one of the more primitive *Panax* plants, laying a solid foundation for subsequent evolutionary research on the genus *Panax*.

In addition, we also established a detailed transcript database of *P. notoginseng* through sequencing and analysis of different tissues from 1- to 4-year-old plants. Through comparative transcriptome analysis, we explored the molecular regulation mechanism of tubercles, a characteristic phenotype of *P. notoginseng*. The associated DEGs were mainly involved in the biosynthesis of plant hormones such as strigolactone, cytokinin, and auxin. The synergistic effects of these phytohormones result in the production of a tubercle phenotype, and further study of the functions of related DEGs will more fully reveal the molecular mechanisms of tubercle formation.

We next explored the saponin biosynthesis pathway in *P. notoginseng* plants at temporal and spatial levels. We compared the expression patterns of saponin biosynthesis genes

in the same tissues of 1- to 4-year-old plants and found that most genes in tissues other than stems were highly expressed in 3- or 4-year-old plants. This indicates that as plant age increases, saponin biosynthesis gene expression levels also increase, as does the content of accumulated saponins. The quality of *P. notoginseng* harvested after more than 3 years of growth is therefore optimal, but because of diseases, insect pests, and continuous cropping obstacles, most materials circulated in the market are 3-year-old *P. notoginseng*. At the spatial level, most pathway genes were specifically expressed in flowers, and a few were highly expressed in rhizomes and roots, including the postmodification UGT enzyme genes *PnUGT2*, *PnUGT3*, and *PnUGT4*. These results indicate that saponin compounds or their precursors may be synthesized in the flowers first and then transferred to the roots or further modified in the roots, consistent with a previous report.

The ultimate step in the saponin biosynthesis pathway is glycosylation catalyzed by UGTs. This is the most critical step in determining the structure and pharmacological effects of the compounds, and we therefore focused on identifying candidate UGT genes. First, we conducted a systematic evolutionary analysis of all *P. notoginseng* genes that contained the conserved GT domain. As expected, we obtained five UGT genes that catalyzed the glycosylation of ginsenosides. Second, we performed WGCNA analysis on all genes annotated as UGTs and key enzyme genes of the *P. notoginseng* saponin biosynthetic pathway and screened out seven modules of highly correlated genes. Among these seven modules, two (module blue and module green) contained genes with identified functions, indicating that the genes enriched in these modules were likely to participate in the biosynthesis of saponins. Third, we conducted a consistency analysis of expression profiles and identified 20 UGT genes with high expression levels and expression patterns consistent with those of pathway genes. Combining the results of the two analyses above, we identified candidate UGT genes to lay a foundation for further comprehensive analysis of the complete notoginsenoside biosynthesis pathway.

In summary, we constructed a high-quality, chromosome-level *P. notoginseng* reference genome as a comprehensive genetic inventory for evolutionary phylogenomic studies of *Panax* plants. Using detailed transcriptome data, we explored the molecular mechanism of tubercle formation, investigated the biosynthesis pathway of saponins, and provided many promising candidate genes to fully reveal the biosynthetic pathway of notoginsenosides in *P. notoginseng*.

MATERIALS AND METHODS

Plant materials, DNA extraction, and library construction

Individual plants of *P. notoginseng* (Burk.) F. H. Chen were collected in August 2019 from Wenshan County, Yunnan Province, China (26°49′55″N, 100°3′20″E, 2630 m above sea level). Fresh and healthy leaves were harvested, immediately frozen in liquid nitrogen, and preserved at −80°C. High-quality genomic DNA was extracted from the *P. notoginseng leaves u*sing the modified phenol-chloroform isoamyl alcohol extraction method. The quality and quantity of the isolated DNA were assessed using a NanoPhotometer (Implen, CA, USA) and a Qubit 2.0 Fluorometer (Life Technologies, CA, USA). Illumina (350 bp), PacBio, and Hi-C libraries were constructed following the operation guide for each technology.

Genome sequencing, assembly, and quality assessment

For PacBio libraries, the whole genome was sequenced on the PacBio Sequel II System based on single-molecule real-time sequencing technology, and 284.07 Gb (~106.79×) of data were obtained. The Illumina library was sequenced on the Illumina HiSeq X Ten platform following standard Illumina protocols. After filtering out adapter sequences and low-quality and duplicated reads, we obtained 231.06 Gb (~86.86×) of clean data. The subreads obtained from PacBio libraries were assembled into contigs using Canu (v1.8), and the consensus genome was polished by referring to the Illumina reads with BWA (v0.7.9a) and Pilon (v1.22). For Hi-C libraries, Illumina HiSeq X Ten was used for sequencing with PE150, and a total of 340.83 Gb (~128.13×) of data were retained. Finally, based on Hi-C technology using BWA-mem and LACHESIS, the final genome was 2.66 Gb in size, and the contig and scaffold N50 were 1.12 and 216.47 Mb, respectively. We used BUSCO (v3.0.1, default parameters), Illumina reads, and transcriptome mapping to the *P. notoginseng* genome with BWA-mem to confirm the high quality of the assembled genome.

Genome annotation

We used homology-based, *de novo*, and transcriptome-based predictions to predict the protein-coding genes in the *P. notoginseng* genome. The gene sets predicted by various strategies were integrated into a non-redundant and more complete gene set using EVidenceModeler. Gene functional annotation was performed mainly by searching against various functional databases, such as Swiss-Prot, NT (Nucleotide Sequence Database), NR (Non-Redundant Protein Sequence Database), Pfam, eggNOG (Evolutionary Genealogy of Genes: Non-supervised Orthologous Groups), and GO. Repetitive sequences were annotated using an *ab initio* prediction method and a homolog-based approach. We detected noncoding RNA by comparison with known noncoding RNA libraries and Rfam, and we also predicted rRNAs, snRNAs, microRNAs, and so on.

Analysis of genomic evolution and WGD events

We used the OrthoMCL package (1.4) to identify and cluster gene families (clusters) from *P. notoginseng* and seven other plant species: *P. ginseng*, *D. carota*, *V. vinifera*, *C. annuum* L., *G. uralensis*, *A. thaliana*, and *O. sativa*. After gene family clustering, we aligned all 458 single-copy gene protein sequences using MUSCLE and constructed a phylogenetic tree using PhyML. Based on the gene family cluster analysis and after filtering gene families with abnormal gene numbers in individual species, we used the CAFÉ program to identify the expansion and contraction of gene families in each species. To explore the evolution of the *P. notoginseng* genome, we calculated the 4DTv of syntenic blocks and the distribution of synonymous substitutions per synonymous site (K_s) to identify WGD events.

Integrated genomic and transcriptomic analysis

One- to four-year-old *P. notoginseng* plants were collected from Wenshan County, Yunnan Province, China. There were three biological replicates for each sample, and samples were taken at least five meters apart. After harvesting, we subdivided the plants into different tissue parts, including the root (xylem), stem, leaf, flower, rhizome, fibril, periderm, phloem, and tubercle. All samples were transported on dry ice, washed with ultrapure water three times, immediately frozen in liquid nitrogen, and stored at −80°C before RNA extraction. Total RNA was extracted from each tissue using a modified cetyltrimethylammonium bromide method. The RNA purity was checked using a kaiaoK5500 spectrophotometer (Kaiao, Beijing, China), and the RNA integrity and concentration were assessed using the RNA Nano 6000 Assay Kit for the Bioanalyzer 2100 system (Agilent Technologies, CA, USA). cDNA libraries were constructed using the NEBNext Ultra RNA Library Prep Kit for Illumina (New England Biolabs, USA) following the manufacturer's recommendations. After cluster

generation, the libraries were sequenced on an Illumina NovaSeq S2 platform, and 150 bp paired-end reads were generated.

Genes encoding key enzymes thought to be involved in the saponin biosynthetic pathway were annotated by BLAST (2.2.28). Their predicted proteins were aligned with the Pfam database using HMMER (3.1b1), and their expression levels in different tissues were obtained from transcriptome data. We used MeV software (4.9.0) to create a heatmap of gene expression and analyze gene expression patterns. In addition, we identified transcription factor genes in the *P. notoginseng* genome by comparison with the PlantTFDB database. We used an R script to calculate the Pearson correlation coefficients between transcription factors and genes in batches and Cytoscape software to draft the correlation map.

Screening and functional verification of candidate UGT genes

Multiple sequence alignments were generated using DNAMAN to visualize the conserved motifs. For phylogenetic tree analysis, the amino acid sequences of UGTs from other species were downloaded from the National Center for Biotechnology Information (NCBI) database and aligned using ClustalW. Then, a neighbor-joining tree was built using MEGA X software (Kumar et al., 2016) with 1000 bootstrap iterations. *P. notoginseng* cDNA was prepared using the PrimeScript 1st Strand cDNA Synthesis Kit (Takara, Dalian, China). After designing primers, we cloned a total of 32 UGT genes, and the PCR products were ligated into the N-terminal MBP fusion expression vector HIS-MBP-pET28a (HIS, histidine; MBP, maltose-binding protein) (Li et al., 2018) according to the protocol of the Seamless Cloning Kit (Beyotime, Shanghai, China). We transformed the successfully sequenced positive strains into *E. coli* BL21 (DE3) (Transgen Biotech, Beijing, China) and maintained the cultures in Luria-Bertani liquid medium with kanamycin (50 μg/mL) at 37°C in a shaking incubator until the optical density at 600 nm reached 0.6–0.8. Then, 1 M isopropyl β-D-thiogalactopyranoside was added to a final concentration of 50 μM, and cultures were maintained at 16°C and 120 rpm for 16 h to allow expression of recombinant proteins. pET28a-transformed *E. coli* BL21 (DE3) cells were treated in parallel as a control. The recombinant cells were harvested by centrifugation at 10 000 *g* and 4°C, then resuspended in 100 mM phosphate buffer (pH 8.0) that contained 1 mM phenylmethanesulfonylfluoride and sonicated in an ice-water bath for 10 min (lysed for 5 s, paused for 5 s). The sample lysates were centrifuged for 20 min at 12 000 *g* and 4°C to separate crude enzymes from cell debris. A UGT activity assay was performed in a total volume of 100 μl that contained 100 mM crude enzyme buffer (pH 8.0), 1 mM UDP-glucose, and 0.1 mM acceptor substrate for 2 h in a 35°C water bath and was terminated by the addition of 200 μl methanol. Precipitated proteins were removed by centrifugation (10 000 *g* for 10 min) and filtered through 0.22 μm filters before injection. Glycosylated products were detected using ultra-high-performance liquid chromatography coupled with quadrupole time-of-flight mass spectrometry (UPLC/Q-TOF-MS, Waters, Milford, MA) using a Waters ACQUITY UPLC HSS T3 analytical column (2.1 × 100 mm, 1.8 μm). Data analysis was performed using MassLynx software (version 4.1). Standards of saponin compounds and UDP-glucose were purchased from Yuanye Bio-Technology (Shanghai, China). To screen additional candidate UGT genes, we also conducted WGCNA using R and expression profile consistency analysis.

Data availability

The data supporting the findings of this work are available within the paper and its Supplemental Information files. The nucleotide sequencing data for UGT genes identified in this study have been deposited at NCBI GenBank under accession numbers MT551198 to MT551202. The genome sequence data of *P. notoginseng* have been deposited under NCBI BioProject number PRJNA658419https://www.Ncbi.nlm.nih.gov/bioproject/SUB7934826. In addition, the whole-genome sequence data reported in this paper have been deposited in the Genome Warehouse in the National Genomics Data Center (National Genomics Data Center and Partners, 2020), Beijing Institute of Genomics (China National Center for Bioinformation), Chinese Academy of Sciences, under accession number GWHAOSA00000000 and are publicly accessible at https://bigd.big.ac.cn/gsa.

SUPPLEMENTAL INFORMATION

Supplemental Information is available at *Plant Communications Online*.

FUNDING

We acknowledge support from the National Natural Science Foundation of China (nos. 81891010, 81891013), the Key Project at central government level: The ability establishment of sustainable use for valuable Chinese medicine resources (no. 2060302-1806-03), the High-level Teachers in Beijing Municipal Universities in the Period of 13th Five-year Plan (no. CIT&TCD20170324), and the National Program for Special Support of Eminent Professionals.

AUTHOR CONTRIBUTIONS

W.G., L.H., and Z.J. conceived and initiated the study. Z.J., T.L., and W.Y. performed the genome sequencing and bioinformatics analyses. X.C. provided the original plant material of *P. notoginseng*. Z.J. performed most of the experiments with the assistance of Y.Z., T.H., B.M., Y. Lu, J.G., J.Z., Y. Liu, N.L., X.W., and Y.S., and Y.T. provided assistance with chemical experiments. Z.J. wrote the manuscript and Y.Z., T.L., L.T., W.G., and L.H. revised the manuscript. All authors read and approved the final manuscript.

ACKNOWLEDGMENTS

The authors declare no competing interests.

Received: July 20, 2020
Revised: August 25, 2020
Accepted: September 17, 2020
Published: September 20, 2020

REFERENCES

Briskin, D. (2000). Medicinal plants and phytomedicines. Linking plant biochemistry and physiology to human health. Plant Physiol. **124**:507–514.

Carelli, M., Biazzi, E., Panara, F., Tava, A., Scaramelli, L., Porceddu, A., Graham, N., Odoardi, M., Piano, E., Arcioni, S., et al. (2011). *Medicago truncatula* CYP716A12 is a multifunctional oxidase involved in the biosynthesis of hemolytic saponins. Plant Cell **23**:3070–3081.

Chan, P., Thomas, G., and Tomlinson, B. (2002). Protective effects of trilinolein extracted from *Panax notoginseng* against cardiovascular disease. Acta Pharmacol. Sin **23**:1157–1162.

Chen, W., Kui, L., Zhang, G., Zhu, S., Zhang, J., Wang, X., Yang, M., Huang, H., Liu, Y., Wang, Y., et al. (2017). Whole-genome sequencing and analysis of the Chinese herbal plant *Panax notoginseng*. Mol. Plant **10**:899–902.

Collu, G., Unver, N., Peltenburg-Looman, M.G.A., Heijden, R.v.d., Verpoorte, R., and Memelink, J. (2001). Geraniol 10-hydroxylase, a cytochrome P450 enzyme involved in terpenoid indole alkaloid biosynthesis. Fed. Eur. Biochem. Soc. **508**:215–220.

Cui, X., Huang, L., Guo, L., and Liu, D. (2014). Chinese Sanqi industry status and development contermeasures. Chin. J. Chin. Mater. Med. **39**:553–557.

Dai, L., Liu, C., Zhu, Y., Zhang, J., Men, Y., Zeng, Y., and Sun, Y. (2015). Functional characterization of cucurbitadienol synthase and triterpene glycosyltransferase involved in biosynthesis of mogrosides from *Siraitia grosvenorii*. Plant Cell Physiol. **56**:1172–1182.

Dang, X., Miao, J., Chen, A.-q., Li, P., Chen, L., Liang, J.-r., Xie, R.-m., and Zhao, Y. (2015). The antithrombotic effect of RSNK in blood-stasis model rats. J. Ethnopharmacol. **173**:266–272.

Dassanayake, M., Haas, J.S., Bohnert, H.J., and Cheeseman, J.M. (2009). Shedding light on an extremophile lifestyle through transcriptomics. New Phytol. **183**:764–775.

Deng, B., Zhang, P., Ge, F., Liu, D.-Q., and Chen, C.-Y. (2017). Enhancement of triterpenoid saponins biosynthesis in *Panax notoginseng* cells by co-overexpressions of 3-hydroxy-3-methylglutaryl CoA reductase and squalene synthase genes. Biochem. Eng. J. **122**:38–46.

Deng, C., Wang, J., Lu, C., Li, Y., Kong, D., Hong, Y., Huang, H., and Dai, S. (2020). CcMYB6-1 and CcbHLH1, two novel transcription factors synergistically involved in regulating anthocyanin biosynthesis in cornflower. Plant Physiol. Biochem. **151**:271–283.

Duan, L., Xiong, X., Hu, J., Liu, Y., Li, J., and Wang, J. (2017). *Panax notoginseng* saponins for treating coronary artery disease: a functional and mechanistic overview. Front. Pharmacol. **8**. https://doi.org/10.3389/fphar.2017.00702.

Fukushima, E.O., Seki, H., Ohyama, K., Ono, E., Umemoto, N., Mizutani, M., Saito, K., and Muranaka, T. (2011). CYP716A subfamily members are multifunctional oxidases in triterpenoid biosynthesis. Plant Cell Physiol. **52**:2050–2061.

Grubb, C.D., Zipp, B.J., Kopycki, J., Schubert, M., Quint, M., Lim, E.K., Bowles, D.J., Pedras, M.S., and Abel, S. (2014). Comparative analysis of *Arabidopsis* UGT74 glucosyltransferases reveals a special role of UGT74C1 in glucosinolate biosynthesis. Plant J. **79**:92–105.

Gui, Q., Yang, Y., Ying, S., and Zhang, M. (2013). Xueshuatong improves cerebral blood perfusion in elderly patients with lacunar infarction. Neural Regen. Res. **8**:792–801.

Han, G., Lu, C., Guo, J., Qiao, Z., Sui, N., Qiu, N., and Wang, B. (2020). C2H2 zinc finger proteins: master regulators of abiotic stress responses in plants. Front. Plant Sci. **11**:115.

Han, J.Y., Hwang, H.S., Choi, S.W., Kim, H.J., and Choi, Y.E. (2012). Cytochrome P450 CYP716A53v2 catalyzes the formation of protopanaxatriol from protopanaxadiol during ginsenoside biosynthesis in *Panax ginseng*. Plant Cell Physiol **53**:1535–1545.

Han, J.Y., Kim, H.J., Kwon, Y.S., and Choi, Y.E. (2011). The Cyt P450 enzyme CYP716A47 catalyzes the formation of protopanaxadiol from dammarenediol-II during ginsenoside biosynthesis in *Panax ginseng*. Plant Cell Physiol. **52**:2062–2073.

Heitz, T., Widemann, E., Lugan, R., Miesch, L., Ullmann, P., Desaubry, L., Holder, E., Grausem, B., Kandel, S., Miesch, M., et al. (2012). Cytochromes P450 CYP94C1 and CYP94B3 catalyze two successive oxidation steps of plant hormone jasmonoyl-isoleucine for catabolic turnover. J. Biol. Chem. **287**:6296–6306.

Höfer, R., Dong, L., André, F., Ginglinger, J.-F., Lugan, R., Gavira, C., Grec, S., Lang, G., Memelink, J., Krol, S.V.D., et al. (2013). Geraniol hydroxylase and hydroxygeraniol oxidase activities of the CYP76 family of cytochrome P450 enzymes and potential for engineering the early steps of the (seco)iridoid pathway. Metab. Eng. **20**:221–232.

Irmler, S., Schroder, G., St-Pierre, B., Crouch, N., Hotze, M., Schmidt, J., Stract, D., Matern, U., and Schroder, J. (2000). Indole alkaloid biosynthesis in *Catharanthus roseus*: new enzyme activities and identification of cytochrome P450 CYP72A1 as secologanin synthase. Plant J. **24**:797–804.

Itkin, M., Davidovich-Rikanati, R., Cohen, S., Portnoy, V., Doron-Faigenboim, A., Oren, E., Freilich, S., Tzuri, G., Baranes, N., Shen, S., et al. (2016). The biosynthetic pathway of the nonsugar, high-intensity sweetener mogroside V from *Siraitia grosvenorii*. Proc. Natl. Acad. Sci. U S A **113**:E7619–E7628.

Jaillon, O., Aury, J.M., Noel, B., Policriti, A., Clepet, C., Casagrande, A., Choisne, N., Aubourg, S., Vitulo, N., Jubin, C., et al. (2007). The grapevine genome sequence suggests ancestral hexaploidization in major angiosperm phyla. Nature **449**:463–467.

Jia, L., Zuo, T., Zhang, C., Li, W., Wang, H., Hu, Y., Wang, X., Qian, Y., Yang, W., and Yu, H. (2019). Simultaneous profiling and holistic comparison of the metabolomes among the flower buds of *Panax ginseng, Panax quinquefolius*, and *Panax notoginseng* by UHPLC/IM-QTOF-HDMSE-based metabolomics analysis. Molecules **24**:2188.

Jiang, D., Rong, Q., Chen, Y., Yuan, Q., Shen, Y., Guo, J., Yang, Y., Zha, L., Wu, H., Huang, L., et al. (2017). Molecular cloning and functional analysis of squalene synthase (SS) in *Panax notoginseng*. Int. J. Biol. Macromol **95**:658–666.

Jin, J.F., Wang, Z.Q., He, Q.Y., Wang, J.Y., Li, P.F., Xu, J.M., Zheng, S.J., Fan, W., and Yang, J.L. (2020). Genome-wide identification and expression analysis of the NAC transcription factor family in tomato (*Solanum lycopersicum*) during aluminum stress. BMC Genomics **21**:288.

Kim, N.H., Jayakodi, M., Lee, S.C., Choi, B.S., Jang, W., Lee, J., Kim, H.H., Waminal, N.E., Lakshmanan, M., van Nguyen, B., et al. (2018). Genome and evolution of the shade-requiring medicinal herb *Panax ginseng*. Plant Biotechnol. J. **16**:1904–1917.

Kumar, S., Stecher, G., and Tamura, K. (2016). MEGA7: molecular evolutionary genetics analysis version 7.0 for bigger datasets. Mol. Biol. Evol. **33**:1870–1874.

Laloum, T., Martin, G., and Duque, P. (2018). Alternative splicing control of abiotic stress responses. Trends Plant Sci. **23**:140–150.

Lee, T., Grinshpun, S.A., Kim, K.Y., Iossifova, Y., Adhikari, A., and Reponen, T. (2006). Relationship between indoor and outdoor airborne fungal spores, pollen, and (1→3)-β-D-glucan in homes without visible mold growth. Aerobiologia **22**:227–235.

Li, S.F., Allen, P.J., Napoli, R.S., Browne, R.G., Pham, H., and Parish, R.W. (2020). MYB-bHLH-TTG1 regulates *Arabidopsis* seed coat biosynthesis pathways directly and indirectly via multiple tiers of transcription factors. Plant Cell Physiol. **61**:1005–1018.

Li, Y., Lin, H.X., Wang, J., Yang, J., Lai, C.J., Wang, X., Ma, B.W., Tang, J.F., Li, Y., Li, X.L., et al. (2018). Glucosyltransferase capable of catalyzing the last step in neoandrographolide biosynthesis. Org. Lett. **20**:5999–6002.

Lim, E.K., Baldauf, S., Li, Y., Elias, L., Worrall, D., Spencer, S.P., Jackson, R.G., Taguchi, G., Ross, J., and Bowles, D.J. (2003). Evolution of substrate recognition across a multigene family of glycosyltransferases in *Arabidopsis*. Glycobiology **13**:139–145.

Lim, E.K., Doucet, C.J., Li, Y., Elias, L., Worrall, D., Spencer, S.P., Ross, J., and Bowles, D.J. (2002). The activity of *Arabidopsis* glycosyltransferases toward salicylic acid, 4-hydroxybenzoic acid, and other benzoates. J. Biol. Chem. **277**:586–592.

Liu, J., Jiang, C., Ma, X., and Wang, J. (2018). Notoginsenoside Fc attenuates high glucose-induced vascular endothelial cell injury via upregulation of PPAR-gamma in diabetic Sprague-Dawley rats. Vascul Pharmacol. **109**:27–35.

Lu, J., Li, J., Wang, S., Yao, L., Liang, W., Wang, J., and Gao, W. (2018). Advances in ginsenoside biosynthesis and metabolic regulation. Biotechnol. Appl. Biochem. **65**:514–522.

Luo, H., Sun, C., Sun, Y., Wu, Q., Li, Y., Song, J., Niu, Y., Cheng, X., Xu, H., Li, C., et al. (2011). Analysis of the transcriptome of *Panax notoginseng* root uncovers putative triterpene saponin-biosynthetic genes and genetic markers. BMC Genomics **12**:S5.

Min, S., Jung, S., Cho, K., and Kim, D. (2008). Antihyperlipidemic effects of red ginseng, *Crataegii fructus* and their main constituents ginsenoside Rg3 and ursolic acid in mice. Biomol. Ther. **16**:364–369.

Modolo, L.V., Blount, J.W., Achnine, L., Naoumkina, M.A., Wang, X., and Dixon, R.A. (2007). A functional genomics approach to (iso) flavonoid glycosylation in the model legume *Medicago truncatula*. Plant Mol. Biol. **64**:499–518.

Nafisi, M., Goregaoker, S., Botanga, C.J., Glawischnig, E., Olsen, C.E., Halkier, B.A., and Glazebrook, J. (2007). *Arabidopsis* cytochrome P450 monooxygenase 71A13 catalyzes the conversion of indole-3-acetaldoxime in camalexin synthesis. Plant Cell **19**:2039–2052.

National Genomics Data Center Members and Partners. (2020). Database resources of the national genomics data center in 2020. Nucleic Acids Res. **48**:D24–D33.

Ng, T.B. (2006). Pharmacological activity of sanchi ginseng (*Panax notoginseng*). J. Pharm. Pharmacol. **58**:1007–1019.

Niu, Y., Luo, H., Sun, C., Yang, T.J., Dong, L., Huang, L., and Chen, S. (2014). Expression profiling of the triterpene saponin biosynthesis genes FPS, SS, SE, and DS in the medicinal plant *Panax notoginseng*. Gene **533**:295–303.

Ono, E., Ruike, M., Iwashita, T., Nomoto, K., and Fukui, Y. (2010). Co-pigmentation and flavonoid glycosyltransferases in blue *Veronica persica* flowers. Phytochemistry **71**:726–735.

Pan, C., Hou, Y., An, X., Singh, Gurbakhshish, Chen, M., Yang, Z., Pu, J., and Li, J. (2012). *Panax notoginseng* and its components decreased hypertension via stimulation of endothelial-dependent vessel dilatation. Vasc. Pharmacol. **56**:150–158.

Paul, P., Singh, S.K., Patra, B., Liu, X., Pattanaik, S., and Yuan, L. (2020). Mutually regulated AP2/ERF gene clusters modulate biosynthesis of specialized metabolites in plants. Plant Physiol. **182**:840–856.

Sarkar, D., and Maranas, C.D. (2020). SNPeffect: identifying functional roles of SNPs using metabolic networks. Plant J. **103**:512–531.

Schober, M.S., Burton, R.A., Shirley, N.J., Jacobs, A.K., and Fincher, G.B. (2009). Analysis of the (1,3)-beta-D-glucan synthase gene family of barley. Phytochemistry **70**:713–720.

Shen, Q., Zhang, L., Liao, Z., Wang, S., Yan, T., Shi, P., Liu, M., Fu, X., Pan, Q., Wang, Y., et al. (2018). The genome of *Artemisia annua* provides insight into the evolution of Asteraceae family and artemisinin biosynthesis. Mol. Plant **11**:776–788.

Shibuya, M., Nishimura, K., Yasuyama, N., and Ebizuka, Y. (2010). Identification and characterization of glycosyltransferases involved in the biosynthesis of soyasaponin I in *Glycine max*. FEBS Lett. **584**:2258–2264.

Simao, F.A., Waterhouse, R.M., Ioannidis, P., Kriventseva, E.V., and Zdobnov, E.M. (2015). BUSCO: assessing genome assembly and annotation completeness with single-copy orthologs. Bioinformatics **31**:3210–3212.

Song, C., Zhao, S., Hong, X., Liu, J., Schulenburg, K., and Schwab, W. (2016). A UDP-glucosyltransferase functions in both acylphloroglucinol glucoside and anthocyanin biosynthesis in strawberry (*Fragaria* × *ananassa*). Plant J. **85**:730–742.

Su, P., Du, S., Li, H., Li, Z., Xin, W., and Zhang, W. (2016). Notoginsenoside R1 inhibits oxidized low-density lipoprotein induced inflammatory cytokines production in human endothelial EA.hy926 cells. Eur. J. Pharmacol. **770**:9–15.

Tanaka, K., Hayashi, K.-i., Natsume, M., Kamiya, Y., Sakakibara, H., Kawaide, H., and Kasahara, H. (2014). UGT74D1 catalyzes the glucosylation of 2-oxindole-3-acetic acid in the auxin metabolic pathway in *Arabidopsis*. Plant Cell Physiol. **55**:218–228.

Tu, L., Su, P., Zhang, Z., Gao, L., Wang, J., Hu, T., Zhou, J., Zhang, Y., Zhao, Y., Liu, Y., et al. (2020). Genome of *Tripterygium wilfordii* and identification of cytochrome P450 involved in triptolide biosynthesis. Nat. Commun. **11**:971.

Villano, C., Esposito, S., D'Amelia, V., Garramone, R., Alioto, D., Zoina, A., Aversano, R., and Carputo, D. (2020). WRKY genes family study reveals tissue-specific and stress-responsive TFs in wild potato species. Sci. Rep. **10**:7196.

Wang, D., Wang, J., Shi, Y., Li, R., Fan, F., Huang, Y., Li, W., Chen, N., Huang, L., Dai, Z., et al. (2020). Elucidation of the complete biosynthetic pathway of the main triterpene glycosylation products of *Panax notoginseng* using a synthetic biology platform. Metab. Eng. **61**:131–140.

Wang, P., Wei, Y., Fan, Y., Liu, Q., Wei, W., Yang, C., Zhang, L., Zhao, G., Yue, J., Yan, X., et al. (2015). Production of bioactive ginsenosides Rh2 and Rg3 by metabolically engineered yeasts. Metab. Eng. **29**:97–105.

Wang, T., Guo, R., Zhou, G., Zhou, X., Kou, Z., Sui, F., Li, C., Tang, L., and Wang, Z. (2016). Traditional uses, botany, phytochemistry, pharmacology and toxicology of *Panax notoginseng* (Burk.) F.H. Chen: a review. J. Ethnopharmacol **188**:234–258.

Wei, C., Yang, H., Wang, S., Zhao, J., Liu, C., Gao, L., Xia, E., Lu, Y., Tai, Y., She, G., et al. (2018). Draft genome sequence of *Camellia sinensis* var. *sinensis* provides insights into the evolution of the tea genome and tea quality. Proc. Natl. Acad. Sci. U S A **115**:E4151–E4158.

Wei, W., Wang, P., Wei, Y., Liu, Q., Yang, C., Zhao, G., Yue, J., Yan, X., and Zhou, Z. (2015). Characterization of *Panax ginseng* UDP-glycosyltransferases catalyzing protopanaxatriol and biosyntheses of bioactive ginsenosides F1 and Rh1 in metabolically engineered yeasts. Mol. Plant **8**:1412–1424.

Xia, E., Tong, W., Hou, Y., An, Y., Chen, L., Wu, Q., Liu, Y., Yu, J., Li, F., Li, R., et al. (2020). The reference genome of tea plant and resequencing of 81 diverse accessions provide insights into genome evolution and adaptation of tea plants. Mol. Plant **13**:1013–1026.

Xia, E.H., Zhang, H.B., Sheng, J., Li, K., Zhang, Q.J., Kim, C., Zhang, Y., Liu, Y., Zhu, T., Li, W., et al. (2017). The tea tree genome provides insights into tea flavor and independent evolution of caffeine biosynthesis. Mol. Plant **10**:866–877.

Xie, W., Zhou, P., Qu, M., Dai, Z., Zhang, X., Zhang, C., Dong, X., Sun, G., and Sun, X. (2020). Ginsenoside Re attenuates high glucose-induced RF/6A injury via regulating PI3K/AKT inhibited HIF-1alpha/VEGF signaling pathway. Front. Pharmacol. **11**:695.

Xiong, Y., Chen, L., Man, J., Hu, Y., and Cui, X. (2019). Chemical and bioactive comparison of *Panax notoginseng* root and rhizome in raw and steamed forms. J. Ginseng Res. **43**:385–393.

Xu, C., Wang, W., Wang, B., Zhang, T., Cui, X., Pu, Y., and Li, N. (2019). Analytical methods and biological activities of *Panax notoginseng* saponins: recent trends. J. Ethnopharmacol. **236**:443–465.

Yan, X., Fan, Y., Wei, W., Wang, P., Liu, Q., Wei, Y., Zhang, L., Zhao, G., Yue, J., and Zhou, Z. (2014). Production of bioactive ginsenoside compound K in metabolically engineered yeast. Cell Res. **24**:770–773.

Yu, L., Chen, Y., Shi, J., Wang, R., Yang, Y., Yang, L., Zhao, S., and Wang, Z. (2019). Biosynthesis of rare 20(R)-protopanaxadiol/protopanaxatriol type ginsenosides through *Escherichia coli* engineered with uridine diphosphate glycosyltransferase genes. J. Ginseng Res. **43**:116–124.

Zhang, B., Zhang, J., Zhang, C., Zhang, X., Ye, J., Kuang, S., Sun, G., and Sun, X. (2018). Notoginsenoside R1 protects against diabetic cardiomyopathy through activating estrogen receptor alpha and its downstream signaling. Front. Pharmacol. **9**:1227.

Zhang, B., Zhang, X., Zhang, C., Shen, Q., Sun, G., and Sun, X. (2019). Notoginsenoside R1 protects db/db mice against diabetic nephropathy via upregulation of Nrf2-mediated HO-1 expression. Molecules **24**:247.

Zhang, D., Li, W., Xia, E.-h., Zhang, Q.-j., Liu, Y., Zhang, Y., Tong, Y., Zhao, Y., Niu, Y.-c., Xu, J.-h., et al. (2017a). The medicinal herb *Panax notoginseng* genome provides insights into ginsenoside biosynthesis and genome evolution. Mol. Plant **10**:903–907.

Zhang, E.Y., Gao, B., Shi, H.L., Huang, L.F., Yang, L., Wu, X.J., and Wang, Z.T. (2017b). 20(S)-Protopanaxadiol enhances angiogenesis

via HIF-1alpha-mediated VEGF secretion by activating p70S6 kinase and benefits wound healing in genetically diabetic mice. Exp. Mol. Med. **49**:e387.

Zhang, Q.J., Li, W., Li, K., Nan, H., Shi, C., Zhang, Y., Dai, Z.Y., Lin, Y.L., Yang, X.L., Tong, Y., et al. (2020a). The chromosome-level reference genome of tea tree unveils recent bursts of non-autonomous LTR retrotransposons to drive genome size evolution. Mol. Plant **13**:935–938.

Zhang, S., Zhu, C., Lyu, Y., Chen, Y., Zhang, Z., Lai, Z., and Lin, Y. (2020b). Genome-wide identification, molecular evolution, and expression analysis provide new insights into the APETALA2/ethylene responsive factor (AP2/ERF) superfamily in *Dimocarpus longan* Lour. BMC Genomics **21**:62.

Zhao, Q., Yang, J., Cui, M.Y., Liu, J., Fang, Y., Yan, M., Qiu, W., Shang, H., Xu, Z., Yidiresi, R., et al. (2019). The reference genome sequence of *Scutellaria baicalensis* provides insights into the evolution of wogonin biosynthesis. Mol. Plant **12**:935–950.

Zhong, H., Wu, H., Bai, H., Wang, M., Wen, J., Gong, J., Miao, M., and Yuan, F. (2019). *Panax notoginseng* saponins promote liver regeneration through activation of the PI3K/AKT/mTOR cell proliferation pathway and upregulation of the AKT/Bad cell survival pathway in mice. BMC Comp. Altern. Med. **19**:122.

Plant Communications, Volume *2*

Supplemental Information

The chromosome-level reference genome assembly for *Panax notoginseng* and insights into ginsenoside biosynthesis

Zhouqian Jiang, Lichan Tu, Weifei Yang, Yifeng Zhang, Tianyuan Hu, Baowei Ma, Yun Lu, Xiuming Cui, Jie Gao, Xiaoyi Wu, Yuru Tong, Jiawei Zhou, Yadi Song, Yuan Liu, Nan Liu, Luqi Huang, and Wei Gao

Supporting Information Appendix

The Chromosome-level Reference genome Assembly for *Panax notoginseng* and Insights into Ginsenoside Biosynthesis

Zhouqian Jiang[1], Lichan Tu[1,2], Weifei Yang[3], Yifeng Zhang[1,2], Tianyuan Hu[1], Baowei Ma[1], Yun Lu[1], Xiuming Cui[4], Yuru Tong[2], Jie Gao[1], Xiaoyi Wu[1], Jiawei Zhou[1], Yadi Song[1], Yuan Liu[1], Nan Liu[1], Luqi Huang[5], Wei Gao[1,2,6*]

[1]School of Traditional Chinese Medicine, Capital Medical University, Beijing, China

[2]School of Pharmaceutical Sciences, Capital Medical University, Beijing, China

[3]Annoroad Gene Technology, Beijing, China

[4]Faculty of Life Science and Technology, Kunming University of Science and Technology, Kunming, China

[5]State Key Laboratory Breeding Base of Dao-di Herbs, National Resource Center for Chinese Materia Medica, China Academy of Chinese Medical Sciences, Beijing, China

[6]Advanced Innovation Center for Human Brain Protection, Capital Medical University, Beijing, China

*Corresponding Authors:

Wei Gao: weigao@ccmu.edu.cn

Luqi Huang: huangluqi01@126.com

Tel/Fax: 010-83916572

Table of contents

Supplementary Section S1 - Genome sequencing, assembly and evaluation

1.1 Plant materials

The *P. notoginseng* plant used for genome sequencing were collected from Wenshan County, Yunnan Province, China in August 2019. Fresh and healthy leaves were harvested and immediately frozen on liquid nitrogen after collection, followed by the preservation at -80℃ in the laboratory prior to DNA extraction.

1.2 Estimation of genome size using *K-mer* analysis

To estimation the genome size of *P. notoginseng* by using the *K-mer* analysis, we selected 231.06 Gb pair-end reads and generated the *21-mer* frequency distribution. The distribution of the *21-mer* depends on the characteristics of the genome and follows a Poisson's distribution. We estimated that the genome size was 1.67 Gb. Based on the *21-mer* analysis, we also estimated the heterozygosity ratio and the proportion of repeated sequences in the genome, which were 0.21% and 70.09% respectively (**Supplementary Table 1**). Considering that the higher repetitive sequence of the genome may lead to inaccurate *K-mer* analysis, we chose *K*=35 for a second prediction and finally the genome size was estimated to be 2.35Gb (**Supplementary Figure 1**).

1.3 Library construction and genome sequencing

High-quality genomic DNA was extracted from the leaves using a phenol chloroform isoamyl alcohol extraction method. The quality and quantity of the isolated DNA were separated checked by Nanophotometer® (IMPLEN, CA, USA) and Qubit® 2.0 Fluorometer (Life Technologies, CA, USA). Then the genomic DNA was broken into random fragments. DNA sequencing libraries were constructed according to the standard Illumina library preparation protocols. Paired-end library with insert size of 350 bp was constructed according to the manufacturer's instructions (Illumina, San Diego, CA). The constructed library was sequenced using Illumina HiSeq X Ten Platform by following the standard Illumina protocols. After filtering out the adapter sequences and the low-quality and duplicated reads, we obtained a total of 231.06

Gb(~86.86x) of clean data.

For PacBio libraries (English et al., 2012), we needed at least 10 μg of sheared DNA. The whole genome was sequenced on the PacBio Sequel System (**Supplementary URLs**) based on the single-molecular real-time (SMRT) sequencing technology. The template library was constructed using SMRTbell Template Prep Kit 1.0 (product code 100-259-100) and SMRTbell Damage Repair Kit (product code 100-465-900). Following the procedure described in the PacBio brochure, the high-quality DNA was fragmented and concentrated. The fragments were bead-purified, damage-repaired, and used as the ~20 kb SMRTbell templates. A total of 284.07 Gb (~106.79x) of data were obtained.

DNA from young leaves of the same *P. notoginseng* plant was used to constructed the Hi-C library. Grind the sample with 2% formaldehyde to fix the chromatin. After the cross-linking of the sample was completed, leaf cell lysis was performed and chromatin digestion was performed using *Mbol* endonucleases. After biotin labeling, blunt end linking and DNA purification, Hi-C sample was prepared and entered into the standard library construction process **(Supplementary Figure 2)**. After the constructed libraries were qualified by quality controlling, Illumina HiSeq X Ten was used for sequencing and the sequencing strategy used was PE150. Finally, a total of 340.83 Gb (~128.13x) data was retained **(Supplementary Table 2**).

1.4 Genome assembly

The reads exported by Sequel II™ Systems were quality evaluated with the in-built High-Quality Region Finder (HQRF) which identified the longest high quality regain each read generated by a singly-loaded DNA polymerase according to the ratio of signal to noise (Chakraborty et al., 2016; Hackl et al., 2014). The quality reads obtained were assembled into contigs using Canu (v1.5; **Supplementary URLs**) (Koren et al., 2017). The consensus genome was subjected to a final round of base-error correction (polish) by referring to the Ilumina reads with BWA (v0.7.9a) and Pilon (v1.22; **Supplementary URLs**) (BJ et al., 2014). The total length of this assembly version was 2.66 Gb with a contig N50 size of 1.21 Mb. Then, the Hi-C sequencing data were aligned to the

assembled scaffold by BWA-mem and the contigs were clustered onto chromosomes with LACHESIS (**Supplementary URLs**; **Supplementary Table 3**), the final genome was 2.66 Gb and the contig and scaffold N50 were 1.12 Mb and 216.47 Mb respectively (**Table 1 and Supplementary Table 4**).

1.5 Evaluation of assembly quality

We applied three methods to evaluate the quality of our assembled genome. First, we mapped clean reads from Illumina PE libraries to the genome using BWA mem. The distribution of the sequencing depth at each position was calculated using SAMtools. Nearly 99.82% of the clean reads could be mapped to the assembly genome, which covered 97.97% of the assembled sequence (**Supplementary Table 5**). Second, the completeness of the genome was evaluated with BUSCO (Benchmarking Universal Single-Copy Orthologs, v3.0.1, default parameters; **Supplementary URLs**) (Simao et al., 2015) based on the homologous database. We found 96.6% complete BUSCOs in the *P. notoginseng* genome (**Supplementary Table 6**). Third, the RNA sequencing (RNA-seq) reads of *P. notoginseng* generated in this study were assembled using Trinity, and these samples came from different tissue of different parts of *P. notoginseng* plants. According to the mapping rate (mostly ranging from 94%~97%) of each sample, the assembly had good coverage of the gene regions. Collectively, BUSCO, short-insert size read mapping and transcriptome analysis proved the high quality of the genome assembly, which was adequate enough for subsequent genome analyses in this study.

Supplementary Section S2 - Genome Annotation

2.1 Annotation of repeat sequences

Repetitive sequences are an important part of the genome including two categories, tandem repeat and interspersed repeats. In this study, two strategies were used to predict the repetitive sequences, which were *de novo* approach and homology approach respectively. For the *de novo* approach, RepeatModeler (**Supplementary URLs**) was used in this strategy. *De novo* repeat sequence library was established firstly, and then repeat sequences were predicted by repeatmasker software RepeatScout (**Supplementary URLs**). In addition, the *ab* initio prediction method was also used to find tandem repeat sequences in the genome by the software Tandem Repeats Finder (TRF). For the homology-based approach, it was based on repeated sequence database Repdase. RepeatMasker (version 3.3.0; **Supplementary URLs**) and RepeatProteinMask used to predict sequences similar to known repeat sequences (**Supplementary Table 7**). According to the integrated statistics of the prediction results obtained above, the proportion of repetitive sequences in the *P. notoginseng* genome was 85.85%. The most abundant repetitive element repeat type was LTR, which accounted for 58.88% of the genome (**Supplementary Figure 3 and Supplementary Table 8**).

2.2 Annotation of protein-coding genes

We used homology-based prediction, *de novo* prediction and transcriptome-based prediction to predict the protein-coding genes in the *P. notoginseng* genome. Proteins from the four known species (*Arabidopsis thaliana*, *Daucus carota*, *Panax ginseng*, *P. notoginseng*-pub) were used as homology evidence to search against *P. notoginseng* genome using tblastn (evalue 1e-5), and the gene structure were predicted by GeneWise with default parameter (**Supplementary URLs**; **Supplementary Figure 4**). For the *de novo* prediction, software based on the statistical characteristics of genomic sequence data (such as codon frequency, exon-intron distribution) was used to predict gene structure. The software used in this study contained Augustus, SNAP and GeneMark

(**Supplementary URLs**). To carry out the RNA-Seq aided gene prediction, clean RNA-Seq reads were assembled into transcripts using Trinity, then aligned to our genome assembly and predicted gene structure using PASA (**Supplementary URLs**). Synthesizing the above forecast results, the gene sets predicted by various strategies were integrated into a non-redundant and more complete gene set by EVidenceModeler (EVM; **Supplementary URLs**). Finally, a total of 37,606 genes were predicted from the *P. notoginseng* genome (**Supplementary Table 9**). By predicting the structure of the genes, we also obtained information of gene features such as the distributions of mRNA length, exon length, exon number, intron length and CDS length and so on (**Supplementary Table 10**).

2.3 Functional annotation protein-coding genes

The function annotation of genes is mainly to compare the predicted gene sets with various functional databases, so that can able to understand the function of genes and their role in life activities. The protein database used in this study included Swissprot, NT, NR, PFAM, eggNOG, and GO (**Supplementary URLs**). A total of 36,154 genes were predicted to be functional, accounting for 96.14% of all genes in the *P. notoginseng* genome (**Supplementary Table 11**).

2.4 Annotation of noncoding RNA genes

Noncoding RNA, refers to RNA that can't translate into proteins, such as rRNA, tRNA, snRNA, miRNA and so on, all have important biological functions. miRNA can degrade its target gene or inhibit translation into protein, and play an important role for gene silencing. tRNA and rRNA directly participate in protein synthesis. As well as, snRNA mainly involves in the processing of RNA precursors, which is the important component of RNA shear body. By comparing with known noncoding RNA libraries, Rfam, we can obtain the prediction of rRNA, snRNA, miRNA and so on. The tRNA sequences in genome were predicted by the software tRNAscan-SE (**Supplementary URLs**). Finally, we obtained 14,430 miRNA genes, 1513 tRNA genes, 3018 rRNA genes and 8174 snRNA genes in *P. notoginseng* genome (**Supplementary Table 12**).

Supplementary Section S3 - Evolution and cluster of gene family

3.1 Identification of gene families

Using the OrthoMCL package (Li et al., 2003) (version 1.4), we identified the gene families (clusters) between *P. notoginseng* and seven other plant species, including *P. ginseng*, *D. carota*, *V. vinifera*, *C. annuum*, *G. uralensis*, *A. thaliana*, *O. sativa*. First, the gene set of each species was filtered (**Supplementary Figure 5 and Supplementary Table 13**). If there were multiple alternative splicing transcripts for a gene, only the transcript with the longest coding region was retained for further analysis. Second, in order to ensure the reliability of the encoded protein, genes encoding length less than 50 amino acids were excluded. Then, an all-vs-all BLASTP (version 2.2.28) was performed with an E-value threshold of 1e-5. Finally, clustering was conducted using the Markov cluster algorithm (MCL) integrated in the OrthoMCL package. In total, 27,501 gene families comprising 232,394 genes were identified among these eight plant species and used for subsequent comparative analysis. According to the classification results of gene families, specific gene families within species and gene families shared between species could be found. A total of 1072 gene families containing 2879 genes unique to the *P. notoginseng* genome were found (**Supplementary Figure 6**). To functionally annotate these unique genes, we performed Gene Ontology (GO) and KEGG pathway enrichment analysis by using Fisher's exact test with false discovery rate (FDR) corrections (**Supplementary Figure 7 and Supplementary Table 14**).

3.2 Phylogenetic tree and divergence estimation

After gene family clustering, we aligned all 458 single-copy gene protein sequences by MUSCLE (**Supplementary URLs**) (Edgar, 2004). Then the four-fold degenerate synonymous site (4DTv) were employed to construct phylogenetic trees. PhyML software (Guindon et al., 2010) used the maximum likelihood method (Guindon and Gascuel, 2003) to construct the species phylogenetic tree (ML TREE). 4DTv of genes in each single-copy gene family are often used to estimate the substitution rate and the

divergence time between species. This analysis needed to be added to the phylogenetic tree of the species with the calibration time first (Benton and Donoghue, 2007; Blanc and Wolfe, 2004). According to the supergene sequence integrated in the phylogenetic analysis, the MCMCtree software (**Supplementary URLs**) in the PAML software package (Yang, 2007) was used to estimate the divergence time using the BRMC method (International Brachypodium, 2010; Sanderson, 2003). The MCMCtree running parameters were as follows: burn-in=20,000; sample-frequency=2. *O. sativa* was designated as an outgroup of the phylogenetic tree. The calibration times of the divergence between *O. sativa* and *A. thaliana* (130.7-160.6 MYA), *A. thaliana* and *G. uralensis* (124.3-132.1 MYA), *G. uralensis* and *V. vinifera* (117.8-127.5 MYA), *V. vinifera* and *C. annuum* (109.6-116.3 MYA), *D. carota* and *P. notoginseng* (48.3-70.1 MYA) were obtained from the TimeTree website (**Supplementary URLs**). The divergence time between *P. notoginseng* and *P. ginseng*, *C. annuum* and *D. carota* were estimated to be approximately 4.2 MYA and 91.6 MYA respectively (**Supplementary Figure 8A**).

3.3 Expansion and contraction of gene family

Based on the cluster analysis results of gene families and after filtering gene families with abnormal gene numbers in individual species, we used the CAFÉ program(De Bie et al., 2006) to identify the expansion and contraction of gene families of each species. A random birth and death model were used to study changes in gene families along each lineage of the phylogenetic tree. We used the probabilistic graphical model (PGM) to simulate the gain and loss of genes under the phylogenetic tree and conducted hypothesis testing to analyze the expansion and contraction of gene families. Using conditional likelihoods as the test statistics, we calculated the corresponding p-values in each lineage, and a p-value of 0.05 was used to identify families that were significantly expanded and contracted. Finally, we determined that 989 gene families were expanded and 1823 gene families were contracted (**Supplementary Figure 8B**). By conducting enrichment analysis of GO and KEGG on gene families, results showed that expanded gene families mainly enriched in GO terms such as transposition, fatty

281 acid biosynthetic process, respiratory chain, catalytic activity and so on
282 (**Supplementary Table 15**). Contracted gene families mainly enriched in GO terms
283 (**Supplementary Table 16**) such as protein phosphorylation, protein modification
284 process, beta-glucan biosynthetic process, 1,3-beta-D-glucan synthase complex, purine
285 nucleotide binding and so on (**Supplementary Figure 9**).
286

Supplementary Section S4 - Analysis of whole-genome duplication

4.1 Identification of WGD events of *P. notoginseng*

To further explore the evolution of the *P. notoginseng* genome, we searched for whole genome duplication (WGD) in our assembled *P. notoginseng* genome. WGD events are widespread in the plant genome and are considered to be an important driving force for the evolution of plant genomes. The protein sequences from *P. notoginseng*, *V. vinifera* and *D. carota* were searched against themselves using blastp ($E<1e^{-5}$) to identify syntenic blocks. Then the alignment results were subjected to McscanX (Huang et al., 2009; Schmutz et al., 2010) to determine syntenic blocks. In addition, the protein sequences from *P. notoginseng* were compared with *V. vinifera*, *D. carota* and *P. ginseng*. We calculated the 4DTv (fourfold degenerate synonymous sites of the third codons) for syntenic segments from the concatenated alignments constructed by fourfold degenerate sites of all gene pairs found in each segment and plotted the distribution of the 4DTv values (**Figure 2B**). There were two peaks at approximately 0.16 and 0.50 found in the *P. notoginseng* genome, and the first peak at approximately 0.50 revealed the core eudicot gamma triplication event. The second peak at approximately 0.16 indicated that *P. notoginseng* underwent another WGD event after diverging from *V. vinifera* and *D. carota*.

To verify the above conjecture, we conducted a collinear comparison analysis of the *P. notoginseng* and *V. vinifera* genome. Jcvi was used for identify syntenic blocks and plotted their relationship (**Figure 2C and Supplementary Figure 10**). From the results, we could find that there was a 1:2 collinear relationship between *P. notoginseng* and *V. vinifera* genome (**Supplementary Figure 10**).

4.2 Estimate the timing of the WGD event in *P. notoginseng*

To estimate the timing of the WGD event in *P. notoginseng*, we calculated the *Ks* (synonymous substitution rate) value of the gene pair within and between species using the default parameters of the software wgd (Zwaenepoel and Van de Peer, 2019), and then summed the results and the distribution of the *Ks* values was plotted

(**Supplementary Figure 12**). The results of the *Ks* distribution were consistent with the 4DTv values, and showed a main peak at approximately 0.38, which indicated that a recent WGD event occurred in the *P. notoginseng* genome. Then we calculated the time of WGD event of *P. notoginseng* according to the method reported in the literature (Qin et al., 2014), and summarized the WGD events of each published genome for centralized display (Iorizzo et al., 2016; Tu et al., 2020; Vanneste et al., 2014). The WGD event occurred approximately 29.6 MYA in *P. notoginseng* genome.

Supplementary Section S5 - Analysis of genes related to terpenes biosynthesis pathway

5.1 Identification and phylogenetic analysis of genes

The biosynthesis pathways of terpenoids in plants have been comprehensively explained, and research on *Panax* L. plants has attracted extensive interest from researchers. To identify the terpenoid biosynthesis-related genes in the *P. notoginseng* genome, we used two methods to analyze the genes in 8 species. For genes with corresponding domains in Pfam database such as *CYP450*, *DXR*, *DXS*, *HDR*, *HDS*, *HMGR*, *HMGS*, *MCS*, *MCT*, *MDD*, *PMK*, *SE*, *SS*, *UGT*, we used HMMER (3.1b1) to annotation and searched for each species to obtain copies of genes in different species. For genes where the corresponding domain in the Pfam database was not found, such as *AACT*, *CMK*, *DS*, *FPS*, *GGPPS*, *GPS*, *IPI*, *MVK*, we first downloaded the homologous sequences of genes in different species from NCBI and then compared the sequences by blast (2.2.28) (setting parameter: e value: $1e^{-5}$, coveraged > 50%, identity > 50%; **Supplementary URLs**) to obtain gene copies (**Supplementary Table 17**). After obtaining the gene sequences, we constructed the phylogenetic tree with each gene using the protein sequences in 8 species using MEGA-X (**Supplementary Figure 13-14**), the genetic relationship among the three species *P. notoginseng*, *P. ginseng* and *D. carota* was relatively close.

5.2 Analysis of the duplication of homologous gene pairs

After counting the genes in the terpenoid biosynthetic pathway, we found that most of the genes had multiple copies, so we analyzed the replication time of these multicopy gene pairs. We used the default parameter of wgd software to calculate the Ka value and Ks value of gene pairs, and then converted the Ks value to years (**Supplementary Table 18**). Finally, the results were presented in the form of pictures using Adobe Illustrator (**Supplementary Figure 15**).

Supplementary Section S6 - Transcriptomic analysis and transcription factor regulation

6.1 Sample collections and RNA isolation of tissue transcriptome

One- to four-year-old *P. notoginseng* plants were collected from Wenshan County, Yunnan Province, China. After harvested, we subdivided the plant into different tissue parts, including root (xylem), stem, leaf, flower, rhizome, fibril, periderm, phloem and tubercle (**Supplementary Figure 16-17**). All collected samples were transported by dry ice, washed with ultrapure water three times, immediately frozen on liquid nitrogen and stored at -80 °C prior to RNA extraction. Total RNA for each tissue was extracted using Trizol method. Generally, three biological replicates from each tissue were collected.

6.2 RNA sequencing and assembly

The RNA purity was checked using the kaiaoK5500®Spectrophotometer (Kaiao, Beijing, China) and the RNA integrity and concentration was assessed using the RNA Nano 6000 Assay Kit of the Bioanalyzer 2100 system (Agilent Technologies, CA, USA). Then, the integrate RNA was used in cDNA library construction and Illumina sequencing. The cDNA library was constructed using the NEBNext Ultra RNA Library Prep Kit for Illumina (NEB), following the manufacturer's recommendations. After cluster generation, the libraries were sequenced on an Illumina novaseq S2 platform and 150 bp paired-end reads were generated.

In order to guarantee the data quality which was used to analysis, Raw data was filter (**Supplementary Table 19**) with following steps: trim primer sequence from the reads; remove the contaminated reads for adapters; remove the low quality reads; remove the reads whose N base more than 5% for total bases. Bowtie2 v2.2.3 was used for building the genome index, and Clean Data was then aligned to the reference genome using HISAT2 v2.1.0 (**Supplementary Figure 18-19**). The filtered sequences were mapped on the *P. notoginseng* genome and the mapping rate ranged from 90%-96%, indicating a high quality of our genome.

6.3 Transcriptome analysis

ASprofile software was used to analyze and count the alternative splicing events of each sample in this study and rMats to classify and count the alternative splicing events in different groups (**Supplementary Figure 20 and Supplementary Table 20**). We also used Cuffcompare to detect new transcription and discovered some new unknown genes and laid the foundation for a more comprehensive analysis of transcript information. SNP and InDel were detected by Samtools (**Supplementary Figure 21 and Supplementary Table 21**).

Reads Count for each gene in each sample was counted by HTSeq v0.6.0, and FPKM (Fragments Per Kilobase Million Mapped Reads) was then calculated (**Supplementary Figure 22 and 23**). To explore the gene-level regulation of the formation of the root morphological characteristics, we conducted a comparative analysis between the different root groups to screen for differentially expressed genes (DEGs). DESeq2 was employed for differential gene expression analysis between two samples with biological replicates. Genes with $q \leq 0.05$ and $|\log2\_ratio| \geq 1$ were identified as DEGs. The GO and KEGG enrichment of differentially expressed genes were performed and considered to be significantly enriched with $q < 0.05$. After screening the DEGs between the periderm group and tubercle group, and GO enrichment analysis results showed that DEGs, which were highly expressed in tubercle group, were mainly enriched in secondary root formation, terpene catabolic process, shoot axis formation, strigolactone biosynthetic process (**Supplementary Figure 24**), etc. By annotating these DEGs, we found a series of genes related to the biosynthesis of phytohormone (**Supplementary Table 22**), such as the carotenoid cleavage dioxygenase 7 (CCD7) and CCD8 genes involved in the biosynthesis of strigolactone, hydroxylase and dehydrogenase genes related to cytokinin, expansin related genes, etc.

6.4 Analysis of saponin biosynthesis and regulation mechanism

Through comparison with the PlnatTFDB database, we identified a total of 2150 transcription factor genes from the *P. notoginseng* genome, which were classified into 57 subfamilies. Among these subfamilies, bHLH transcription factor, ERF transcription

factor, NAC transcription factor, MYB transcription factor, C2H2 transcription factor, MYB-related transcription factor contained a large number of gene copies (**Supplementary Table 23**). To investigate the role of transcription factors in terpenoid biosynthesis pathway, we studied the correlation between transcription factors and key enzyme genes. We first used R to calculate the Pearson correlation coefficient between transcription factors and genes in batches (set a significant correlation parameter $p<0.05$). Then, we selected the strong correlation gene pair whose correlation coefficient is greater than 0.7 and used Cytoscape software to draw the correlation map (**Figure 2D**). From the correlation map, several subfamilies had a strong correlation include bHLH transcription factor, ERF transcription factor, MYB transcription factor, WRKY transcription factor, indicating that these genes may participate in terpenoid biosynthesis process by regulating the expression of key enzyme genes. In addition, we also studied the temporal (**Figure 3**) and spatial (**Supplementary Figure 25**) expression profiles of saponin pathway genes during the growth and development of *P. notoginseng*, with a view to more fully revealing the production and development of saponins in *P. notoginseng* plants.

Supplementary Section S7 - Analyzing key enzyme genes of ginsenosides pathway and functional verification of UGT genes

7.1 Phylogenetic analysis of UGT and CYP450 genes

By comparison with the Pfam database, we identified 336 CYP450 genes and 158 UGT genes from the *P. notoginseng* genome. Then we downloaded the gene sequences of each subfamily from NCBI (**Supplementary Table 25-26**), used MEGA-X software to construct the phylogenetic tree, and modified the evolution trees on the online website iTOL (**Supplementary Figure 26 and Figure 3A**) (Letunic and Bork, 2019).

7.2 Function verification of candidate UGT genes

7.2.1 Gene cloning and expression vector construction

After sampling, *P. notoginseng* plants were frozen immediately in liquid nitrogen and

ground into powder for isolation of total RNA using Trizol (Invitrogen, Carlsbad, CA, USA) as the manufacture's instruction and then converted into cDNA using PrimeScript® RT reagent Kit with gDNA eraser (Takara, Dalian, China). Among the gene sequences obtained through systematic evolution and homologous alignment, we designed primers and cloned 32 open reading frames of UGT genes (**Supplementary Figure 27 and Supplementary Table 27**), the cloned open reading frames (ORFs) of UGT genes were inserted into *pEASY*®-Blunt Cloning Vector (TransGen Biotech, Beijing, China) independently. After the cloned gene was sequenced successfully, we connected them to the expression vector HIS-MBP-PreSc-pET28a (Li et al., 2018b) using Seamless Cloning Kit (Beyotime, Shanghai, China) as the manufacture's instruction.

7.2.2 Induced protein expression and functional verification

After successful construction, the expression vector was transformed into *E. coli* BL21 (DE3) (Transgen Biotech, Beijing, Chain), and the recombinant *E. coli* BL21 (DE3) strain was cultured in LB medium (with 50μg/mL kanamycin) at 37 ℃ at 200 rpm until the OD_{600} reached 0.6-0.8. Cool the bacterial solution on ice and add IPTG to a final concentration of 50 μM. After incubation at 16 ℃ at 120 rpm for 16h, the cells were harvested by centrifugation at 4 ℃ and suspended in 100 mM phosphate buffer (pH 8.0), 1mM PMSF. The resuspension solution was disrupted by ultrasonication and the mixture was centrifuged at 4 ℃ at 12000 *g* for 20 min, so that protein and cell debris were successfully separated. The supernatant was used for enzymatic assays. The pET28a-transformed *E. coli* BL21 (DE3) cells were treated in parallel as a control. Next, we checked whether the vectors expressed protein by SDS-PAGE protein electrophoresis, and used the crude enzyme to carry out the enzymatic reaction of glycosylation. Generally, the reaction was carried out in a 100 μL volume containing 100 mM crude enzyme buffer (pH 8.0), 1mM UDP-glucose, 0.1 mM acceptor substrate for 2h in a 35 ℃ water bath and was terminated by adding 100 μL methanol. At first, we used PPD and PPT as substrates and then use monoglucosides such as Rh_2, F_1 as substrates to verify whether UGT genes have catalytic functions. The mixed solution

was allowed to stand overnight at 4 ℃. The extraction was passed through a 0.22 μM organic filter membrane, and the resulting solution was tested by UPLC/Q-TOF-MS (ultrahigh-performance liquid chromatography coupled with quadrupole time-of-flight mass spectrometry) (**Supplementary Figure 28-31**). The following Q-TOF-MS parameters were used: the experiment was performed in the ESI (-) ionization mode; scan range, 50-1500 Da; scan time, 0.2 s; cone voltage, 40 V; source temperature, 100 ℃; dissolved gas temperature, 450 ℃; cone gas flow rate, 50 L/h; desolvation flow rate, 900 L/h; collision energy, 20-50V. The mass accuracy was corrected by a lock spray with leucine enkephalin (200 pg/μL, 10 μL/min) as the reference (m/z 556.2766 ESI (+) and 554.2620 ESI (–)).

The UPLC separation was performed using an Agilent Technologies 1290 Infinity II system (Agilent Technologies, Santa Clara, CA, USA) with a Waters ACQUITY UPLC HSS T3 analytical column (2.1 mm x 100 mm, 1.8 μm) kept at 35 ℃. The mobile phases were a mixture of 0.1% (v/v) acetic acid in water (A) and acetonitrile (B), and the flow rate was 0.3 mL/min. The gradient elution was programmed as follows: 0–2.0 min, 20–28% B; 2.0–3.0 min, 28–36% B; 3.0–10.0 min, 36–40% B; 10.0–15.0 min, 40–64% B; 15.0–17.0 min, 64–90% B; 17.0–22.0 min, 90–20% B. The injection volume was 1 μL for each sample.

7.3 Screen for candidate UGT genes involved in the saponin biosynthetic pathway

7.3.1 WGCNA analysis of UGT genes

We used the WGCNA software package in the R to perform the analysis on the genes annotated as glucosyltransferases or glycosyltransferases and saponins pathway genes in *P. notoginseng* genome (**Supplementary Figure 33**). First of all, we sorted and filtered the genes expression data, genes with a variance of 0 in the expression between different samples were filtered out. In addition, genes with a gene expression level of 0 that exceeded 10% of the total number of samples were also filtered out. Based on the filtered data, the hierarchical clustering was used to draw the sample tree, and the relationship between different samples could be seen from the dendrogram. Then we used the pickSoftThreshold function to calculate the soft threshold (β value). From the

result graph, we can see that when β value was 10, the correlation threshold was the highest. Finally, we used the function blockwiseModules to construct the modules present in these UGT genes, and obtained a total of 7 different modules **(Supplementary Table 28)**. In addition, the genes in the saponin biosynthesis pathway were mainly concentrated in the four modules: green, turquoise, red and brown.

7.3.2 Identification and expression profiling of genes related to terpenoids biosynthesis

Through the transcriptome data, we obtained the expression levels of the genes related to terpenoid biosynthesis in each group of samples, and used MEV software to draw the heat maps (**Supplementary Figure 34**). According to their expression patterns in different samples, these genes could be divided into three categories: most genes were highly expressed in flowers; some gens were highly expressed in various parts of roots; only a small part of genes were highly expressed in leaves. On this basis, we also screened a series of candidate UGT genes by comparing the expression patterns of pathway genes and annotated UGT genes **(Supplementary Figure 35 and Supplementary Table 29)**.

Supplementary URLs

PacBio Sequel System: https://www.pacb.com/products-and-services/pacbio-systems/sequel/

Canu: https://github.com/marbl/canu

Blasr: https://github.com/ PacificBiosciences/blasr

Smrt Link: https://downloads.pacbcloud.com/public/software/installers/smrtlink_5.0.1.9585.zip

Pilon: https://github.com/broadinstitute/pilon

LACHESIS: http://shendurelab.github.io/LACHESIS/

BUSCO: http://busco.ezlab.org/

RepeatModeler: http://www.repeatmasker.org/RepeatModeler/

RepeatScout: http://www.repeatmasker.org/

RepBase: https://www.girinst.org/server/RepBase/index.php

RepeatMasker: http://www.repeatmasker.org/

RepeatProteinMask: http://www.repeatmasker.org/

Blast: http://blast.ncbi.nlm.nih.gov/Blast.cgi

Genewise: http://www.ebi.ac.uk/~birney/wise2

Augustus: http://augustus.gobics.de/

SNAP: https://github.com/KorfLab/SNAP

GeneMark: http://exon.gatech.edu/GeneMark/

PASA: http://pasa.sourceforge.net/

EVidenceModeler: http://evidencemodeler.github.io/

Swissprot: https://web.expay.org/docs/swiss-prot_guideline.html

NT: https://www.ncbi.nlm.nih.gov/nucleotide/

NR: ftp://ftp.ncbi.nlm.nih.gov/blast/db/FASTA/nr.gz

PFAM: http://xfam.org/

eggNOG: http://eggnogdb.embl.de/

GO: http://geneontology.org/page/go-database

KEGG: http://www.kegg.jp/

Rfam: http://rfam.xfam.org/

552 tRNAsacn-SE: http://lowelab.ucsc.edu/tRNAscan-SE/

553 Mummer 4.0: https://github.com/mummer4/mummer

554 MUSCLE: http://www.drive5.com/muscle/

555 ENSEMBL database: http://www.ensembl.org/index.html

556 PlantTFDB: planttfdb.cbi.pku.edu.cn/ iTOL: https://itol.embl.de/itol.cgi

557 MCMCtree: http://abacus.gene.ucl.ac.uk/software/paml.html

558 TimeTree: http://www.time.org/

559

References

Aoki, K., Yano, K., Suzuki, A., Kawamura, S., Sakurai, N., Suda, K., Kurabayashi, A., Suzuki, T., Tsugane, T., Watanabe, M., et al. (2010). Large-scale analysis of full-length cDNAs from the tomato (*Solanum lycopersicum*) cultivar Micro-Tom, a reference system for the Solanaceae genomics. BMC GENOMICS 11:210.

Augustin, M.M., Ruzicka, D.R., Shukla, A.K., Augustin, J.M., Starks, C.M., O'Neil-Johnson, M., McKain, M.R., Evans, B.S., Barrett, M.D., Smithson, A., et al. (2015). Elucidating steroid alkaloid biosynthesis in *Veratrum californicum*: production of verazine in Sf9 cells. Plant J 82:991-1003.

Bak, S., Kahn, R., Nielsen, H., Moller, B., and Halkier, B. (1998). Cloning of three A-type cytochromes p450, CYP71E1, CYP98, and CYP99 from *Sorghum bicolor* (L.) Moench by a PCR approach and identification by expression in *Escherichia coli* of CYP71E1 as a multifunctional cytochrome p450 in the biosynthesis of the cyanogenic glucoside dhurrin. Plant Mol Biol 36:393-405.

Benton, M.J., and Donoghue, P.C. (2007). Paleontological evidence to date the tree of life. Mol Biol Evol 24:26-53.

BJ, W., T, A., T, S., M, P., A, A., S, S., A., C.C., Zeng, Q., Wortman, J., Young, S.K., et al. (2014). Pilon: An Integrated Tool for Comprehensive Microbial Variant Detection and Genome Assembly Improvement. PLoS ONE 9:e112963.

Blanc, G., and Wolfe, K.H. (2004). Widespread paleopolyploidy in model plant species inferred from age distributions of duplicate genes. Plant Cell 16:1667-1678.

Brazier-Hicks, M., and Edwards, R. (2005). Functional importance of the family 1 glucosyltransferase UGT72B1 in the metabolism of xenobiotics in Arabidopsis thaliana. Plant J 42:556-566.

Chakraborty, M., Baldwin-Brown, J.G., Long, A.D., and Emerson, J.J. (2016). Contiguous and accurate *de novo* assembly of metazoan genomes with modest long read coverage. Nucleic Acids Res 44:e147.

Chen, B., Chen, J., Du, Q., Zhou, D., Wang, L., Xie, J., Li, Y., and Zhang, D. (2018). Genetic variants in microRNA biogenesis genes as novel indicators for secondary growth in Populus. New Phytol 219:1263-1282.

Chen, H., Wu, B., Nelson, D.R., Wu, K., and Liu, C. (2014). Computational Identification and Systematic Classification of Novel Cytochrome P450 Genes in *Salvia miltiorrhiza*. PLOS ONE 9:e115149.

Chen, H.Y., and Li, X. (2017). Identification of a residue responsible for UDP-sugar donor selectivity of a dihydroxybenzoic acid glycosyltransferase from Arabidopsis natural accessions. Plant J 89:195-203.

Courtney, K.J., Percival, F.W., Hallaban, D.L., Christoffersen, R.E., and Hallahan, D.L. (1996). The Electronic Plant Gene Register. Plant Physiol 112:445-446.

De Bie, T., Cristianini, N., Demuth, J.P., and Hahn, M.W. (2006). CAFE: a computational tool for the study of gene family evolution. Bioinformatics 22:1269-1271.

Edgar, R.C. (2004). MUSCLE: multiple sequence alignment with high accuracy and high throughput. Nucleic Acids Res 32:1792-1797.

Eljounaidi, K., Cankar, K., Comino, C., Moglia, A., Hehn, A., Bourgaud, F.,

Bouwmeester, H., Menin, B., Lanteri, S., and Beekwilder, J. (2014). Cytochrome P450s from Cynara cardunculus L. CYP71AV9 and CYP71BL5, catalyze distinct hydroxylations in the sesquiterpene lactone biosynthetic pathway. Plant Science 223:59-68.

English, A.C., Richards, S., Han, Y., Wang, M., Vee, V., Qu, J., Qin, X., Muzny, D.M., Reid, J.G., Worley, K.C., et al. (2012). Mind the gap: upgrading genomes with Pacific Biosciences RS long-read sequencing technology. PLoS One 7:e47768.

Feng, Q., Zhang, Y., Hao, P., Wang, S., Fu, G., Huang, Y., Li, Y., Zhu, J., Liu, Y., Hu, X., et al. (2002). Sequence and analysis of rice chromosome 4. Nature 420:316-320.

Fukushima, E.O., Seki, H., Ohyama, K., Ono, E., Umemoto, N., Mizutani, M., Saito, K., and Muranaka, T. (2011). CYP716A Subfamily Members are Multifunctional Oxidases in Triterpenoid Biosynthesis. Plant Cell Physiol 52:2050-2061.

Guindon, S., Dufayard, J.F., Lefort, V., Anisimova, M., Hordijk, W., and Gascuel, O. (2010). New algorithms and methods to estimate maximum-likelihood phylogenies: assessing the performance of PhyML 3.0. Syst Biol 59:307-321.

Guindon, S., and Gascuel, O. (2003). A simple, fast, and accurate algorithm to estimate large phylogenies by maximum likelihood. Syst Biol 52:696-704.

Guo, J., Ma, X., Cai, Y., Ma, Y., Zhan, Z., Zhou, Y.J., Liu, W., Guan, M., Yang, J., Cui, G., et al. (2016a). Cytochrome P450 promiscuity leads to a bifurcating biosynthetic pathway for tanshinones. New Phytol 210:525-534.

Guo, J., Zhou, Y.J., Hillwig, M.L., Shen, Y., Yang, L., Wang, Y., Zhang, X., Liu, W., Peters, R.J., Chen, X., et al. (2013). CYP76AH1 catalyzes turnover of miltiradiene in tanshinones biosynthesis and enables heterologous production of ferruginol in yeasts. Proc Natl Acad Sci U S A 110:12108-12113.

Guo, L., Yang, R., and Gu, Z. (2016b). Cloning of genes related to aliphatic glucosinolate metabolism and the mechanism of sulforaphane accumulation in broccoli sprouts under jasmonic acid treatment. J Sci Food Agr 96:4329-4336.

Hackl, T., Hedrich, R., Schultz, J., and Forster, F. (2014). proovread: large-scale high-accuracy PacBio correction through iterative short read consensus. Bioinformatics 30:3004-3011.

Han, J.Y., Hwang, H.S., Choi, S.W., Kim, H.J., and Choi, Y.E. (2012). Cytochrome P450 CYP716A53v2 catalyzes the formation of protopanaxatriol from protopanaxadiol during ginsenoside biosynthesis in *Panax ginseng*. Plant Cell Physiol 53:1535-1545.

Han, J.Y., Kim, H.J., Kwon, Y.S., and Choi, Y.E. (2011). The Cyt P450 enzyme CYP716A47 catalyzes the formation of protopanaxadiol from dammarenediol-II during ginsenoside biosynthesis in *Panax ginseng*. Plant Cell Physiol 52:2062-2073.

Hansen, E., Osmani, S., Kristensen, C., Moller, B., and Hansen, J. (2009). Substrate specificities of family 1 UGTs gained by domain swapping. Phytochemistry 70:473-482.

Hou, B., Lim, E., Higgins, G., and Bowles, D.J. (2004). N-glucosylation of cytokinins

by glycosyltransferases of Arabidopsis thaliana. J Biol Chem 279:47822-47832.
Hu, T.T., Pattyn, P., Bakker, E.G., Cao, J., Cheng, J.F., Clark, R.M., Fahlgren, N., Fawcett, J.A., Grimwood, J., Gundlach, H., et al. (2011). The *Arabidopsis lyrata* genome sequence and the basis of rapid genome size change. Nat Genet 43:476-481.
Huang, L., Li, J., Ye, H., Li, C., Wang, H., Liu, B., and Zhang, Y. (2012). Molecular characterization of the pentacyclic triterpenoid biosynthetic pathway in *Catharanthus roseus*. Planta 236:1571-1581.
Huang, S., Li, R., Zhang, Z., Li, L., Gu, X., Fan, W., Lucas, W.J., Wang, X., Xie, B., Ni, P., et al. (2009). The genome of the cucumber, *Cucumis sativus* L. Nature Genetics 41:1275-1281.
International Brachypodium, I. (2010). Genome sequencing and analysis of the model grass *Brachypodium distachyon*. Nature 463:763-768.
International Rice Genome Sequencing, P. (2005). The map-based sequence of the rice genome. Nature 436:793-800.
Iorizzo, M., Ellison, S., Senalik, D., Zeng, P., Satapoomin, P., Huang, J., Bowman, M., Iovene, M., Sanseverino, W., Cavagnaro, P., et al. (2016). A high-quality carrot genome assembly provides new insights into carotenoid accumulation and asterid genome evolution. Nat Genet 48:657-666.
Jia, H.M., Jia, H.J., Cai, Q.L., Wang, Y., Zhao, H.B., Yang, W.F., Wang, G.Y., Li, Y.H., Zhan, D.L., Shen, Y.T., et al. (2019). The red bayberry genome and genetic basis of sex determination. Plant Biotechnol J 17:397-409.
Jones, P., Messner, B., Nakajima, J.-I., Schäffner, A.R., and Saito, K. (2003). UGT73C6 and UGT78D1, Glycosyltransferases Involved in Flavonol Glycoside Biosynthesis in *Arabidopsis thaliana*. J Biol Chem 278:43910-43918.
Jung, S.-C., Kim, W., Park, S.C., Jeong, J., Park, M.K., Lim, S., Lee, Y., Im, W.-T., Lee, J.H., Choi, G., et al. (2014). Two Ginseng UDP-Glycosyltransferases Synthesize Ginsenoside Rg3 and Rd. Plant Cell Physiol 55:2177-2188.
Kahn, R., Bak, S., Svendsen, I., Halkier, B., and Moller, B. (1997). Isolation and reconstitution of cytochrome P450ox and in vitro reconstitution of the entire biosynthetic pathway of the cyanogenic glucoside dhurrin from sorghum. Plant Physiol 115:1661-1670.
Kim, B.-G., Sung, S.H., and Ahn, J.-H. (2012). Biological synthesis of quercetin 3-O-N-acetylglucosamine conjugate using engineered *Escherichia coli* expressing UGT78D2. Appl Microbiol Biot 93:2447-2453.
Knoch, E., Sugawara, S., Mori, T., Nakabayashi, R., Saito, K., and Yonekura-Sakakibara, K. (2017). UGT79B31 is responsible for the final modification step of pollen-specific flavonoid biosynthesis in *Petunia hybrida*. Planta 247:779-790.
Koren, S., Walenz, B.P., Berlin, K., Miller, J.R., Bergman, N.H., and Phillippy, A.M. (2017). Canu: scalable and accurate long-read assembly via adaptive k-mer weighting and repeat separation. Genome Res 27:722-736.
Kovinich, N., Saleem, A., Arnason, J.T., and Miki, B. (2010). Functional characterization of a UDP-glucose:flavonoid 3-O-glucosyltransferase from the

692 seed coat of black soybean (*Glycine max* (L.) Merr.). Phytochemistry 71:1253-
693 1263.
694 KRAUS, P., and KUTCHAN, T. (1995). Molecular-cloning and heterologous
695 expression of a cdna-encoding berbamunine synthase, a c-o phenol-coupling
696 cytochrome-p450 from the higher-plant berberis-stolonifera. P Natl Acad Sci
697 USA 92:2071-2075.
698 Krokida, A., Delis, C., Geisler, K., Garagounis, C., Tsikou, D., Peña-Rodríguez, L.M.,
699 Katsarou, D., Field, B., Osbourn, A.E., and Papadopoulou, K.K. (2013). A
700 metabolic gene cluster in *Lotus japonicusd* iscloses novel enzyme functions and
701 products in triterpene biosynthesis. New Phytol 200:675-690.
702 Lanot, A., Hodge, D., Jackson, R.G., George, G.L., Elias, L., Lim, E.K., Vaistij, F.E.,
703 and Bowles, D.J. (2006). The glucosyltransferase UGT72E2 is responsible for
704 monolignol 4-O-glucoside production in *Arabidopsis thaliana*. Plant J 48:286-
705 295.
706 Lanot, A., Hodge, D., Lim, E.K., Vaistij, F.E., and Bowles, D.J. (2008). Redirection of
707 flux through the phenylpropanoid pathway by increased glucosylation of
708 soluble intermediates. Planta 228:609-616.
709 Letunic, I., and Bork, P. (2019). Interactive Tree Of Life (iTOL) v4: recent updates and
710 new developments. Nucleic Acids Res 47:W256-W259.
711 Li, L., Cheng, H., Gai, J., and Yu, D. (2007). Genome-wide identification and
712 characterization of putative cytochrome P450 genes in the model legume
713 *Medicago truncatula*. Planta 226:109-123.
714 Li, L., Stoeckert, C.J., Jr., and Roos, D.S. (2003). OrthoMCL: identification of ortholog
715 groups for eukaryotic genomes. Genome Res 13:2178-2189.
716 Li, Q., Yu, H.M., Meng, X.F., Lin, J.S., Li, Y.J., and Hou, B.K. (2018a). Ectopic
717 expression of glycosyltransferase UGT76E11 increases flavonoid accumulation
718 and enhances abiotic stress tolerance in Arabidopsis. Plant Biol (Stuttg) 20:10-
719 19.
720 Li, Q.S., Lin, X.M., Qiao, R.Y., Zheng, X.Q., Lu, J.L., Ye, J.H., and Liang, Y.R. (2017).
721 Effect of fluoride treatment on gene expression in tea plant (*Camellia sinensis*).
722 Sci Rep 7:9847.
723 Li, X.J., Chen, X.J., Guo, X., Yin, L.L., Ahammed, G.J., Xu, C.J., Chen, K.S., Liu, C.C.,
724 Xia, X.J., Shi, K., et al. (2016). DWARF overexpression induces alteration in
725 phytohormone homeostasis, development, architecture and carotenoid
726 accumulation in tomato. Plant Biotechnol J 14:1021-1033.
727 Li, Y., Lin, H.X., Wang, J., Yang, J., Lai, C.J., Wang, X., Ma, B.W., Tang, J.F., Li, Y.,
728 Li, X.L., et al. (2018b). Glucosyltransferase Capable of Catalyzing the Last Step
729 in Neoandrographolide Biosynthesis. Org Lett 20:5999-6002.
730 Lim, C.E., Ahn, J.-H., and Lim, J. (2006). Molecular genetic analysis of tandernly
731 located glycosyltransferase genes, UGT73B1, UGT73B2, and UGT73B3, in
732 Arabidopsis thaliana. J Plant Biol 49:309-314.
733 Lim, E., Higgins, G., Li, Y., and Bowles, D.J. (2003). Regioselectivity of glucosylation
734 of caffeic acid by a UDP-glucose : glucosyltransferase is maintained in planta.
735 Biochem J 373:987-992.

Lim, E.K., Jackson, R.G., and Bowles, D.J. (2005). Identification and characterisation of Arabidopsis glycosyltransferases capable of glucosylating coniferyl aldehyde and sinapyl aldehyde. FEBS Lett 579:2802-2806.

Lin, J.S., Huang, X.X., Li, Q., Cao, Y., Bao, Y., Meng, X.F., Li, Y.J., Fu, C., and Hou, B.K. (2016). UDP-glycosyltransferase 72B1 catalyzes the glucose conjugation of monolignols and is essential for the normal cell wall lignification in *Arabidopsis thaliana*. Plant J 88:26-42.

Lin, X., Kaul, S., Rounsley, S., Shea, T., Benito, M., Town, C., Fujii, C., Mason, T., Bowman, C., Barnstead, M., et al. (1999). Sequence and analysis of chromosome 2 of the plant *Arabidopsis thaliana*. Nature 402:761-+.

Liu, X., Liu, Y., Huang, P., Ma, Y., Qing, Z., Tang, Q., Cao, H., Cheng, P., Zheng, Y., Yuan, Z., et al. (2017). The Genome of Medicinal Plant *Macleaya cordata* Provides New Insights into Benzylisoquinoline Alkaloids Metabolism. Molecular Plant 10:975-989.

Mao, H., Liu, J., Ren, F., Peters, R.J., and Wang, Q. (2016). Characterization of CYP71Z18 indicates a role in maize zealexin biosynthesis. Phytochemistry 121:4-10.

Mayer, K., and Schuller, C., and Wambutt, R., and Murphy, G., and Volckaert, G., and Pohl, T., and Dusterhoft, A., and Stiekema, W., and Entian, K., and Terryn, N., et al. (1999). Sequence and analysis of chromosome 4 of the plant *Arabidopsis thaliana*. Nature 402:769-+.

Mazel, A., and Levine, A. (2002). Induction of glucosyltransferase transcription and activity during superoxide-dependent cell death in Arabidopsis plants. Plant Physiol Bioch 40:133-140.

Miettinen, K., Dong, L., Navrot, N., Schneider, T., Burlat, V., Pollier, J., Woittiez, L., van der Krol, S., Lugan, R., Ilc, T., et al. (2014). The seco-iridoid pathway from *Catharanthus roseus*. Nat Commun 5:3606.

Morant, M., Schoch, G.A., Ullmann, P., Ertunc, T., Little, D., Olsen, C.E., Petersen, M., Negrel, J., and Werck-Reichhart, D. (2007). Catalytic activity, duplication and evolution of the CYP98 cytochrome P450 family in wheat. Plant Mol Biol 63:1-19.

Moses, T., Pollier, J., Almagro, L., Buyst, D., Van Montagu, M., Pedreno, M.A., Martins, J.C., Thevelein, J.M., and Goossens, A. (2014). Combinatorial biosynthesis of sapogenins and saponins in *Saccharomyces cerevisiae* using a C-16 alpha hydroxylase from *Bupleurum falcatum*. Proc Natl Acad Sci U S A 111:1634-1639.

Motamayor, J.C., Mockaitis, K., Schmutz, J., Haiminen, N., Livingstone, D., III, Cornejo, O., Findley, S.D., Zheng, P., Utro, F., Royaert, S., et al. (2013). The genome sequence of the most widely cultivated cacao type and its use to identify candidate genes regulating pod color. GENOME BIOLOGY 14:r53.

Nomura, T., Kushiro, T., Yokota, T., Kamiya, Y., Bishop, G., and Yamaguchi, S. (2005). The last reaction producing brassinolide is catalyzed by cytochrome P-450s, CYP85A3 in tomato and CYP85A2 in Arabidopsis. J Biol Chem 280:17873-17879.

Ohnishi, T., Nomura, T., Watanabe, B., Ohta, D., Yokota, T., Miyagawa, H., Sakata, K., and Mizutani, M. (2006). Tomato cytochrome P450CYP734A7 functions in brassinosteroid catabolism. Phytochemistry 67:1895-1906.

Ono, E., Ruike, M., Iwashina, T., Nomoto, K., and Fukui, Y. (2010). Co-pigmentation and flavonoid glycosyltransferases in blue *Veronica persica* flowers. Phytochemistry 71:726-735.

Oudin, A., Hamdi, S.d., Ouélhazi, L., Chénieux, J.-C., Rideau, M., and Clastre, M. (1999). Induction of a novel cytochrome P450 (CYP96 family) in periwinkle (*Catharanthus roseus*) cells induced for terpenoid indole alkaloid production. Plant Science 149:105-113.

Overkamp, S., Hein, F., and Barz, W. (2000). Cloning and characterization of eight cytochrome P450 cDNAs from chickpea (*Cicer arietinum* L.) cell suspension cultures. Plant Science 155:101-108.

Pham, T., Chen, H., Dai, L., and Vu, T.Q.T. (2016). Isolation a P450 gene in *Pinus armandi* and its expression after inoculation of Leptographium qinlingensis and treatment with methyl jasmonate. Russ J Plant Physl+ 63:111-118.

Priest, D.M., Ambrose, S.J., Vaistij, F.E., Elias, L., Higgins, G.S., Ross, A.R., Abrams, S.R., and Bowles, D.J. (2006). Use of the glucosyltransferase UGT71B6 to disturb abscisic acid homeostasis in *Arabidopsis thaliana*. Plant J 46:492-502.

Qi, X., Bakht, S., Qin, B., Leggett, M., Hemmings, A., Mellon, F., Eagles, J., Werck-Reichhart, D., Schaller, H., Lesot, A., et al. (2006). A different function for a member of an ancient and highly conserved cytochrome P450 family: From essential sterols to plant defense. P Natl Acad Sci USA 103:18848-18853.

Qin, C., Yu, C., Shen, Y., Fang, X., Chen, L., Min, J., Cheng, J., Zhao, S., Xu, M., Luo, Y., et al. (2014). Whole-genome sequencing of cultivated and wild peppers provides insights into Capsicum domestication and specialization. Proc Natl Acad Sci U S A 111:5135-5140.

Ro, D., Arimura, G., Lau, S., Piers, E., and Bohlmann, J. (2005). Loblolly pine abietadienol/abietadienal oxidase PtAO (CYP720B1) is a multifunctional, multisubstrate cytochrome P450 monooxygenase. P Natl Acad Sci USA 102:8060-8065.

Roach, M.J., Johnson, D.L., Bohlmann, J., van Vuuren, H.J.J., Jones, S.J.M., Pretorius, I.S., Schmidt, S.A., and Borneman, A.R. (2018). Population sequencing reveals clonal diversity and ancestral inbreeding in the grapevine cultivar Chardonnay. PLoS Genet 14:e1007807.

Rojas Rodas, F., Rodriguez, T.O., Murai, Y., Iwashina, T., Sugawara, S., Suzuki, M., Nakabayashi, R., Yonekura-Sakakibara, K., Saito, K., Kitajima, J., et al. (2014). Linkage mapping, molecular cloning and functional analysis of soybean gene Fg2 encoding flavonol 3-O-glucoside (1 --> 6) rhamnosyltransferase. Plant Mol Biol 84:287-300.

Saito, S., Hirai, N., Matsumoto, C., Ohigashi, H., Ohta, D., Sakata, K., and Mizutani, M. (2004). Arabidopsis CYP707As encode (+)-abscisic acid 8'-hydroxylase, a key enzyme in the oxidative catabolism of abscisic acid. Plant Physiol 134:1439-1449.

Salanoubat, M., and Lemcke, K., and Rieger, M., and Ansorge, W., and Unseld, M., and Fartmann, B., and Valle, G., and Blocker, H., and Perez-Alonso, M., and Obermaier, B., et al. (2000). Sequence and analysis of chromosome 3 of the plant *Arabidopsis thaliana*. Nature 408:820-822.

Salim, V., Wiens, B., Masada-Atsumi, S., Yu, F., and De Luca, V. (2014). 7-Deoxyloganetic acid synthase catalyzes a key 3 step oxidation to form 7-deoxyloganetic acid in *Catharanthus roseus* iridoid biosynthesis. Phytochemistry 101:23-31.

Sanderson, M. (2003). r8s: inferring absolute rates of molecular evolution and divergence times in the absence of a molecular clock. Bioinformatics 19:301-302.

Schmutz, J., Cannon, S.B., Schlueter, J., Ma, J., Mitros, T., Nelson, W., Hyten, D.L., Song, Q., Thelen, J.J., Cheng, J., et al. (2010). Genome sequence of the palaeopolyploid soybean. Nature 463:178-183.

Schopfer, C., and Ebel, J. (1998). Identification of elicitor-induced cytochrome P450s of soybean (*Glycine max* L.) using differential display of mRNA. Molecular and general genetics 258:315-322.

Seki, H., Ohyama, K., Sawai, S., Mizutani, M., Ohnishi, T., Sudo, H., Akashi, T., Aoki, T., Saito, K., and Muranaka, T. (2008). Licorice beta-amyrin 11-oxidase, a cytochrome P450 with a key role in the biosynthesis of the triterpene sweetener glycyrrhizin. P Natl Acad Sci USA 105:14204-14209.

Seki, H., Sawai, S., Ohyama, K., Mizutani, M., Ohnishi, T., Sudo, H., Fukushima, E.O., Akashi, T., Aoki, T., Saito, K., et al. (2011). Triterpene functional genomics in licorice for identification of CYP72A154 involved in the biosynthesis of glycyrrhizin. Plant Cell 23:4112-4123.

Shaokang Di, F.Y., Felipe Rojas Rodas, Tito O Rodriguez, Yoshinori Murai, Tsukasa Iwashina, Satoko Sugawara, Tetsuya Mori, Ryo Nakabayashi, Keiko Yonekura-Sakakibara, Kazuki Saito, Ryoji Takahashi. (2015). Linkage mapping, molecular cloning and functional analysis of soybean gene Fg3 encoding flavonol 3-O-glucoside/galactoside (1 → 2) glucosyltransferase. BMC Plant Biol 15:126.

Shi, P., Fu, X., Shen, Q., Liu, M., Pan, Q., Tang, Y., Jiang, W., Lv, Z., Yan, T., Ma, Y., et al. (2018). The roles ofAaMIXTA1in regulating the initiation of glandular trichomes and cuticle biosynthesis in *Artemisia annua*. New Phytol 217:261-276.

Shibuya, M., Nishimura, K., Yasuyama, N., and Ebizuka, Y. (2010). Identification and characterization of glycosyltransferases involved in the biosynthesis of soyasaponin I in *Glycine max*. FEBS Lett 584:2258-2264.

Simao, F.A., Waterhouse, R.M., Ioannidis, P., Kriventseva, E.V., and Zdobnov, E.M. (2015). BUSCO: assessing genome assembly and annotation completeness with single-copy orthologs. Bioinformatics 31:3210-3212.

Steele, C., Gijzen, M., Qutob, D., and Dixon, R. (1999). Molecular characterization of the enzyme catalyzing the aryl migration reaction of isoflavonoid biosynthesis in soybean. Arch Biochem Biophys 367:146-150.

Stigliani, A.L., Giorio, G., and D'Ambrosio, C. (2011). Characterization of P450 Carotenoid β- and ε-Hydroxylases of Tomato and Transcriptional Regulation of Xanthophyll Biosynthesis in Root, Leaf, Petal and Fruit. Plant Cell Physiol 52:851-865.

Sun, Y., Chen, Z., Li, J., Li, J., Lv, H., Yang, J., Li, W., Xie, D., Xiong, Z., Zhang, P., et al. (2018). Diterpenoid UDP-Glycosyltransferases from Chinese Sweet Tea and Ashitaba Complete the Biosynthesis of Rubusoside. Mol Plant 11:1308-1311.

Sun, Y., Ji, K., Liang, B., Du, Y., Jiang, L., Wang, J., Kai, W., Zhang, Y., Zhai, X., Chen, P., et al. (2017). Suppressing ABA uridine diphosphate glucosyltransferase (SlUGT75C1) alters fruit ripening and the stress response in tomato. Plant J 91:574-589.

Tabata, S., and Kaneko, T., and Nakamura, Y., and Kotani, H., and Kato, T., and Asamizu, E., and Miyajima, N., and Sasamoto, S., and Kimura, T., and Hosouchi, T., et al. (2000). Sequence and analysis of chromosome 5 of the plant *Arabidopsis thaliana*. Nature 408:823-826.

Tamura, K., Seki, H., Suzuki, H., Kojoma, M., Saito, K., and Muranaka, T. (2016). CYP716A179 functions as a triterpene C-28 oxidase in tissue-cultured stolons of *Glycyrrhiza uralensis*. Plant Cell Rep 36:437-445.

Tamura, K., Teranishi, Y., Ueda, S., Suzuki, H., Kawano, N., Yoshimatsu, K., Saito, K., Kawahara, N., Muranaka, T., and Seki, H. (2017). Cytochrome P450 Monooxygenase CYP716A141 is a Unique beta-Amyrin C-16beta Oxidase Involved in Triterpenoid Saponin Biosynthesis in *Platycodon grandiflorus*. Plant Cell Physiol 58:874-884.

Tanaka, K., Hayashi, K.-i., Natsume, M., Kamiya, Y., Sakakibara, H., Kawaide, H., and Kasahara, H. (2014). UGT74D1 Catalyzes the Glucosylation of 2-Oxindole-3-Acetic Acid in the Auxin Metabolic Pathway in Arabidopsis. Plant Cell Physiol 55:218-228.

Theologis, A., Ecker, J., Palm, C., Federspiel, N., Kaul, S., White, O., Alonso, J., Altafi, H., Araujo, R., Bowman, C., et al. (2000). Sequence and analysis of chromosome 1 of the plant *Arabidopsis thaliana*. Nature 408:816-820.

Trikka, F.A., Nikolaidis, A., Ignea, C., Tsaballa, A., Tziveleka, L.-A., Ioannou, E., Roussis, V., Stea, E.A., Božić, D., Argiriou, A., et al. (2015). Combined metabolome and transcriptome profiling provides new insights into diterpene biosynthesis in *S. pomifera* glandular trichomes. BMC Genomics 16.

Tu, L., Su, P., Zhang, Z., Gao, L., Wang, J., Hu, T., Zhou, J., Zhang, Y., Zhao, Y., Liu, Y., et al. (2020). Genome of *Tripterygium wilfordii* and identification of cytochrome P450 involved in triptolide biosynthesis. Nat Commun 11:971.

Vanneste, K., Baele, G., Maere, S., and Van de Peer, Y. (2014). Analysis of 41 plant genomes supports a wave of successful genome duplications in association with the Cretaceous-Paleogene boundary. Genome Res 24:1334-1347.

Vasav, A.P., and Barvkar, V.T. (2019). Phylogenomic analysis of cytochrome P450 multigene family and their differential expression analysis in *Solanum lycopersicum* L. suggested tissue specific promoters. BMC Genomics 20:116.

Wang, P., Wei, Y., Fan, Y., Liu, Q., Wei, W., Yang, C., Zhang, L., Zhao, G., Yue, J., Yan,

X., et al. (2015). Production of bioactive ginsenosides Rh2 and Rg3 by metabolically engineered yeasts. Metab Eng 29:97-105.

Wang, S., Wang, R., Liu, T., Lv, C., Liang, J., Kang, C., Zhou, L., Guo, J., Cui, G., Zhang, Y., et al. (2019). CYP76B74 Catalyzes the 3 "-Hydroxylation of Geranylhydroquinone in Shikonin Biosynthesis. Plant Physiol 179:402-414.

Wei, W., Wang, P., Wei, Y., Liu, Q., Yang, C., Zhao, G., Yue, J., Yan, X., and Zhou, Z. (2015). Characterization of *Panax ginseng* UDP-Glycosyltransferases Catalyzing Protopanaxatriol and Biosyntheses of Bioactive Ginsenosides F1 and Rh1 in Metabolically Engineered Yeasts. Mol Plant 8:1412-1424.

Weng, J.-K., Li, Y., Mo, H., and Chapple, C. (2012). Assembly of an Evolutionarily New Pathway for alpha-Pyrone Biosynthesis in Arabidopsis. Science 337:960-964.

Wilson, A.E., Wu, S., and Tian, L. (2019). PgUGT95B2 preferentially metabolizes flavones/flavonols and has evolved independently from flavone/flavonol UGTs identified in *Arabidopsis thaliana*. Phytochemistry 157:184-193.

Witte, S., Moco, S., Vervoort, J., Matern, U., and Martens, S. (2009). Recombinant expression and functional characterisation of regiospecific flavonoid glucosyltransferases from *Hieracium pilosella* L. Planta 229:1135-1146.

Wolfgang Schweiger, J.B., Sanghyun Shin, Brigitte Poppenberger, Franz Berthiller, Marc Lemmens, Gary J Muehlbauer, Gerhard Adam. (2012). Validation of a Candidate Deoxynivalenol-Inactivating UDP-glucosyltransferase From Barley by Heterologous Expression in Yeast. Mol Plant Microbe In 23:977-986.

Xie, F., Xiao, P., Chen, D., Xu, L., and Zhang, B. (2012). miRDeepFinder: a miRNA analysis tool for deep sequencing of plant small RNAs. Plant Mol Biol 80:75-84.

Yan, X., Fan, Y., Wei, W., Wang, P., Liu, Q., Wei, Y., Zhang, L., Zhao, G., Yue, J., and Zhou, Z. (2014). Production of bioactive ginsenoside compound K in metabolically engineered yeast. Cell Res 24:770-773.

Yang, Z. (2007). PAML 4: phylogenetic analysis by maximum likelihood. Mol Biol Evol 24:1586-1591.

Yonekura-Sakakibara, K., Tohge, T., Matsuda, F., Nakabayashi, R., Takayama, H., Niida, R., Watanabe-Takahashi, A., Inoue, E., and Saito, K. (2008). Comprehensive flavonol profiling and transcriptome coexpression analysis leading to decoding gene-metabolite correlations in Arabidopsis. Plant Cell 20:2160-2176.

Yonekura-Sakakibara, K., Tohge, T., Niida, R., and Saito, K. (2007). Identification of a flavonol 7-O-rhamnosyltransferase gene determining flavonoid pattern in Arabidopsis by transcriptome coexpression analysis and reverse genetics. J Biol Chem 282:14932-14941.

Yu, H.S., Ma, L.Q., Zhang, J.X., Shi, G.L., Hu, Y.H., and Wang, Y.N. (2011). Characterization of glycosyltransferases responsible for salidroside biosynthesis in *Rhodiola sachalinensis*. Phytochemistry 72:862-870.

Zhang, Y., Xie, K., Liu, A., Chen, R., Chen, D., Yang, L., and Dai, J. (2019). Enzymatic biosynthesis of benzylisoquinoline alkaloid glycosides via promiscuous

glycosyltransferases from *Carthamus tinctorius*. Chinese Chemical Letters 30:443-446.

Zwaenepoel, A., and Van de Peer, Y. (2019). wgd-simple command line tools for the analysis of ancient whole-genome duplications. Bioinformatics 35:2153-2155.

Supplementary Figure Legends

Supplementary Figure 1. *K-mer* analysis for estimating the genome size of *P. notoginseng*. (A) The distribution of numbers of *K-mer* individuals. The red dashed line marks the main peak with depth = 63. **(B)** The distribution of numbers of *K-mer* species.

Supplementary Figure 2. Genome-wide Hi-C map of *P. notoginseng*. Interaction frequency distribution of Hi-C links among chromosomes shows in color key of heatmap ranging from light yellow to dark brown indicated the frequency of Hi-C interaction links from low to high (0−5).

Supplementary Figure 3. Analysis of repetitive sequences in the *P. notoginseng* genome. (A) LTR retrotransposons prediction using different methods; **(B)** Summary of repetitive sequences in the *P. notoginseng* genome; **(C)** Analysis of the divergence of various types of repetitive sequences.

Supplementary Figure 4. Characteristic distribution of *P. notoginseng* annotated genes and comparison with related species. Plant genomes for comparison include *A. thaliana*, *D. carota*, *P. ginseng* and *P. notoginseng*-published.

Supplementary Figure 5. Cluster analysis of gene families of eight species.

Supplementary Figure 6. Venn diagram of distribution of gene families among the seven species. The histogram on the left represents the number of gene families of each species. The red dots and lines on the right represent the gene family's classification between the designated species, and the number of each group is shown by the bar graph above.

Supplementary Figure 7. Enrichment analysis of GO and KEGG in *P. notoginseng*-specific gene families. GO enrichment analysis includes three parts: biological process **(A)**, cellular component **(B)** and molecular function **(C)**. **(D)** KEGG enrichment analysis of *P. notoginseng*-specific genes. The larger the bubble radius, the higher the rich-ratio value and the redder the color of bubble, the higher the degree of enrichment.

Supplementary Figure 8. Evolution analysis of *P. notoginseng* genome. (A) Estimated time of divergence between the eight species in the evolutionary process. **(B)**

Analysis of gene family expansion and contraction between the eight plant genomes.

Supplementary Figure 9. GO enrichment analysis of expanded and contracted gene families of *P. notoginseng* genome. (A) GO enrichment analysis of expanded gene families; **(B)** GO enrichment analysis of contracted gene families; **(C)** Summary of gene numbers expanding and contracting in different categories of GO enrichment analysis.

Supplementary Figure 10. Summary of the syntenic analysis between *P. notoginseng* and *V. vinifera* (n=1 biologically independent samples).

Supplementary Figure 11. Collinear analysis among *D. carota*, *P. notoginseng* and *V. vinifera* genome. The red lines in the genomes of *P. notoginseng* and *V. vinifera* indicate that the 1:2 correspondence between the two collinear regions.

Supplementary Figure 12. Synonymous substitution rate (*Ks*) distributions of syntenic blocks in *P. notoginseng* and comparison with *P. ginseng* and *V. vinifera* genome.

Supplementary Figure 13. Phylogenetic tree of key enzyme genes in terpenoid biosynthetic pathway in 8 species including *P. notoginseng*, *P. ginseng*, *D. carota*, *V. vinifera*, *O. sativa*, *A. thaliana*, *G. uralensis* and *C. annuum* (1). Each phylogenetic tree of terpenoid biosynthetic genes was constructed by using MEGA X with the neighbor-joining method.

Supplementary Figure 14. Phylogenetic trees of key enzyme genes involved in terpenoid biosynthetic pathway in 8 species including *P. notoginseng*, *P. ginseng*, *D. carota*, *V. vinifera*, *O. sativa*, *A. thaliana*, *G. uralensis* and *C. annuum* (2). Each phylogenetic tree of terpenoid biosynthetic genes was constructed by using MEGA X with the neighbor-joining method.

Supplementary Figure 15. Evolution of ginsenoside-associated genes in *P. notoginseng*. (A) Genome duplication in *P. notoginseng*. The calculated Ks value was converted to the divergence time according to T=Ks/2r, where r represents a substitution rate of 6.5×10-9 mutations per site per year for eudicots (n=1 biologically independent samples). **(B)** Duplication event(s) for each gene pair is(are) shown along the timeline from 0 to 150 million years ago with different colors.

Supplementary Figure 16. Overview of clustering of transcriptome samples.

Supplementary Figure 17. Pearson correlation analysis of transcriptome samples. The R^2 value between two random transcripts were indicated in the box, and ranging from white to blue indicted from low to high (0-1).

Supplementary Figure 18. The proportion distribution of various reads before filtering in all samples.

Supplementary Figure 19. The coverage distribution of gene regions mapping on genome in each transcript.

Supplementary Figure 20. Statistics of alternative splicing events. (A) events in each sample; **(B)** different types of alternative splicing events in the comparison groups. TSS: Transcription Start Site; TTS: Transcription Terminal Site; SKIP: Skipped exon; XSKIP: Approximate SKIP; MSKIP: Multi-exon SKIP; XMSKIP: Approximate MSKIP; IR: Intron retention; XIR: Approximate IR; MIR: Multi-IR; XMIR: Approximate MIR; AE: Alternative exon ends (5', 3' or both); XAE: Approximate AE (5' or 3'); A3SS: Alternative 3' splice site; A5SS: Alternative 5' splice site.

Supplementary Figure 21. Variation analysis of each sample. (A) distribution of each variant type; **(B)** according to the detected SNP loci, the frequency of each mutation type has been counted, taking the data results of One1Leaf, Two1Leaf, Two2Flower, Tri3Stem, Tri1Xylem, Fou2Perid as examples; **(C)** according to the detected InDel loci, the frequency of each InDel length has been counted, taking the data results of One1Leaf, Two1Leaf, Two2Flower, Tri3Stem, Tri1Xylem, Fou2Perid as examples.

Supplementary Figure 22. Density distribution diagram of gene expression in each transcriptome sample.

Supplementary Figure 23. Box plot of the overall distribution of gene expression in each transcriptome sample.

Supplementary Figure 24. The exploration of the molecular mechanism of the formation of *P. notoginseng*'s tubercles. (**A**) the display of root morphology of *P. notoginseng*, and the red arrow points to the tubercles. (**B**) GO enrichment analysis of DEGs between the periderm and tubercle group. (**C**) the Directed Acyclic Graph (DAG)

of GO enrichment analysis, the darker color indicates the more significant enrichment and the red is the most significant. The larger the bubble radius, the higher the rich-ratio value and the redder the color of bubble, the higher the degree of enrichment.

Supplementary Figure 25. Spatial expression profile of key enzyme genes in saponin biosynthesis pathway. The genes in red font are the functional UGT cloned in this study.

Supplementary Figure 26. Phylogenetic analysis of CYP450 genes in *P. notoginseng* using MEGA-X.

Supplementary Figure 27. Heat map of the expression of the cloned UGT genes in different transcript samples. The genes marked by five-pointed stars are those with catalytic function identified in this study. In the heat map, the relative expression level from high to low (-2 to 2) is represented by the range from blue to red.

Supplementary Figure 28 The blank control experiments of protein catalytic reaction in this study. (A) Analysis results of *E. coli* no-load control with PPD as the catalytic substrate. **(B)** Analysis results of *E. coli* no-load control with PPT as the catalytic substrate. **(C)** Analysis results of *E. coli* no-load control with ginsenoside F1 as the catalytic substrate. **(D)** Analysis results of *E. coli* no-load control with Rh2 as the catalytic substrate. The molecular ion peaks with 667.4465, 683.4406, 845.496 and 784.00 were extracted respectively, and the mass spectrum in the green box did not match with any corresponding glycoside product, indicating no product was formed.

Supplementary Figure 29. UPLC/Q-TOF analysis results of PnUGT3 protein catalytic reaction. (A) Chromatograms and mass spectrum of ginsenoside Rh1 standard and PnUGT3 catalytic products using PPT as substrate. **(B)** Chromatograms and mass spectrum of ginsenoside Rg1 standard and PnUGT3 catalytic products using F1 as substrate.

Supplementary Figure 30. UPLC/Q-TOF analysis results of PnUGT1 and PnUGT5 protein catalytic reaction. **(A)** Chromatograms and mass spectrum of ginsenoside F1 standard and PnUGT1 catalytic products using PPT as substrate. **(B)** Chromatograms and mass spectrum of ginsenoside CK standard and PnUGT1 catalytic products using PPD as substrate. **(C)** Chromatograms and mass spectrum of

ginsenoside F2 standard and PnUGT1 catalytic products using Rh2 as substrate. **(D)** Chromatograms and mass spectrum of ginsenoside Rh2 standard and PnUGT5 catalytic products using PPD as substrate.

Supplementary Figure 31. UPLC/Q-TOF analysis results of PnUGT2 and PnUGT4 protein catalytic reaction. Chromatograms and mass spectrum of ginsenoside Rg3 standard and PnUGT2 and PnUGT4 catalytic products using Rh2 as substrate.

Supplementary Figure 32. The structural formulas of various saponins in *P. notoginseng*.

Supplementary Figure 33. WGCAN analysis and characterization of corresponding data. (A) Construction of the sample clustering evolutionary tree of transcriptome to screen out outliers. **(B)** Construction the PCA map of transcriptome samples. **(C)** Analysis of network topology for various soft-thresholding powers. When we set R^2=0.9, the optimal candidate threshold to reach this height is 10. **(D)** Visualization of the eigengene network representing the relationships among the modules. The redder the color in the heat map, the stronger the correlation between the two modules.

Supplementary Figure 34. Expression profile of key enzyme genes in saponin biosynthesis pathway. The right side of the heatmap shows the evolutionary tree of genes, and genes with similar expression patterns are clustered into one group.

Supplementary Figure 35. Heat map of expression of UGT genes and genes in terpenoid biosynthesis pathway. The right side of the heatmap shows the evolutionary tree of genes, and genes with similar expression patterns are clustered into one group.

Supplementary Figure 36. Gene clusters involved in saponins biosynthesis found in *P. notoginseng* genome. (A) Gene clusters on chromosomes 1, 2 and their correspondence. **(B)** Gene clusters on chromosomes 6, 8 and their correspondence. Orange lines indicate copies of genes with the same function, and blue lines indicate the correlation between transcription factors and pathway genes.

Supplementary Table legends

Supplementary Table 1. Estimation of genome size of *P. notoginseng* based on *K-mer* analysis.

Supplementary Table 2. Sequencing data statistics of *P. notoginseng*.

Supplementary Table 3. The Statistics of Pseudomolecule based on Hi-C technique.

Supplementary Table 4. Statistic of DNA base composition in the *P. notoginseng* genome.

Supplementary Table 5. Statistics of consistency assessment of the *P. notoginseng* genome.

Supplementary Table 6. Assessment the gene coverage rate using BUSCO.

Supplementary Table 7. Annotation of repetitive sequences in the *P. notoginseng* genome.

Supplementary Table 8. Summary of repetitive sequences in the *P. notoginseng* genome.

Supplementary Table 9. Basic statistical results of gene structure prediction of *P. notoginseng* genome.

Supplementary Table 10. Basic statistical results of gene structure prediction of *P. notoginseng* and relative species.

Supplementary Table 11. Statistical results of gene function annotation of *P. notoginseng* genome.

Supplementary Table 12. Statistical results of non-coding RNA of *P. notoginseng* genome.

Supplementary Table 13. The Statistics of gene clustering to gene families in various species.

Supplementary Table 14. Enriched GO terms of genes in *P. notoginseng*-specific families.

Supplementary Table 15. Enriched GO terms of genes in expanded gene families.

Supplementary Table 16. Enriched GO terms of genes in contracted gene families.

Supplementary Table 17. Copy number variation of genes involved in the ginsenoside biosynthesis in the *P. notoginseng* and seven other plant species.

Supplementary Table 18. *Ks* values and duplication times of genes involved in ginsenoside biosynthesis in *P. notoginseng*.

Supplementary Table 19. Statistics of the information and grouping of transcriptome samples.

Supplementary Table 20. Statistics of alternative splicing events occurred in *P. notoginseng* genome.

Supplementary Table 21. Statistics of variation events occurred in *P. notoginseng* genome.

Supplementary Table 22. Representative genes which are highly expressed in tubercle group.

Supplementary Table 23. Statistics of transcription factors in *P. notoginseng* genome.

Supplementary Table 24. Statistics of FPKM expression in different tissues of some key enzyme genes in the terpene biosynthesis pathway.

Supplementary Table 25. The CYP450 genes used to construct phylogenetic tree in this research.

Supplementary Table 26. The UGT genes used to construct phylogenetic tree in this research.

Supplementary Table 27. Primers for cloning UGT genes in *P. notoginseng* genome.

Supplementary Table 28. Annotation and GO enrichment of candidate UGT genes selected by WGCNA analysis.

Supplementary Table 29. Annotation and GO enrichment of candidate UGT genes screened from the gene expression patterns.

(**Note:** Among these tables, Supplementary Table 19, 20, 21, 24, 28, 29 are placed in a separate excel sheet due to the large content.)

Supplementary Figures

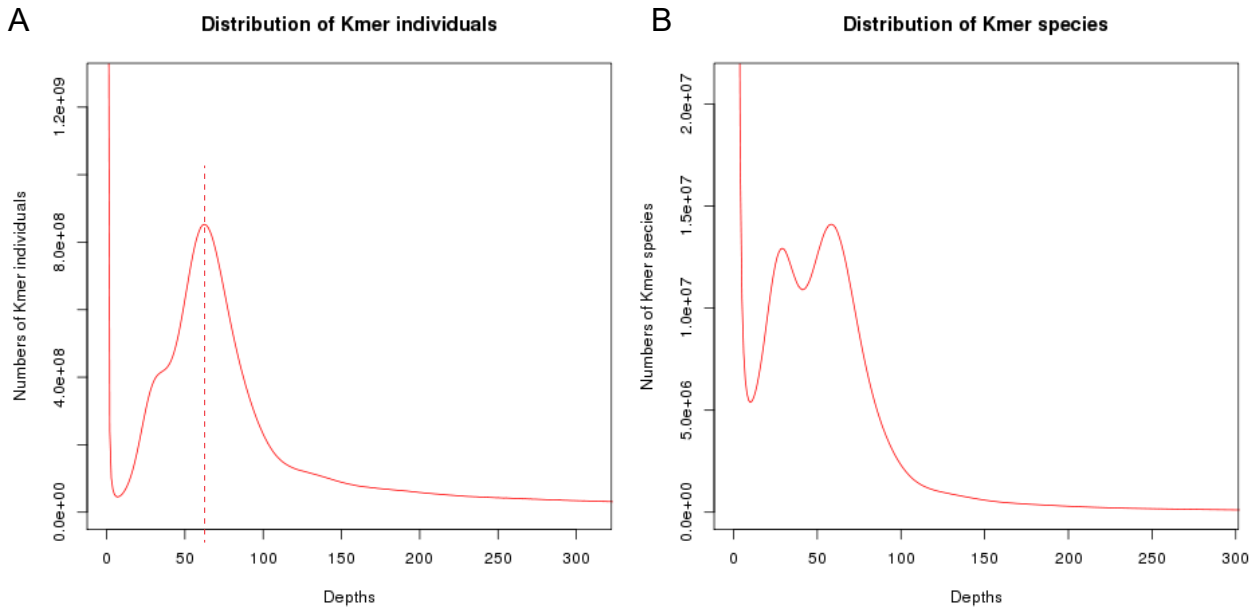

Supplementary Figure 1. *K-mer* analysis for estimating the genome size of *P. notoginseng*. **(A)** The distribution of numbers of *K-mer* individuals. The red dashed line marks the main peak with depth = 63. **(B)** The distribution of numbers of *K-mer* species.

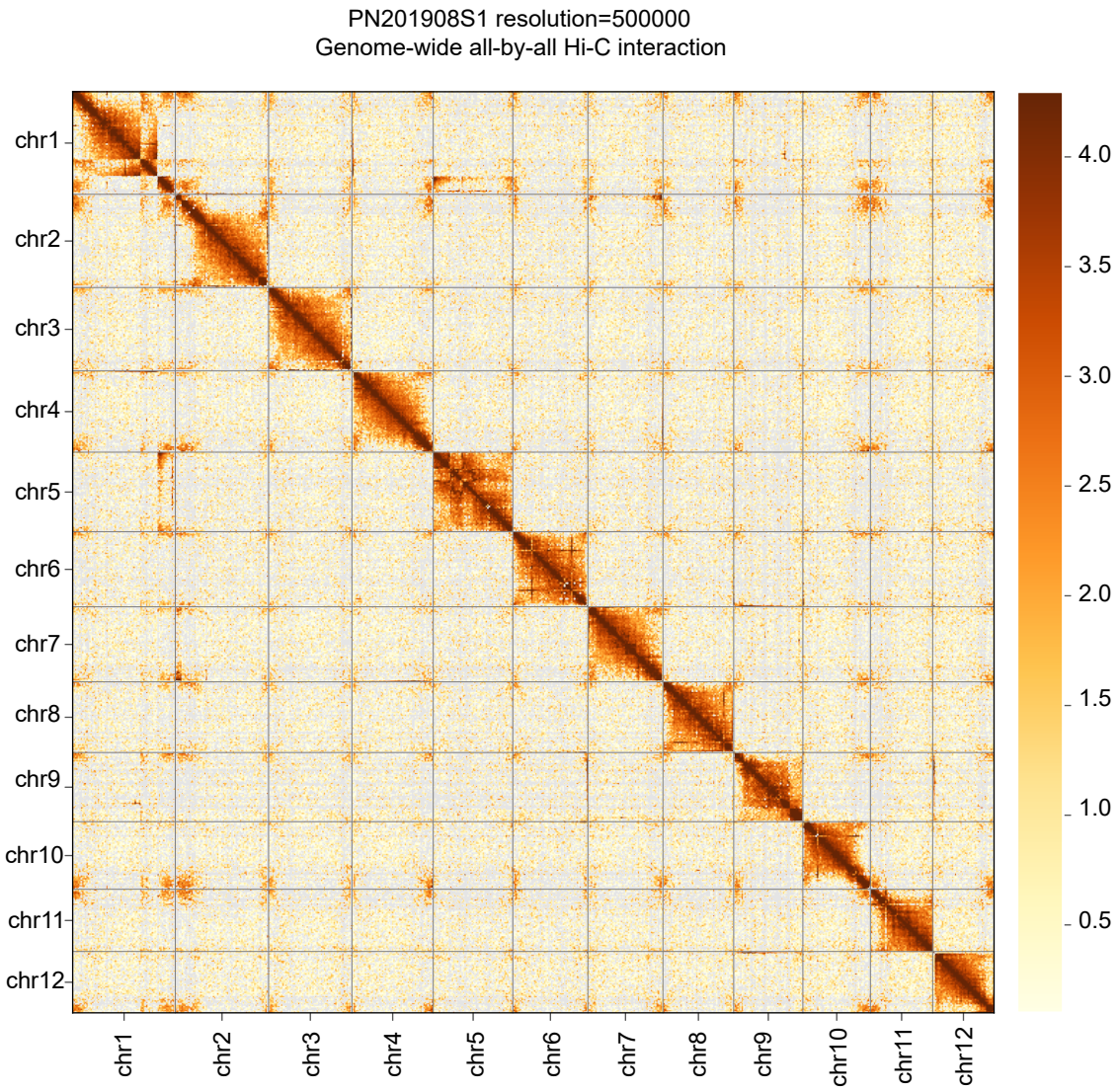

Supplemental Figure 2. Genome-wide Hi-C map of *P. notoginseng*. Interaction frequency distribution of Hi-C links among chromosomes shows in color key of heatmap ranging from light yellow to dark brown indicated the frequency of Hi-C interaction links from low to high (0-5).

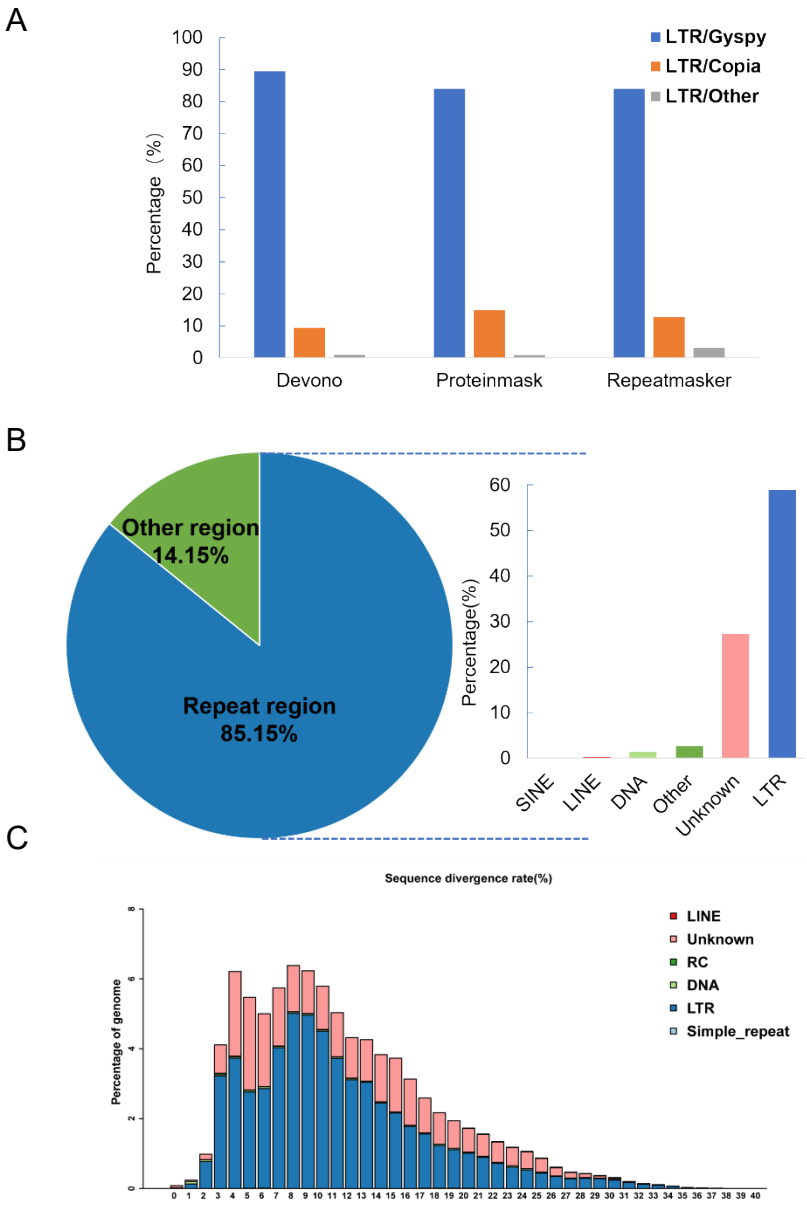

Supplementary Figure 3. Analysis of repetitive sequences in the *P. notoginseng* genome. (**A**) LTR retrotransposons prediction using different methods. (**B**) Summary of repetitive sequences in the *P. notoginseng* genome. (**C**) Analysis of the divergence of various types of repetitive sequences.

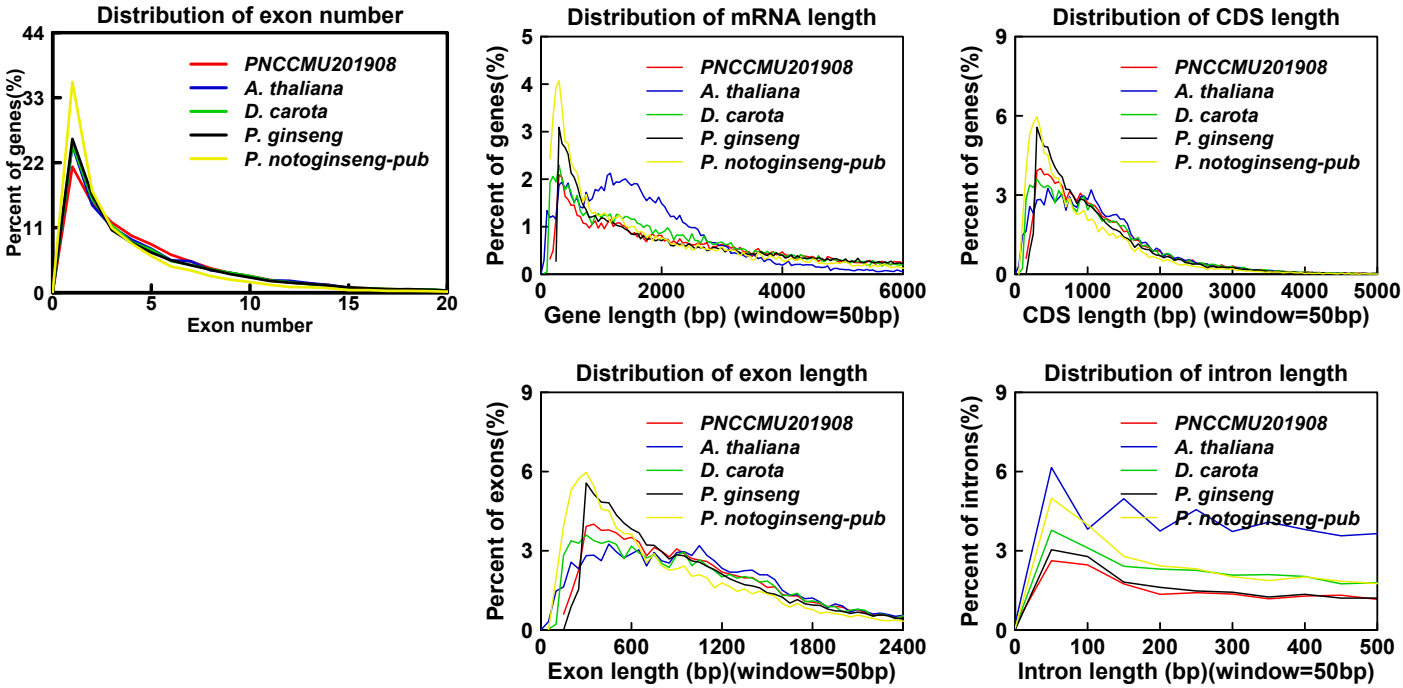

Supplementary Figure 4. Characteristic distribution of *P. notoginseng* annotated genes and comparison with related species. Plant genomes for comparison include *A. thaliana*, *D. carota*, *P. ginseng* and *P. notoginseng*-published.

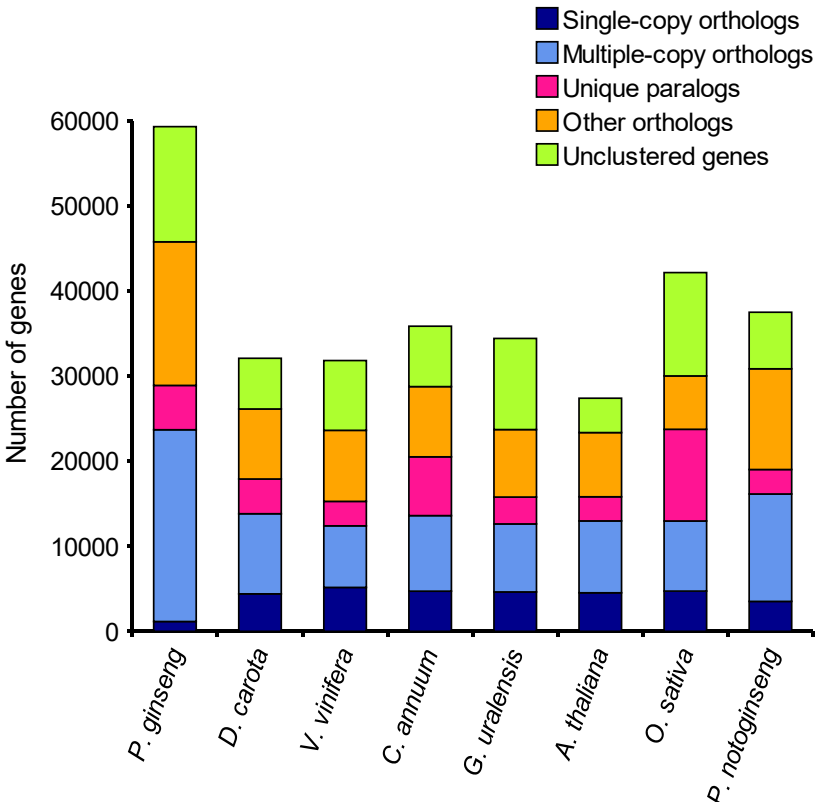

Supplementary Figure 5. Cluster analysis of gene families of eight species.

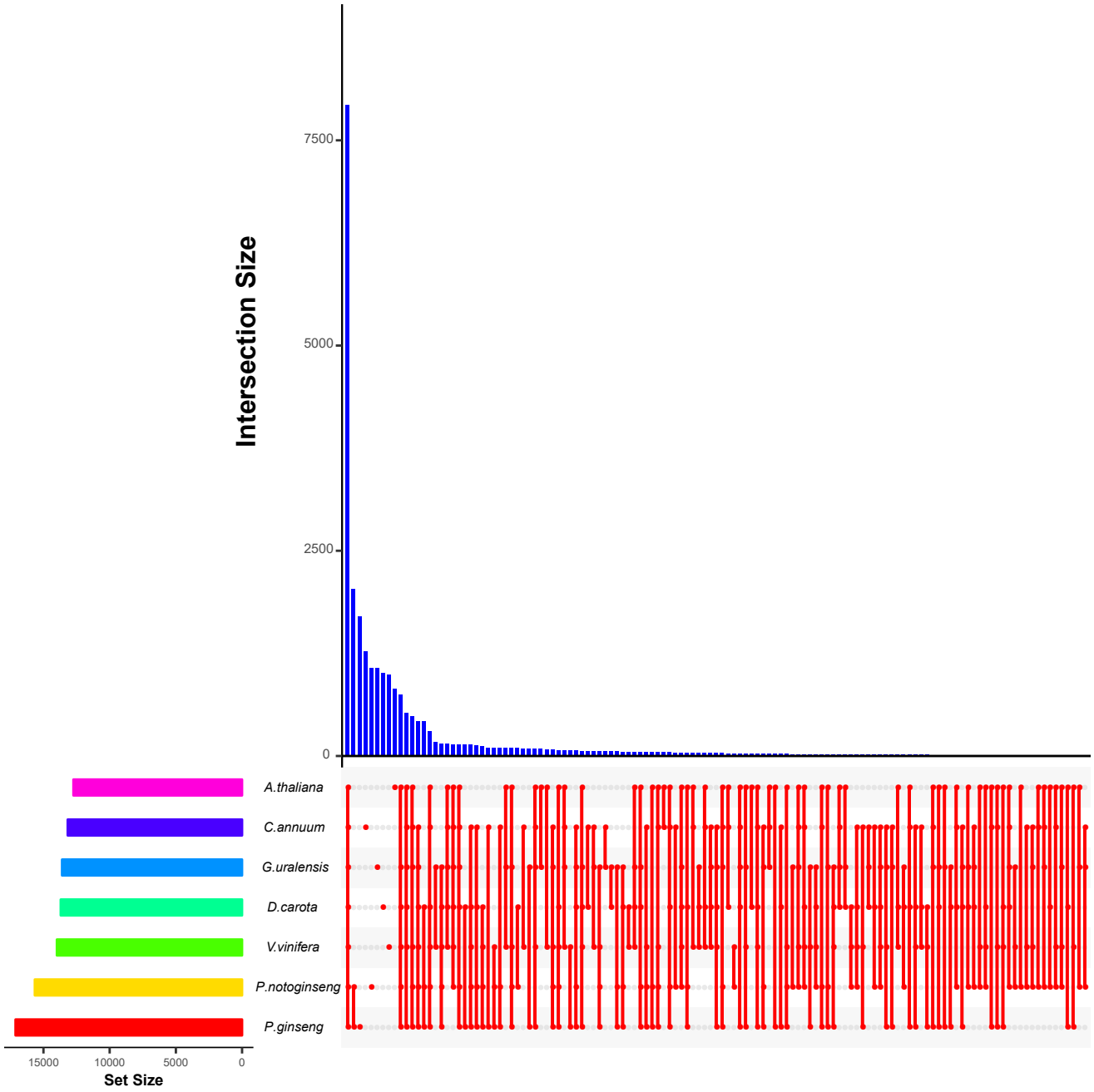

Supplementary Figure 6. Venn diagram of distribution of gene families among the seven species.
The histogram on the left represents the number of gene families of each species. The red dots and lines on the right represent the gene family's classification between the designated species, and the number of each group is shown by the bar graph above.

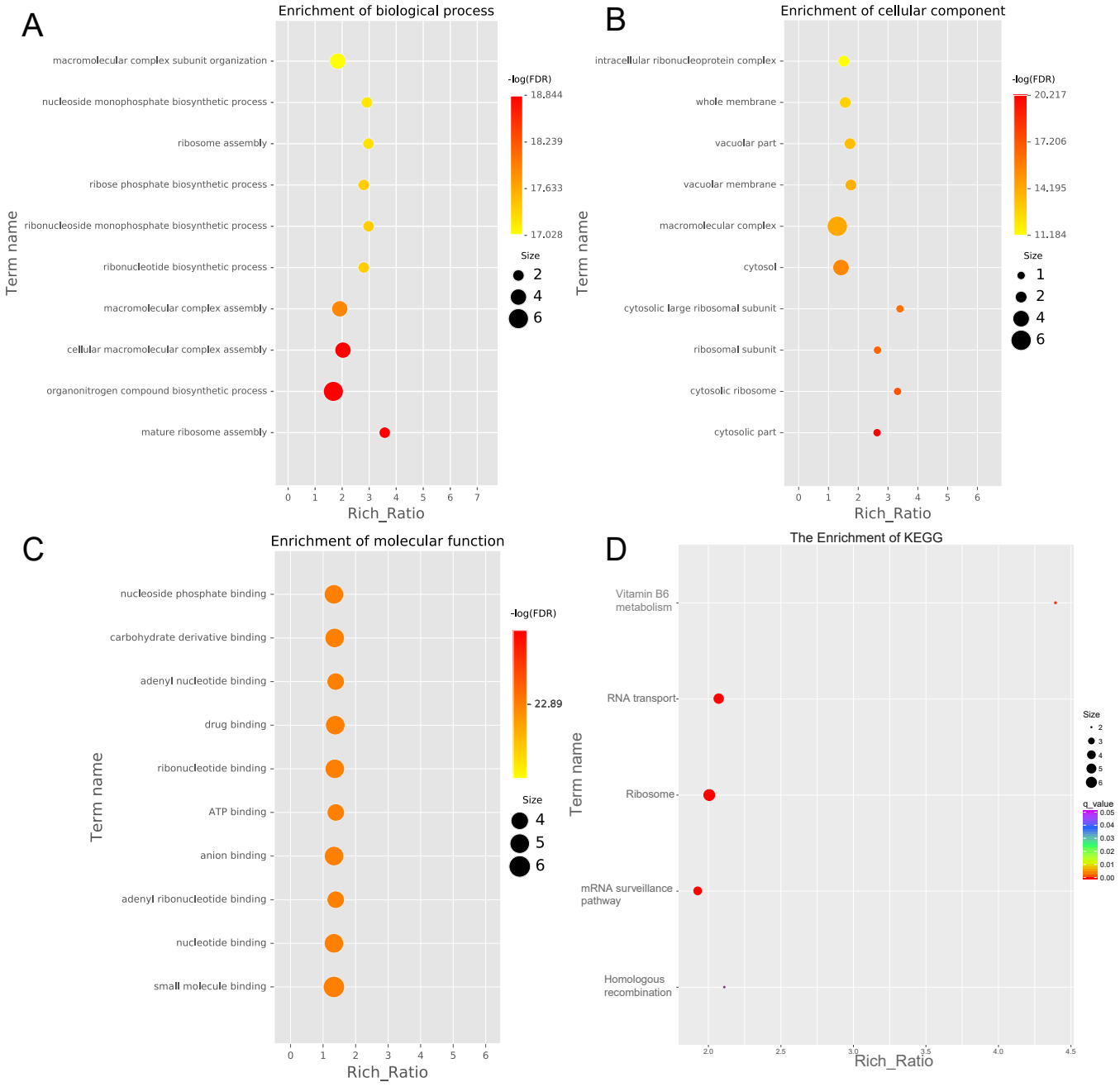

Supplementary Figure 7. Enrichment analysis of GO and KEGG in *P. notoginseng*-specific gene families. GO enrichment analysis includes three parts: biological process **(A)**, cellular component **(B)** and molecular function **(C)**. **(D)** KEGG enrichment analysis of *P. notoginseng*-specific genes. The larger the bubble radius, the higher the rich-ratio value and the redder the color of bubble, the higher the degree of enrichment.

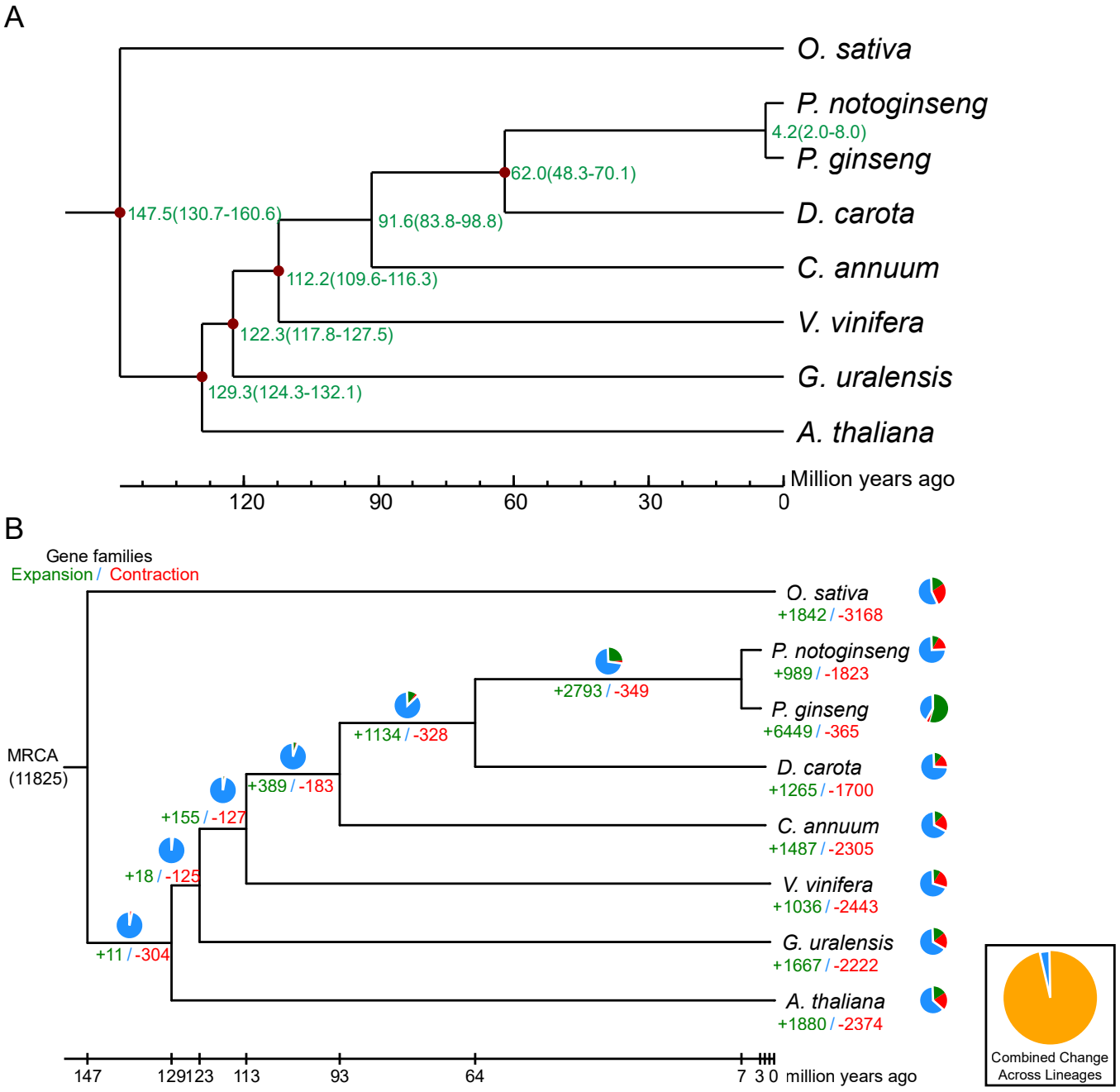

Supplementary Figure 8. Evolution analysis of *P. notoginseng* genome.

(A) Estimated time of divergence between the eight species in the evolutionary process.

(B) Analysis of gene family expansion and contraction between the eight plant genomes.

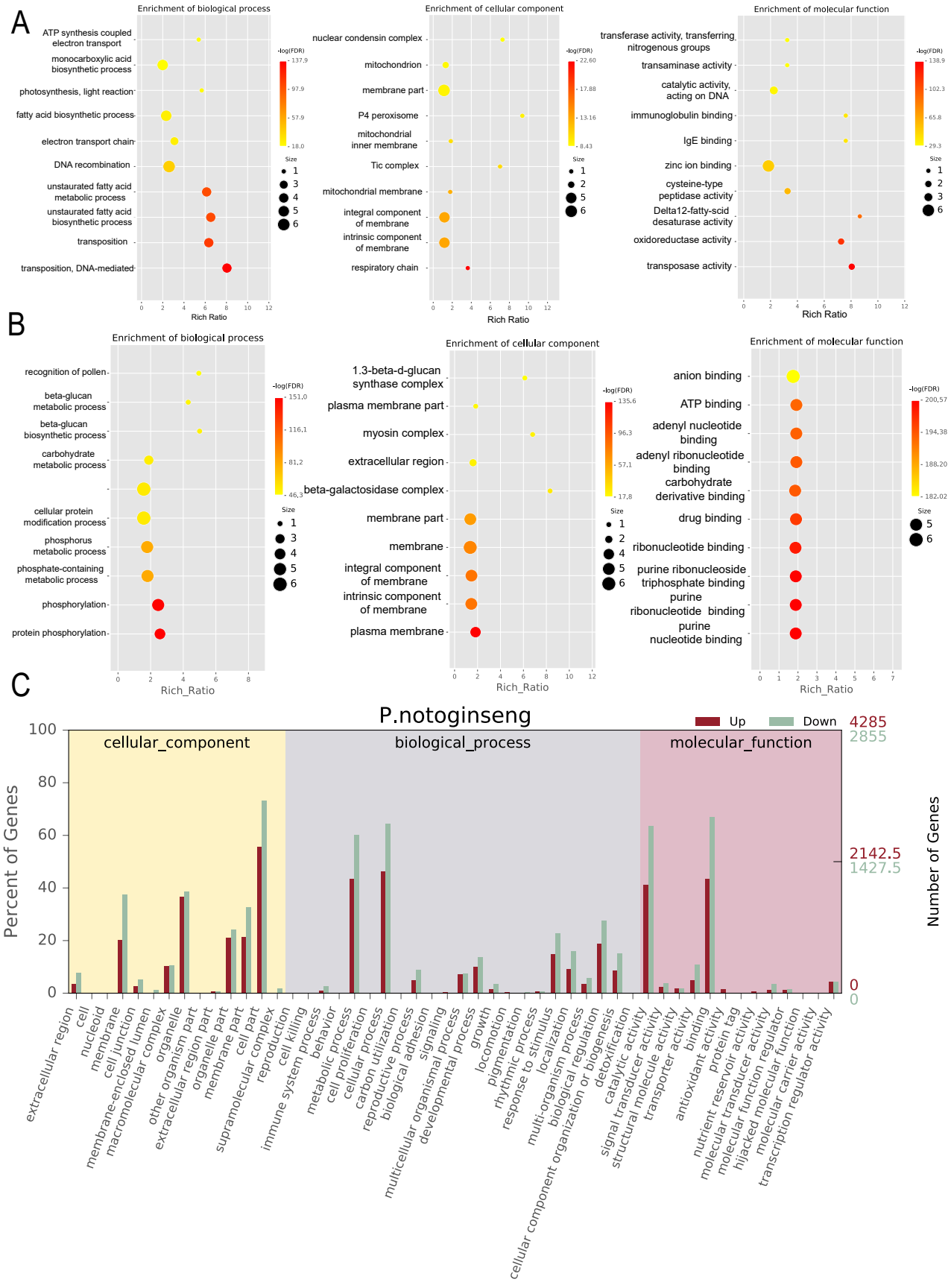

Supplemental Figure 9. GO enrichment analysis of expanded and contracted gene families of *P. notoginseng* genome. (A) GO enrichment analysis of expanded gene families; **(B)** GO enrichment analysis of contracted gene families; **(C)** Summary of gene numbers expanding and contracting in different categories of GO enrichment analysis.

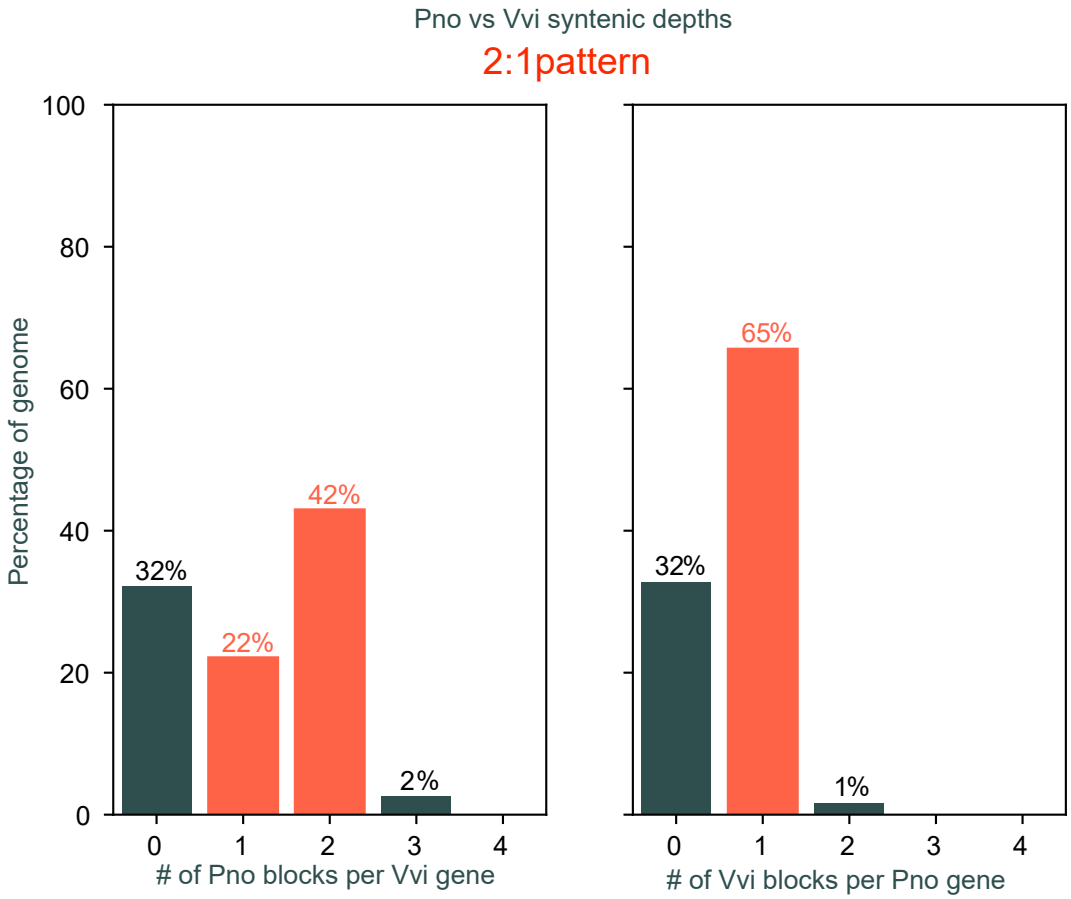

Supplementary Figure 10. Summary of the syntenic analysis between *P. notoginseng* and *V. vinifera* (n=1 biologically independent samples).

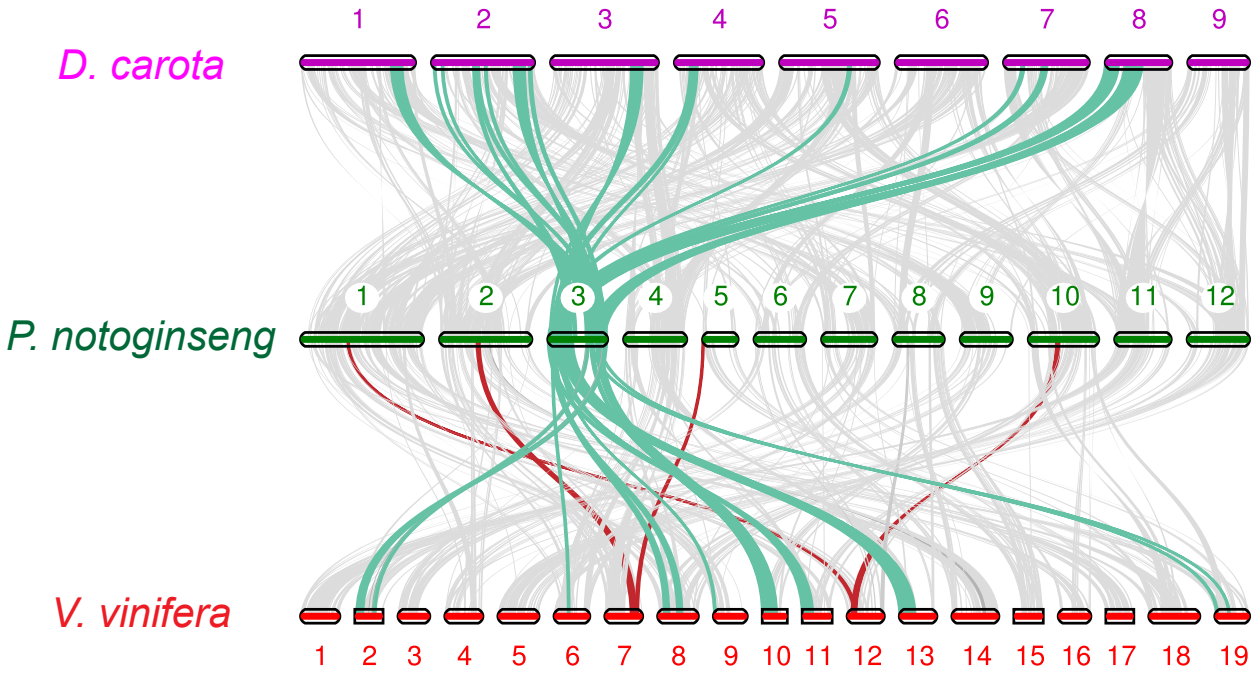

Supplementary Figure 11. Collinear analysis among *D. carota*, *P. notoginseng* and *V. vinifera* genome. The red lines in the genomes of *P. notoginseng* and *V. vinifera* indicate that the 1:2 correspondence between the two collinear regions.

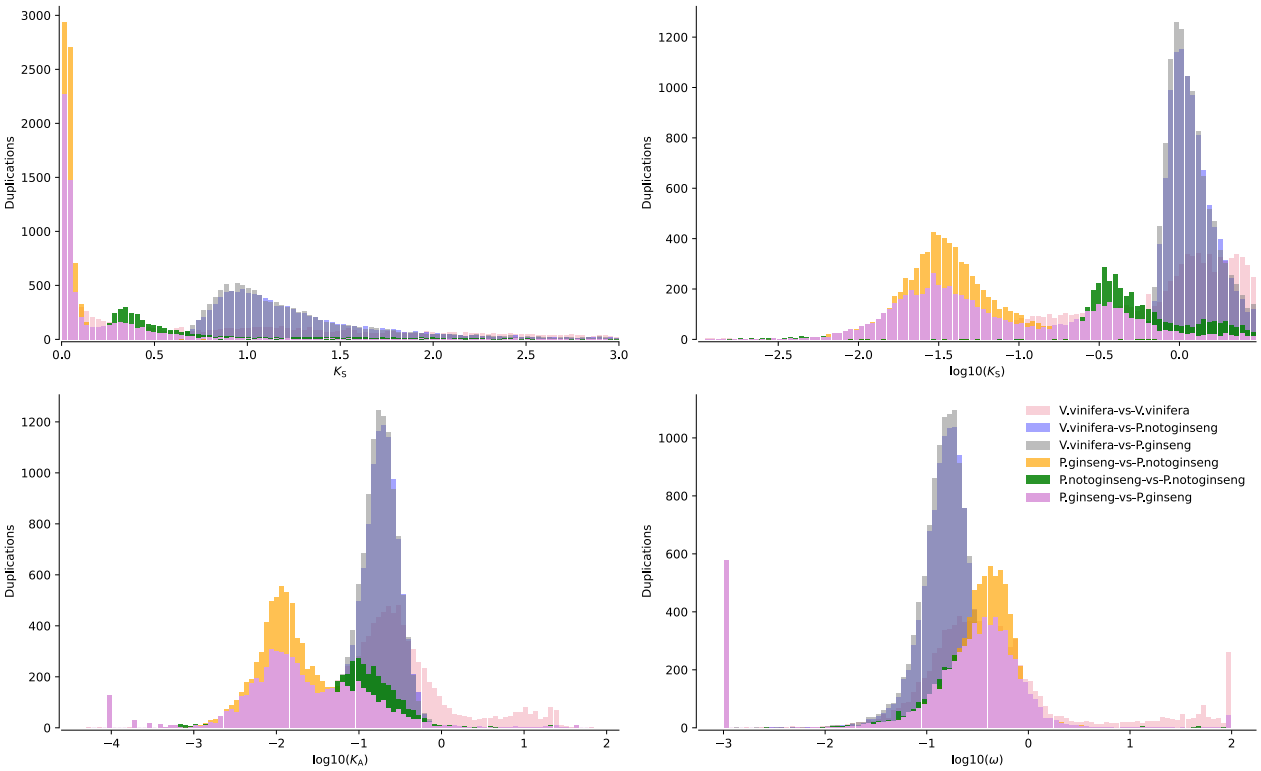

Supplementary Figure 12. Synonymous substitution rate (*Ks*) distributions of syntenic blocks in *P. notoginseng* and comparison with *P. ginseng* and *V. vinifera* genome.

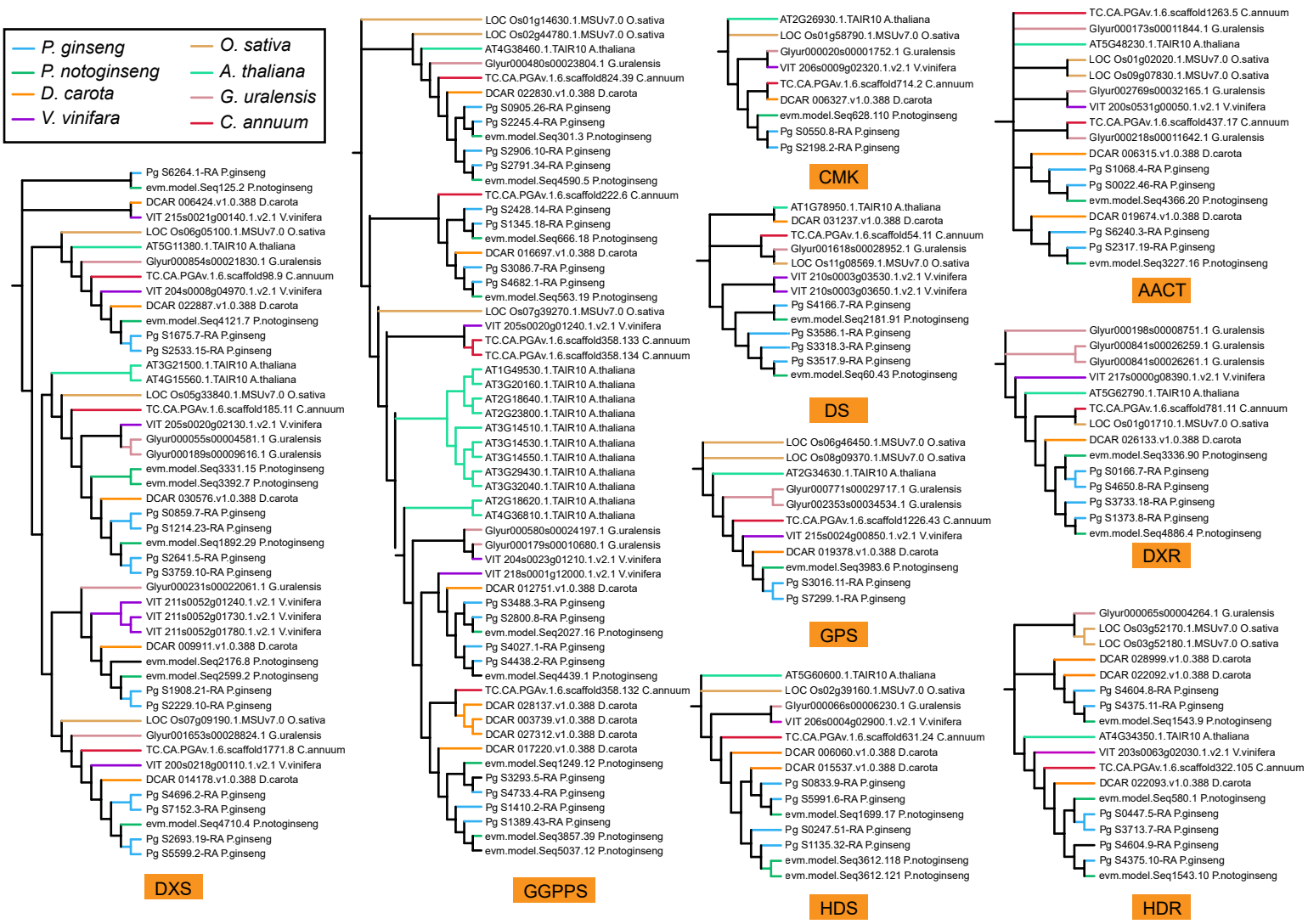

Supplemental Figure 13. Phylogenetic tree of key enzyme genes in terpenoid biosynthetic pathway in 8 species including *P. notoginseng*, *P. ginseng*, *D. carota*, *V. vinifera*, *O. sativa*, *A. thaliana*, *G. uralensis* and *C. annuum* (1). Each phylogenetic tree of terpenoid biosynthetic genes was constructed by using MEGA X with the neighbor-joining method.

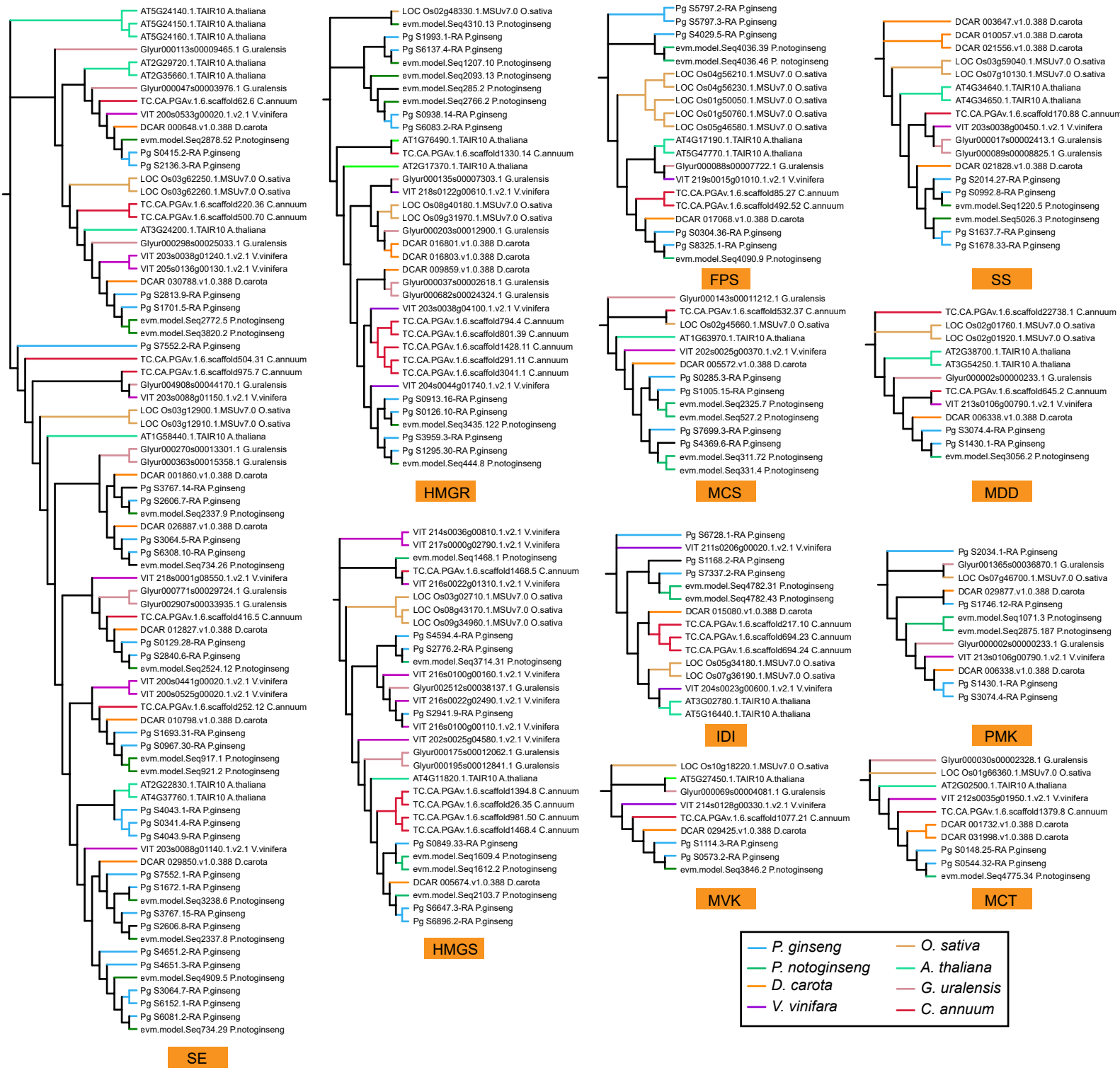

Supplemental Figure 14. Phylogenetic trees of key enzyme genes involved in terpenoid biosynthetic pathway in 8 species including *P. notoginseng*, *P. ginseng*, *D. carota*, *V. vinifera*, *O. sativa*, *A. thaliana*, *G. uralensis* and *C. annuum* (2). Each phylogenetic tree of terpenoid biosynthetic genes was constructed by using MEGA X with the neighbor-joining method.

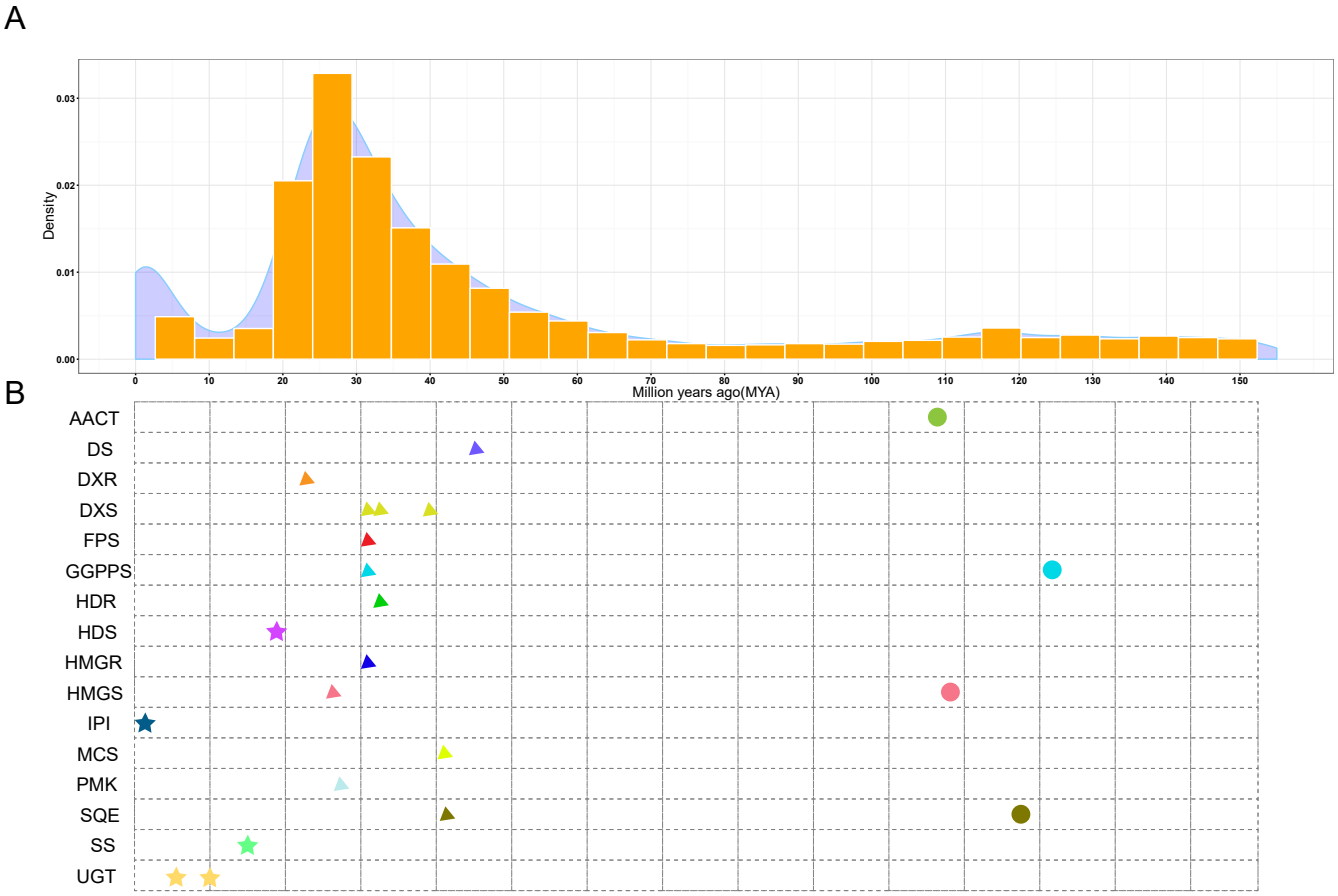

Supplemental Figure 15. Evolution of ginsenoside-associated genes in *P. notoginseng*. **(A)** Genome duplication in *P. notoginseng*. The calculated *Ks* value was converted to the divergence time according to T=*Ks*/2r, where r represents a substitution rate of 6.5×10-9 mutations per site per year for eudicots (n=1 biologically independent samples). **(B)** Duplication event(s) for each gene pair is(are) shown along the timeline from 0 to 150 million years ago with different colors.

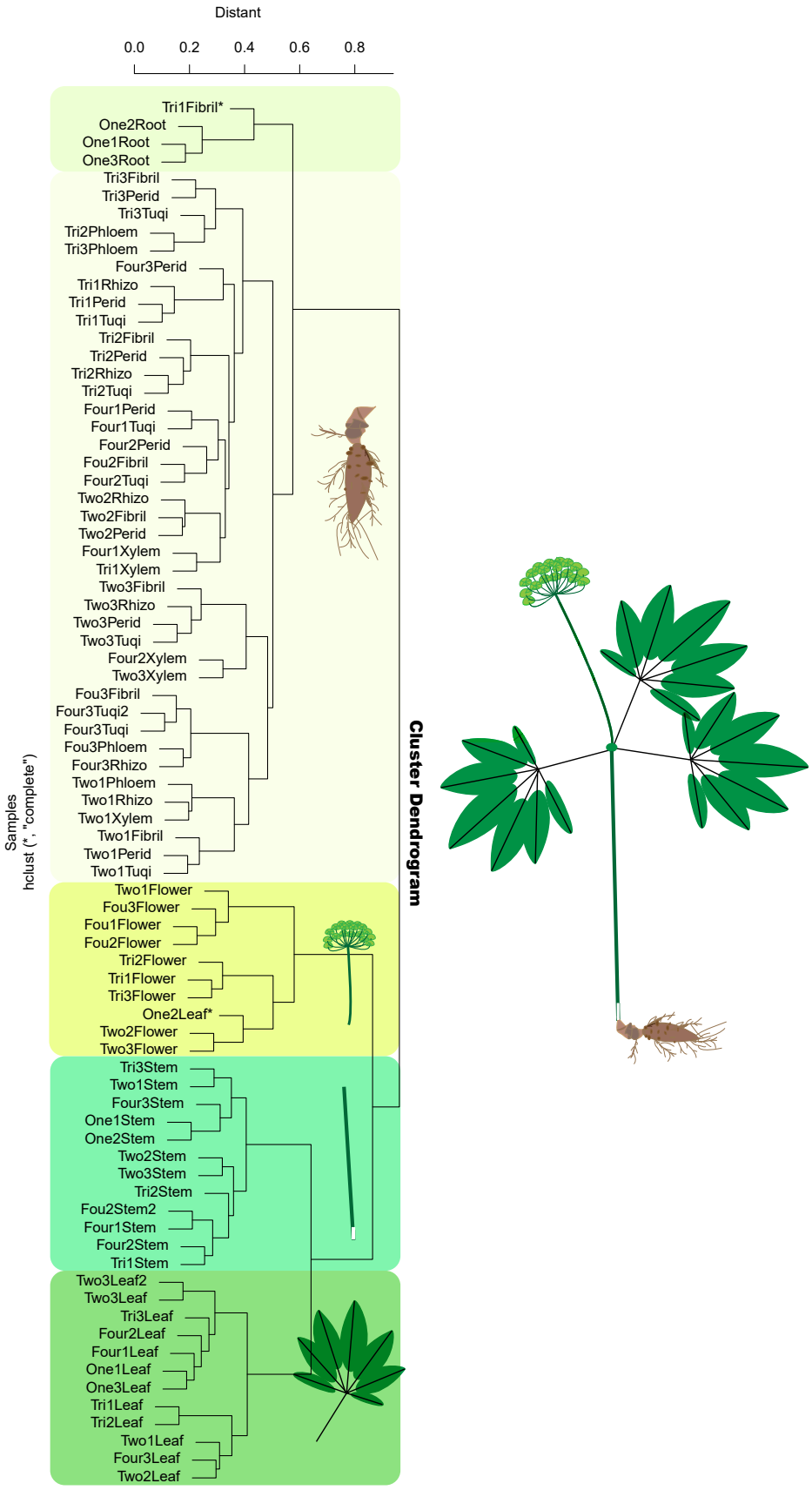

Supplemental Figure 16. Overview of clustering of transcriptome samples.

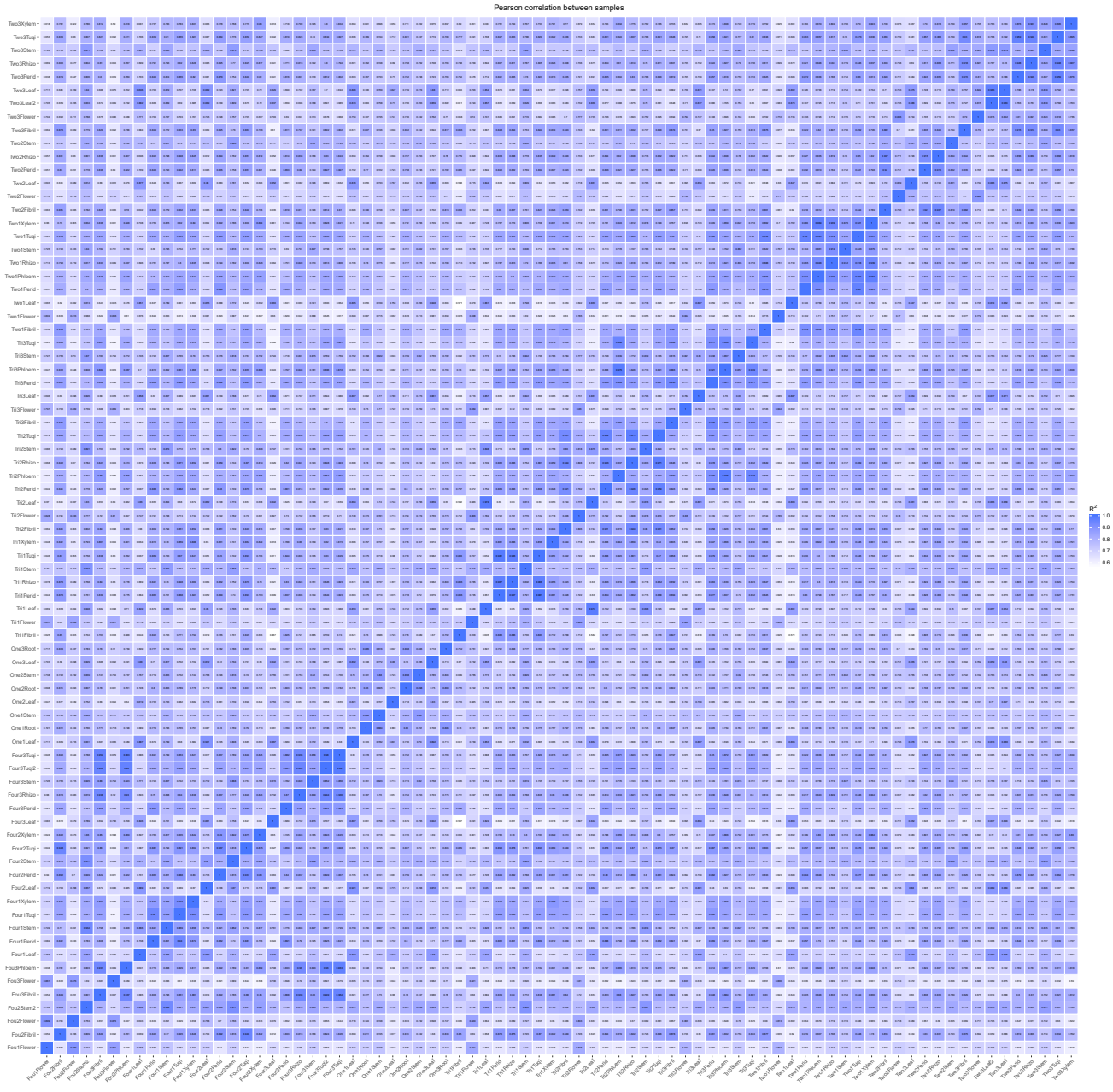

Supplemental Figure 17. Pearson correlation analysis of transcriptome samples.

The R2 value between two random transcripts were indicated in the box, and ranging from white to blue indicted from low to high (0-1).

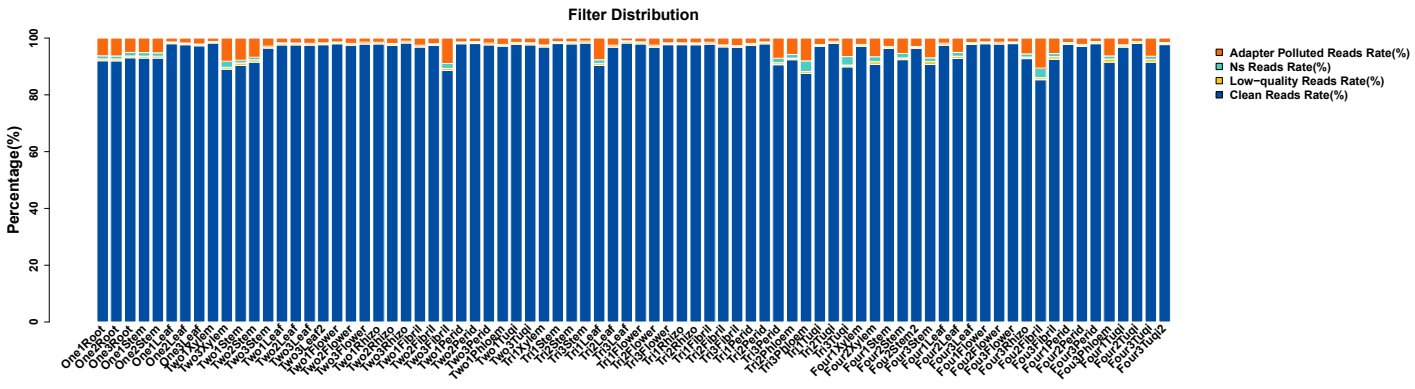

Supplemental Figure 18. The proportion distribution of various reads before filtering in all samples.

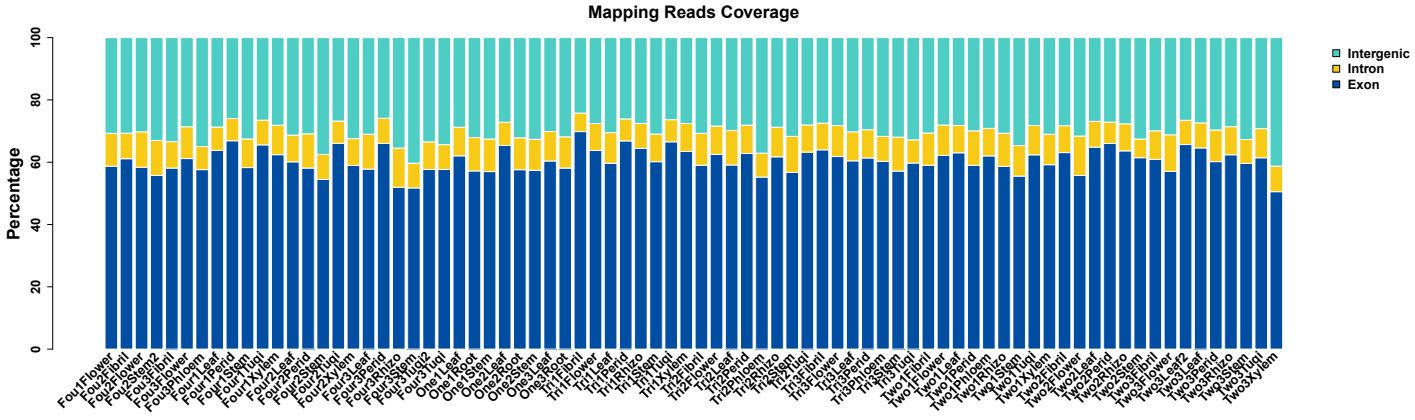

Supplemental Figure 19. The coverage distribution of gene regions mapping on genome in each transcript.

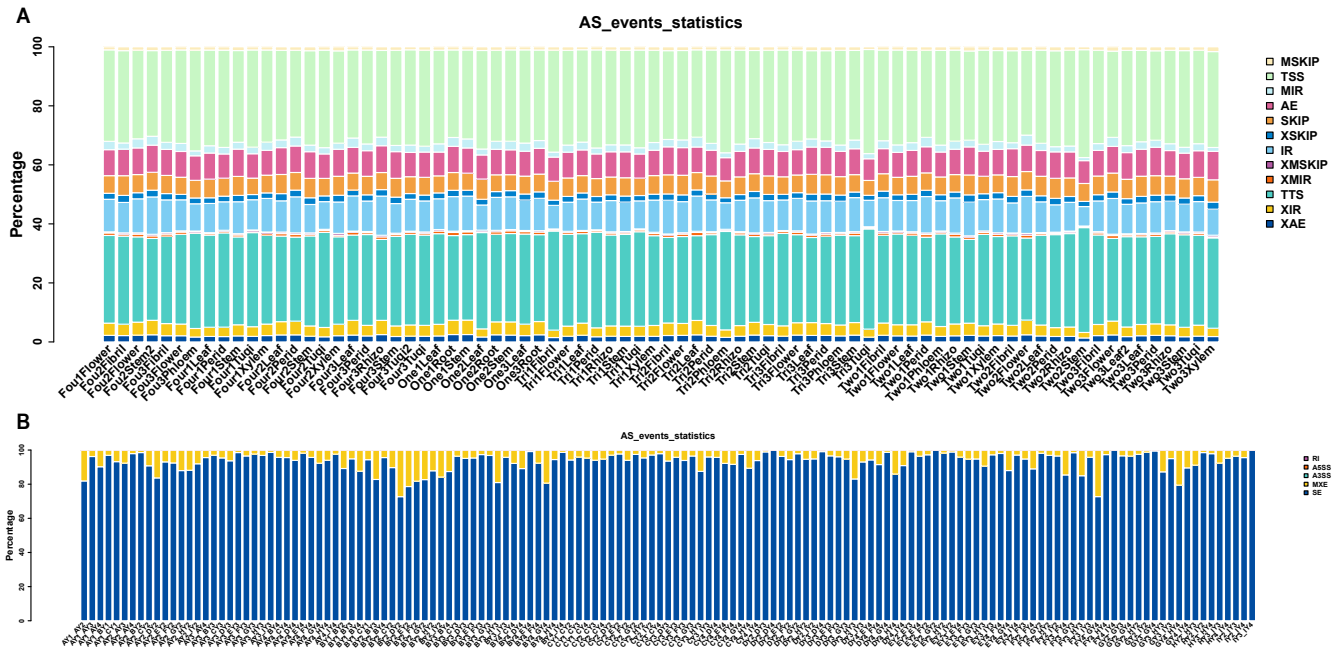

Supplemental Figure 20. Statistics of alternative splicing events. (A) events in each sample; **(B)** different types of alternative splicing events in the comparison groups.

TSS: TranscriptionStart Site; TTS: Transcription Terminal Site; SKIP: Skipped exon; XSKIP: Approximate SKIP; MSKIP: Multi-exon SKIP; XMSKIP: Approximate MSKIP; IR: Intron retention; XIR: Approximate IR; MIR: Multi-IR; XMIR: Approximate MIR; AE: Alternative exon ends (5', 3' or both); XAE: Approximate AE (5' or 3'); A3SS: Alternative 3' splice site; A5SS: Alternative 5' splice site.

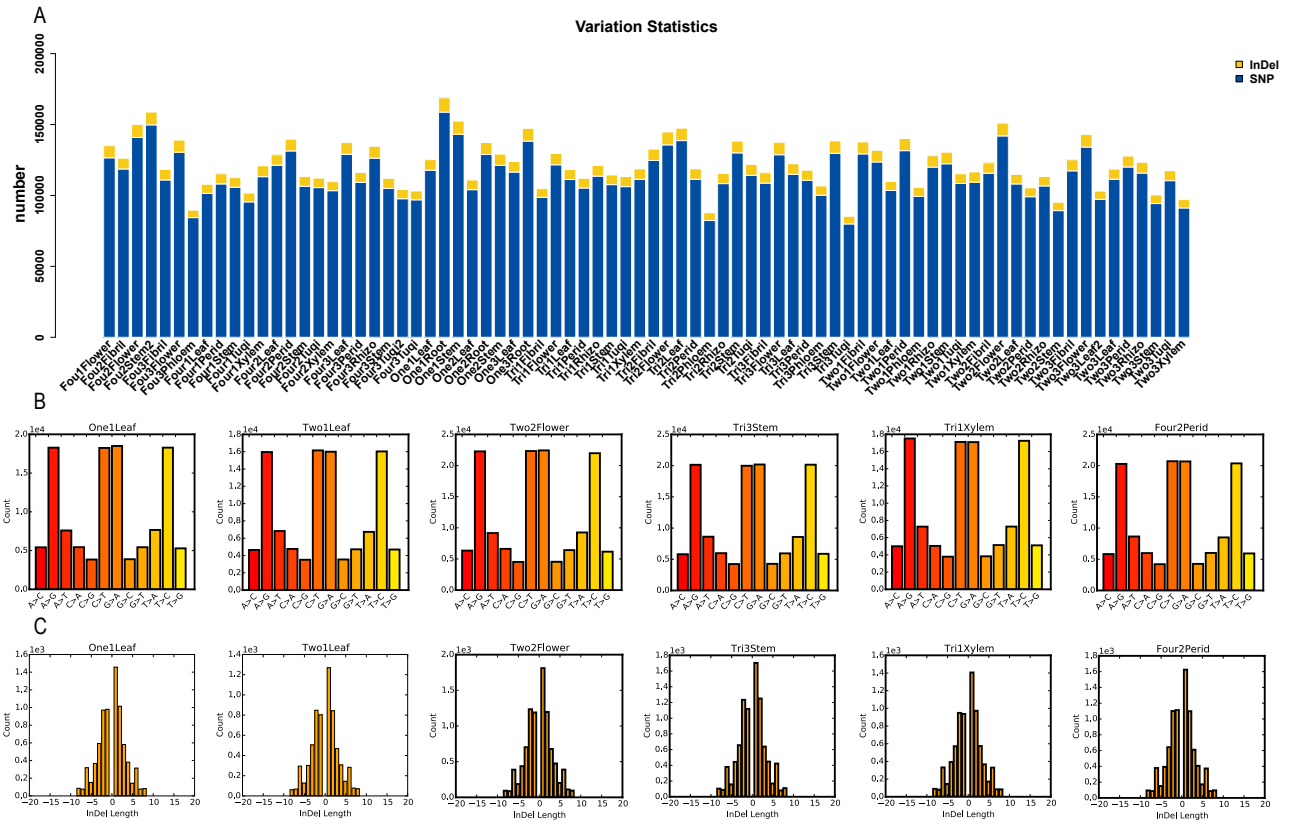

Supplemental Figure 21. Variation analysis of each sample. (A) distribution of each variant type; **(B)** according to the detected SNP loci, the frequency of each mutation type has been counted, taking the data results of One1Leaf, Two1Leaf, Two2Flower, Tri3Stem, Tri1Xylem, Fou2Perid as examples; **(C)** according to the detected InDel loci, the frequency of each InDel length has been counted, taking the data results of One1Leaf, Two1Leaf, Two2Flower, Tri3Stem, Tri1Xylem, Fou2Perid as examples.

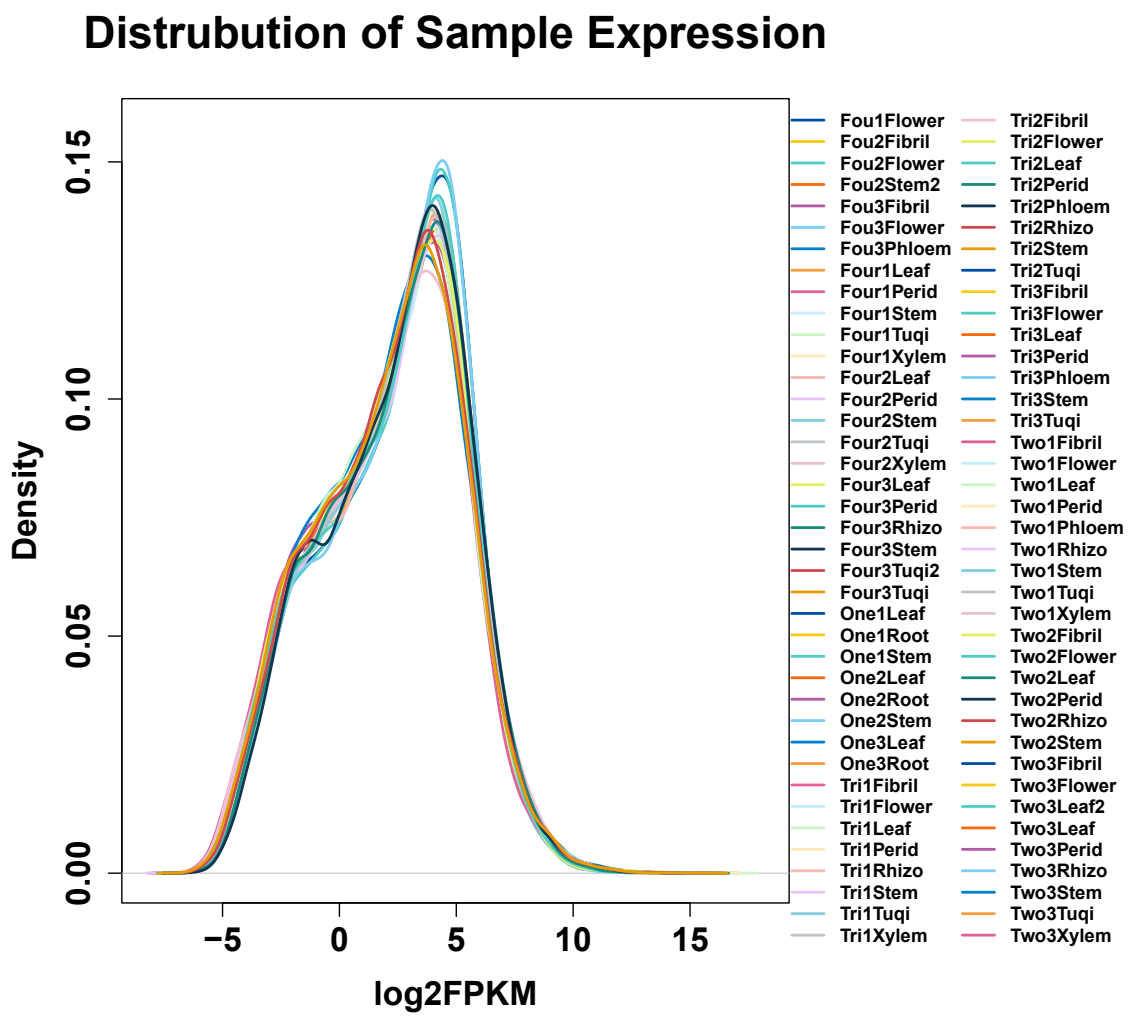

Supplemental Figure 22. Density distribution diagram of gene expression in each transcriptome sample.

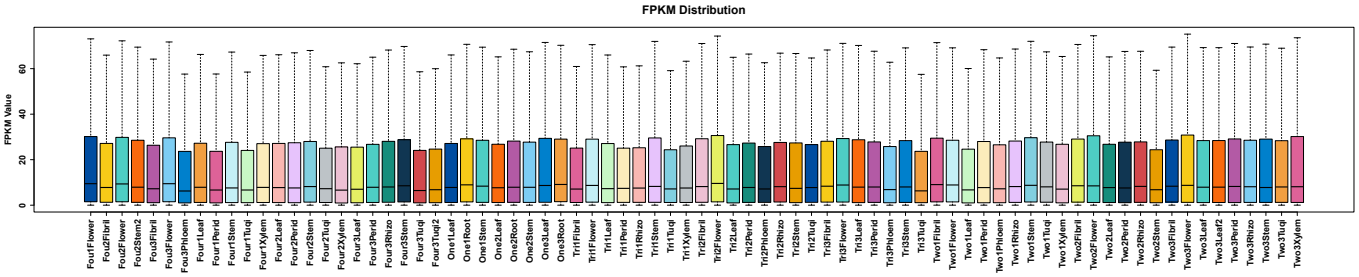

Supplemental Figure 23. Box plot of the overall distribution of gene expression in each transcriptome sample.

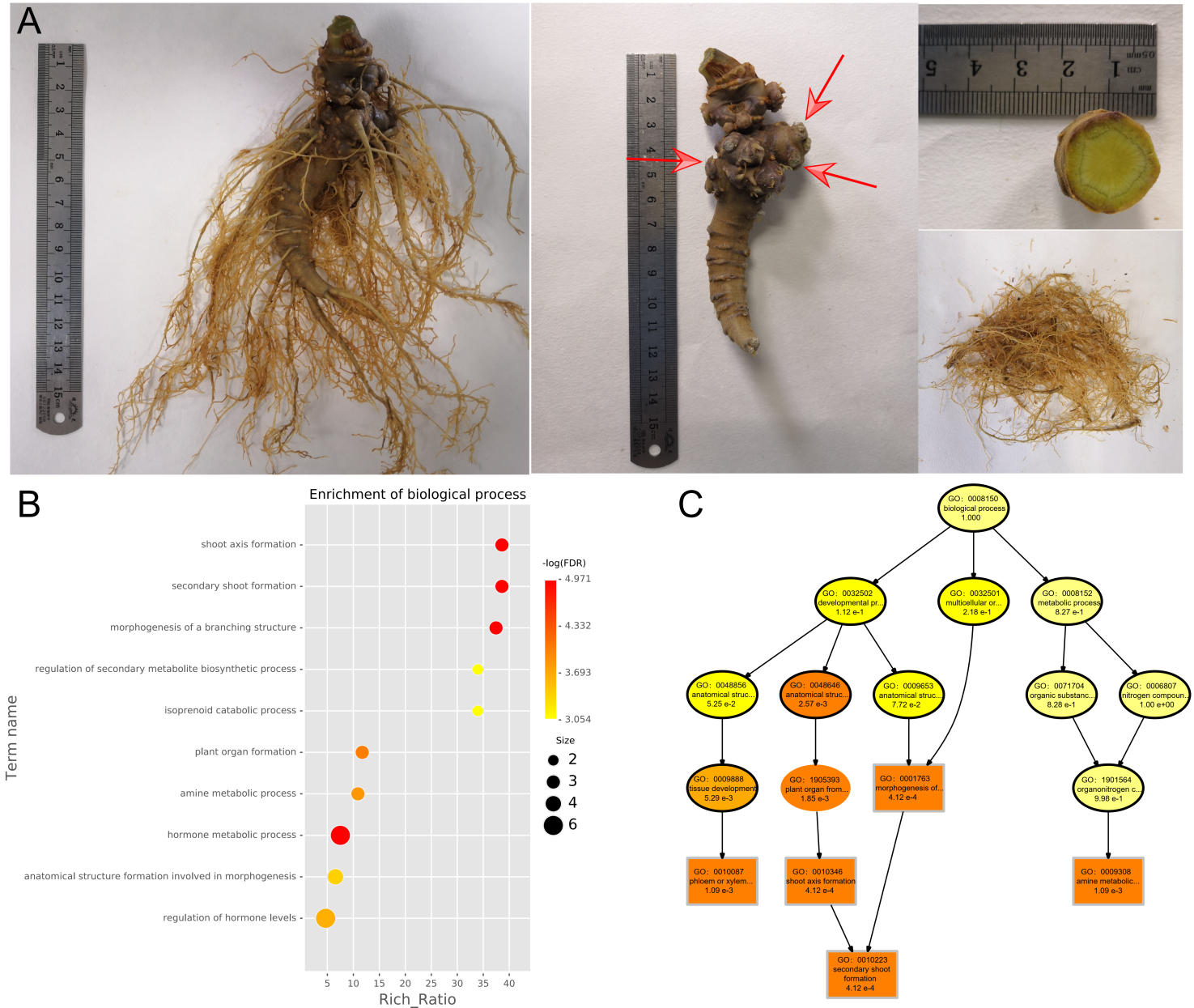

Supplementary Figure 24. The exploration of the molecular mechanism of the formation of *P. notoginseng*'s tubercles. (A) the display of root morphology of *P. notoginseng*, and the red arrow points to the tubercles. **(B)** GO enrichment analysis of DEGs between the periderm and tubercle group. **(C)** the Directed Acyclic Graph (DAG) of GO enrichment analysis, the darker color indicates the more significant enrichment and the red is the most significant. The larger the bubble radius, the higher the rich-ratio value and the redder the color of bubble, the higher the degree of enrichment.

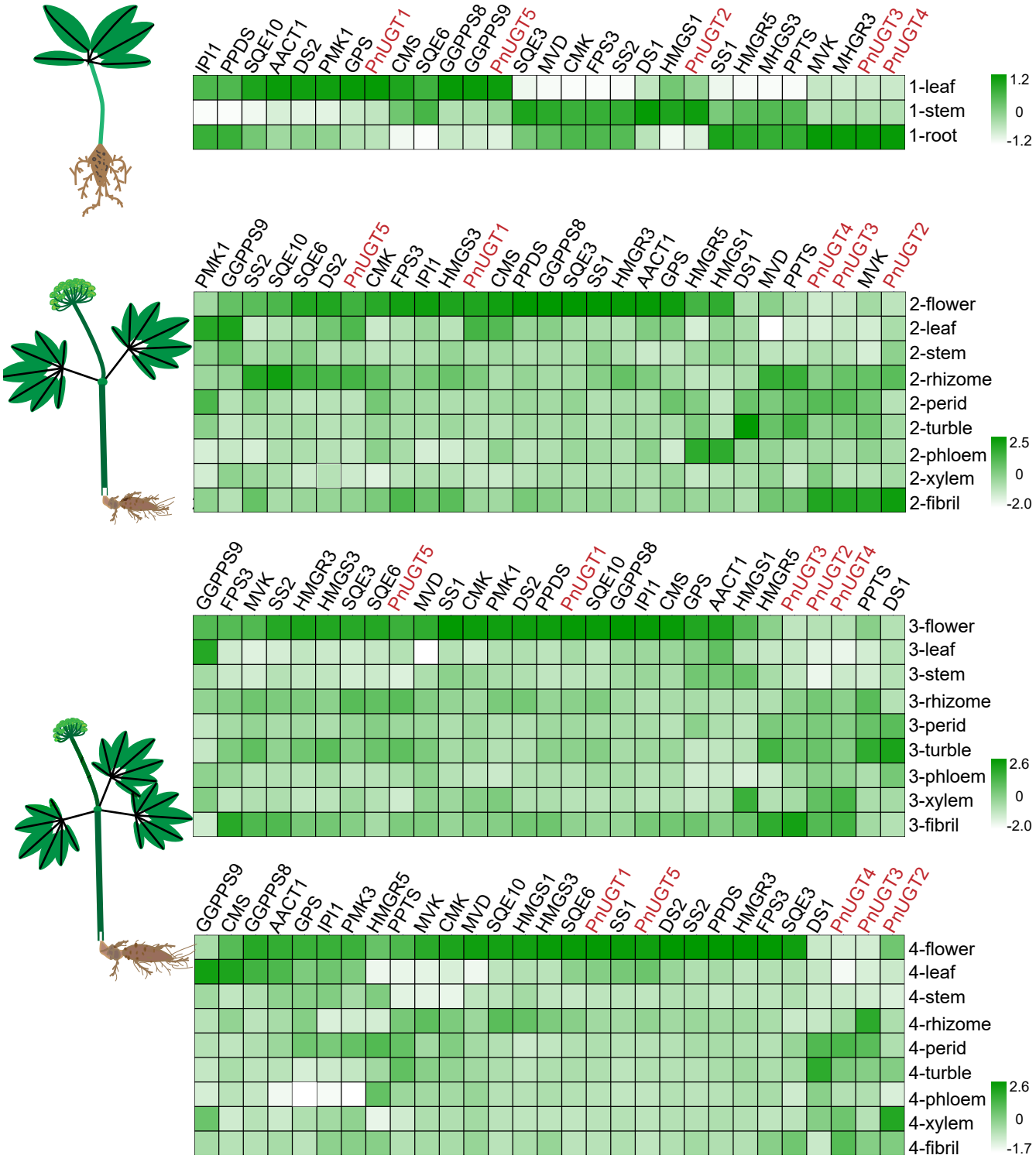

Supplementary Figure 25. Spatial expression profile of key enzyme genes in saponin biosynthesis pathway. The genes in red font are the functional UGT cloned in this study.

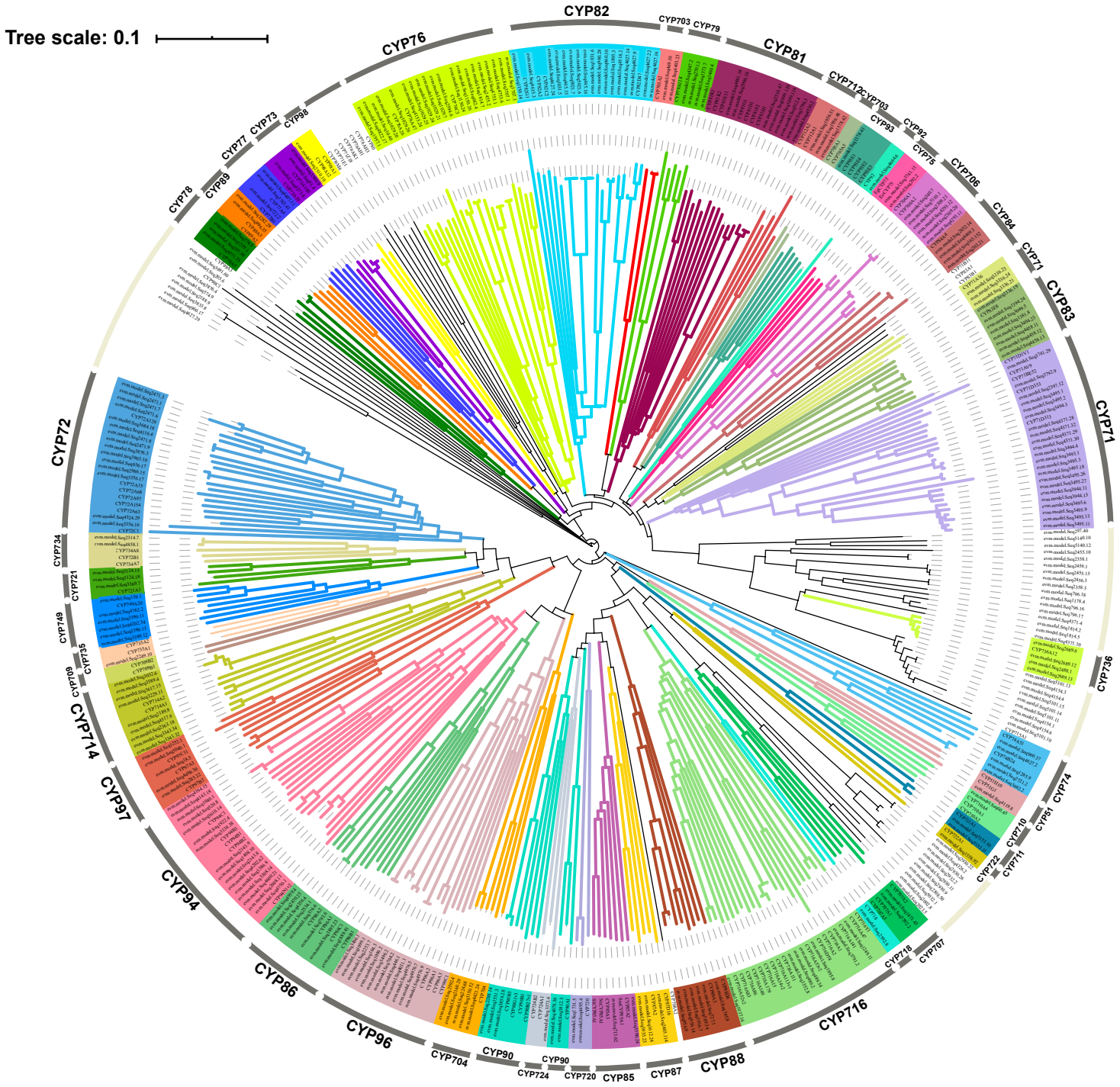

Supplementary Figure 26. Phylogenetic analysis of CYP450 genes in *P. notoginseng* using MEGA-X.

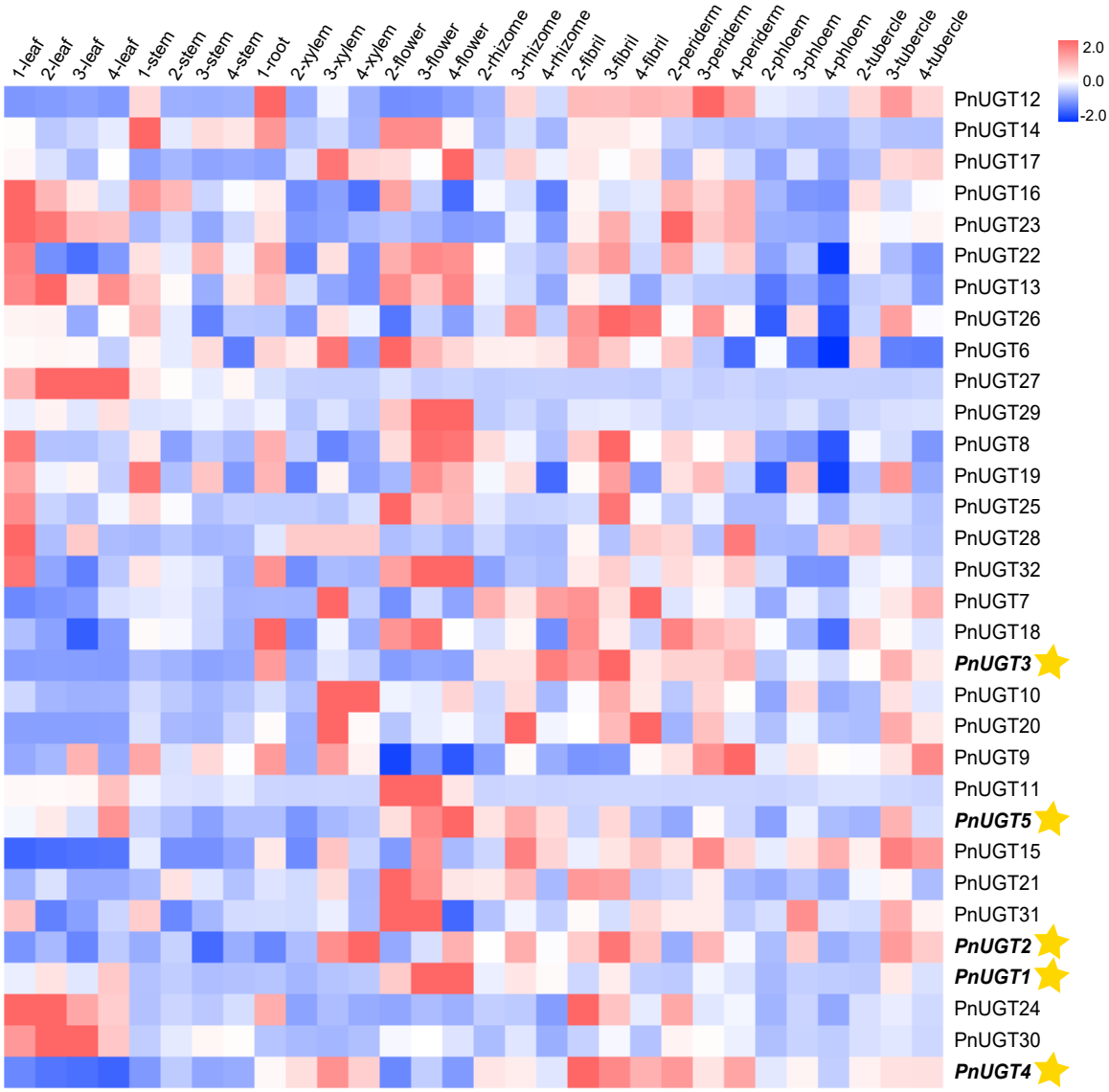

Supplemental Figure 27. Heat map of the expression of the cloned UGT genes in different transcript samples. The genes marked by five-pointed stars are those with catalytic function identified in this study. In the heat map, the relative expression level from high to low (-2 to 2) is represented by the range from blue to red.

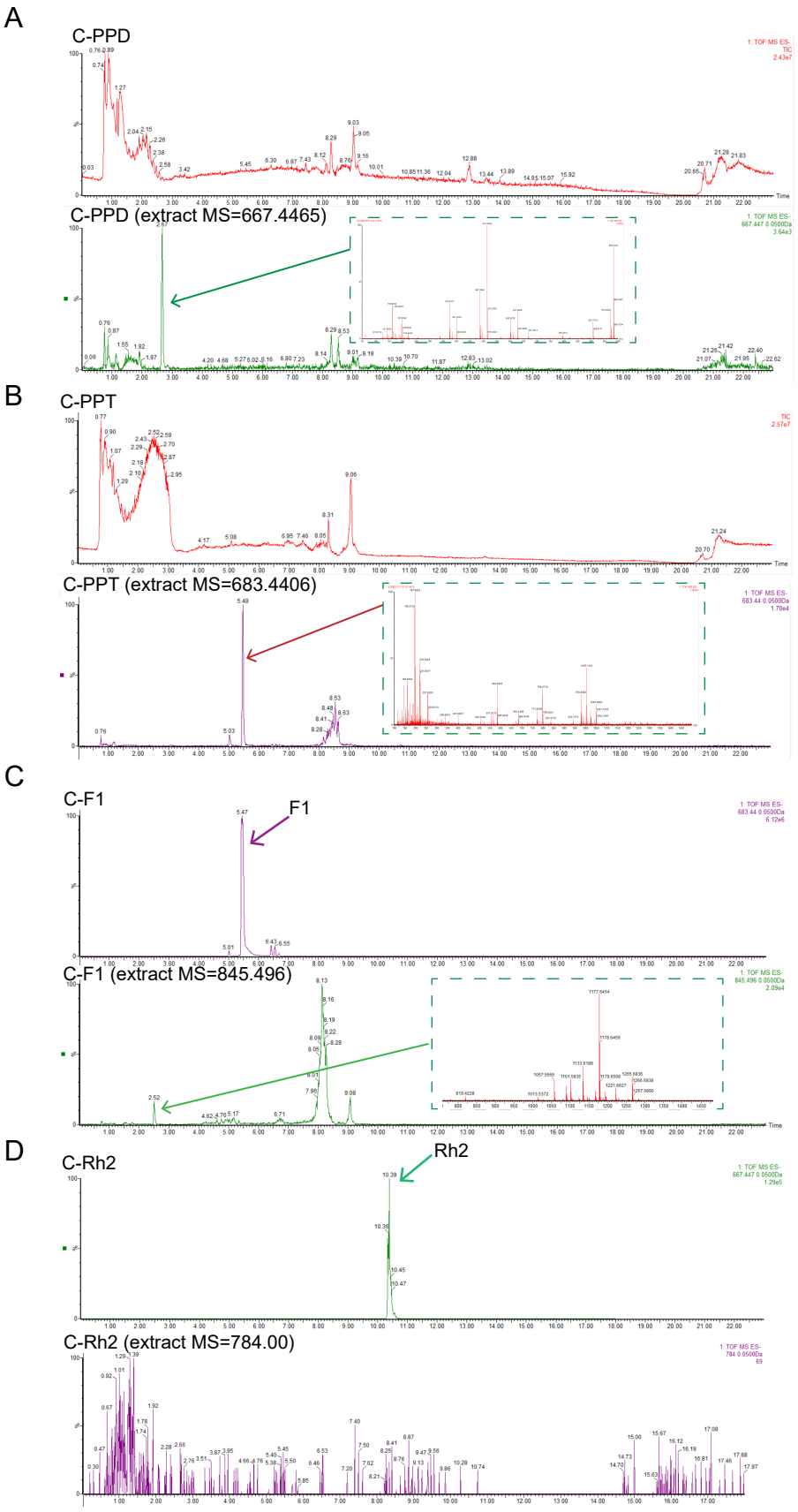

Supplementary Figure 28. The blank control experiments of protein catalytic reaction in this study. **(A)** Analysis results of *E. coli* no-load control with PPD as the catalytic substrate. **(B)** Analysis results of *E. coli* no-load control with PPT as the catalytic substrate. **(C)** Analysis results of *E. coli* no-load control with ginsenoside F1 as the catalytic substrate. **(D)**Analysis results of *E. coli* no-load control with Rh2 as the catalytic substrate. The molecular ion peaks with 667.4465, 683.4406, 845.496 and 784.00 were extracted respectively, and the mass spectrum in the green box did not match with any corresponding glycoside product, indicating no product was formed.

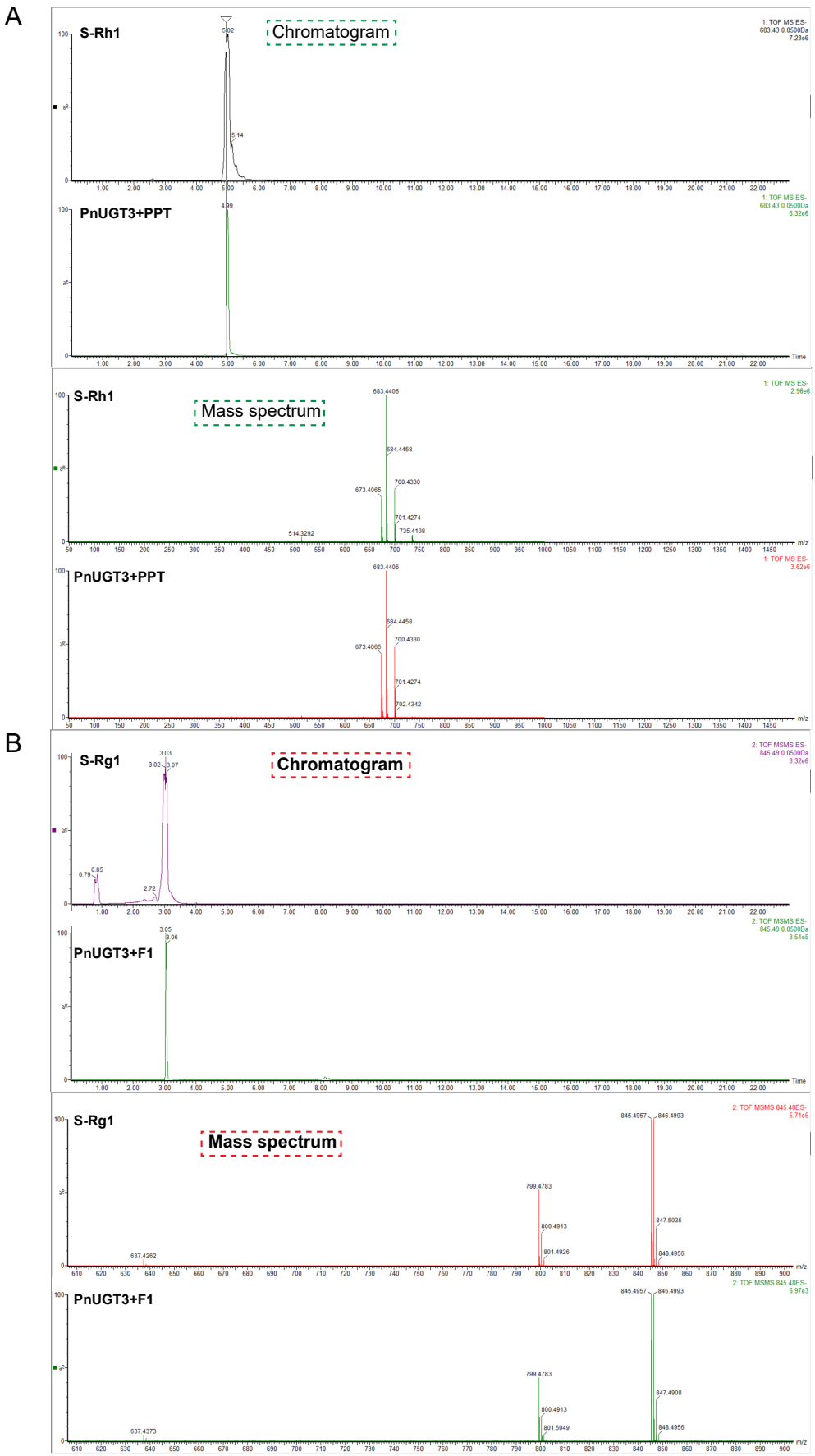

Supplementary Figure 29. UPLC/Q-TOF analysis results of PnUGT3 protein catalytic reaction. **(A)** Chromatograms and mass spectrum of ginsenoside Rh1 standard and PnUGT3 catalytic products using PPT as substrate. **(B)** Chromatograms and mass spectrum of ginsenoside Rg1 standard and PnUGT3 catalytic products using F1 as substrate.

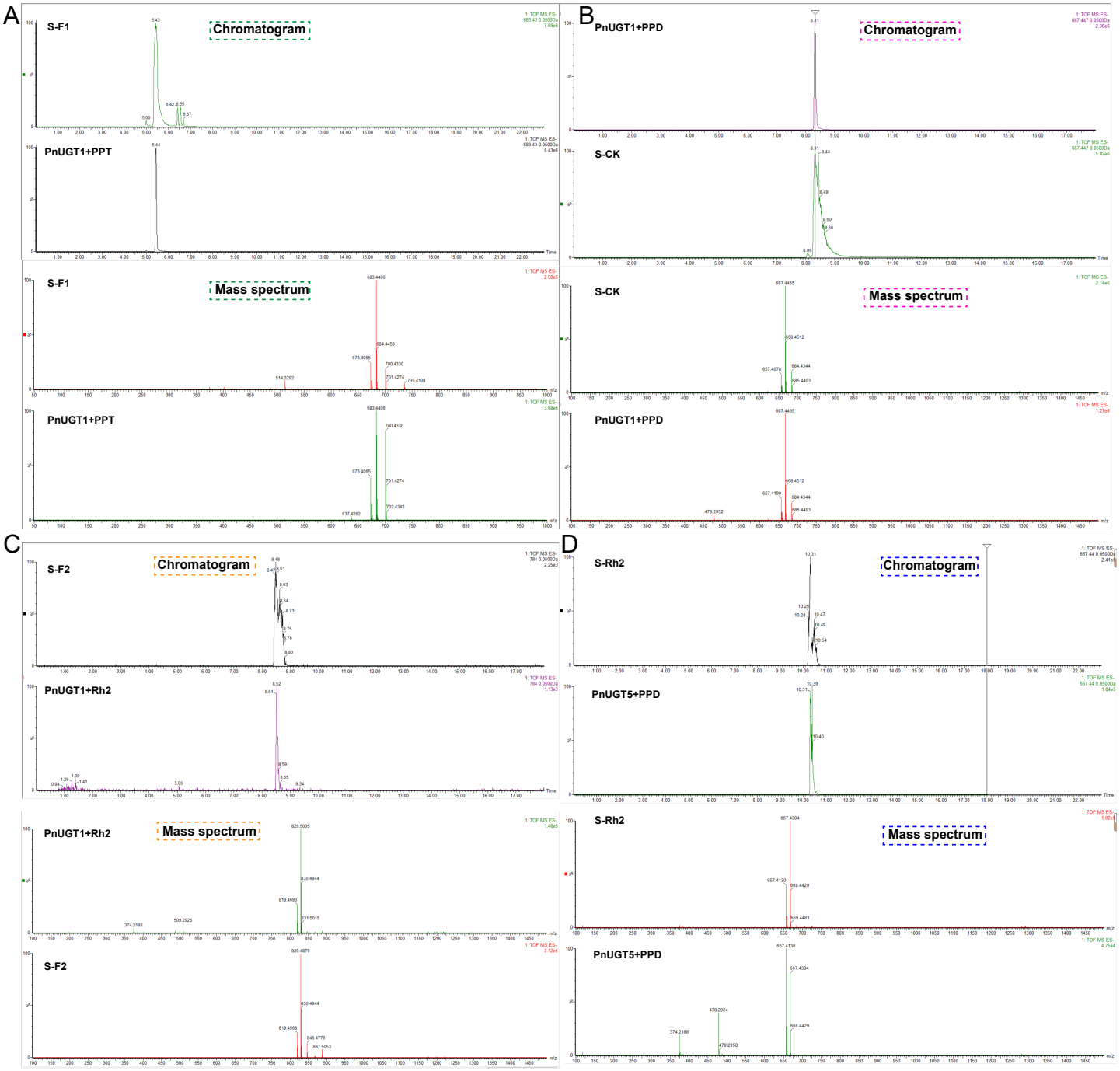

Supplementary Figure 30. UPLC/Q-TOF analysis results of PnUGT1 and PnUGT5 protein catalytic reaction. (A) Chromatograms and mass spectrum of ginsenoside F1 standard and PnUGT1 catalytic products using PPT as substrate. **(B)** Chromatograms and mass spectrum of ginsenoside CK standard and PnUGT1 catalytic products using PPD as substrate. **(C)** Chromatograms and mass spectrum of ginsenoside F2 standard and PnUGT1 catalytic products using Rh2 as substrate. **(D)** Chromatograms and mass spectrum of ginsenoside Rh2 standard and PnUGT5 catalytic products using PPD as substrate.

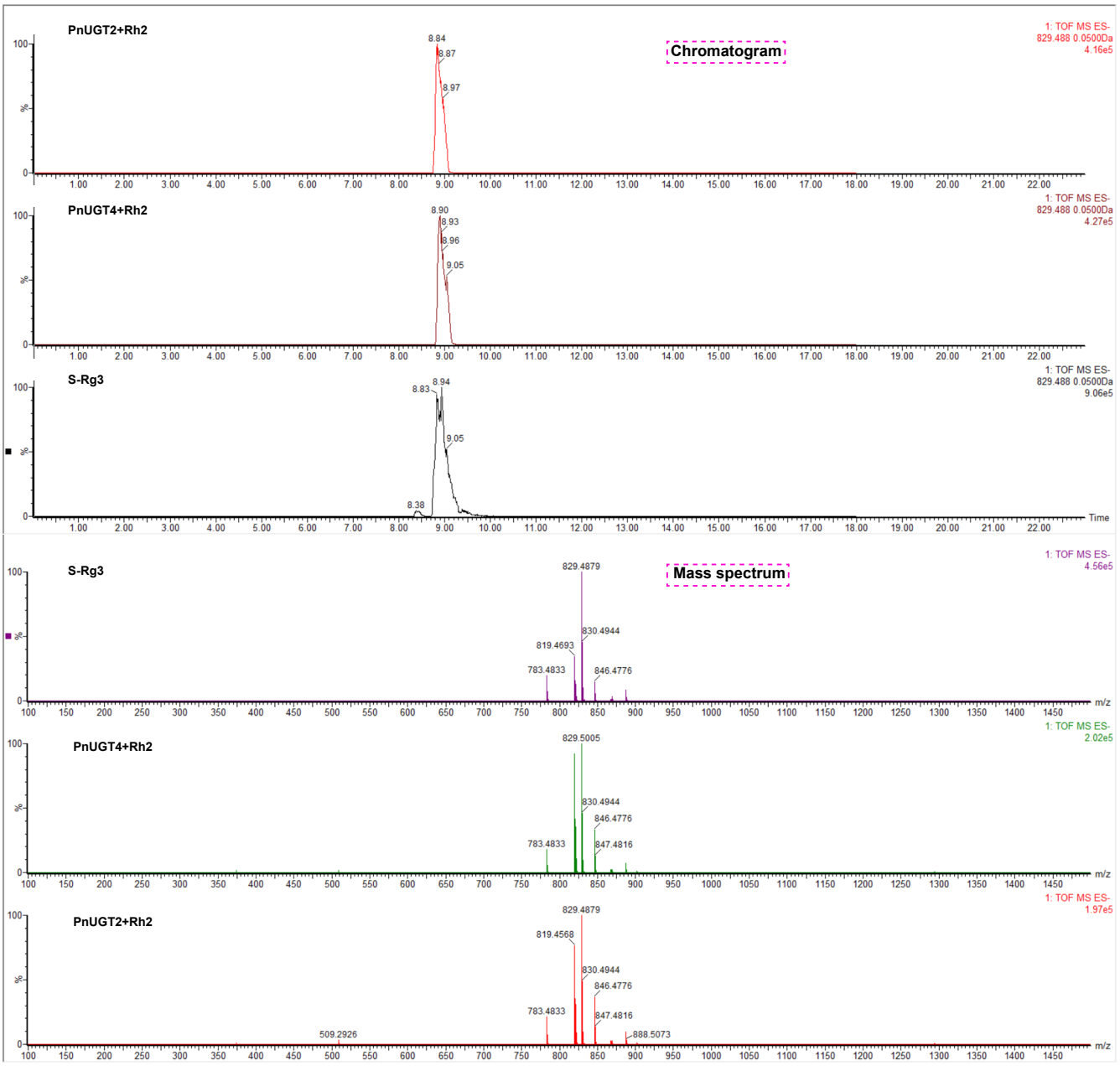

Supplemental Figure 31. UPLC/Q-TOF analysis results of PnUGT2 and PnUGT4 protein catalytic reaction. Chromatograms and mass spectrum of ginsenoside Rg3 standard and PnUGT2 and PnUGT4 catalytic products using Rh2 as substrate.

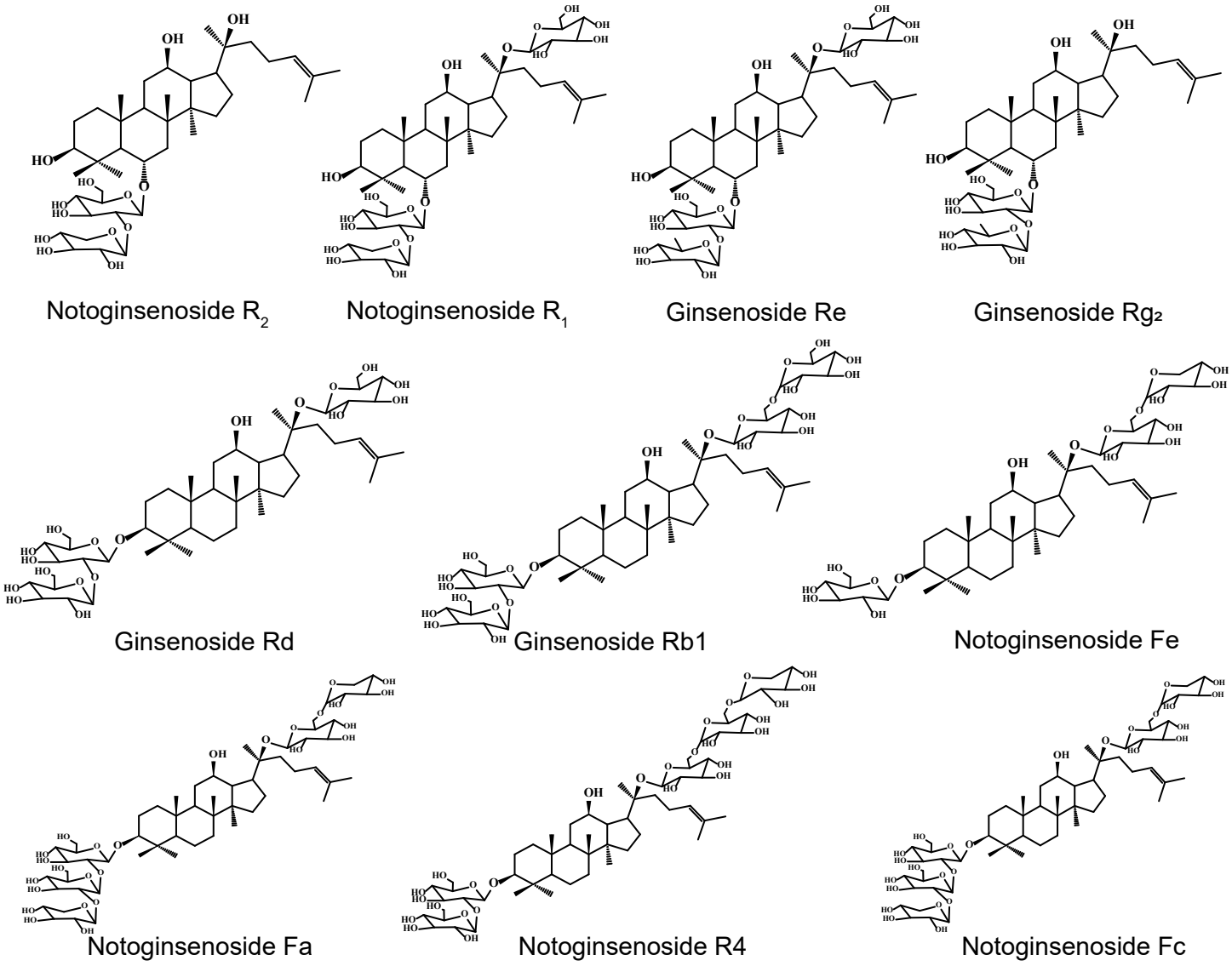

Supplementary Figure 32. The structural formulas of various saponins in *P. notoginseng*.

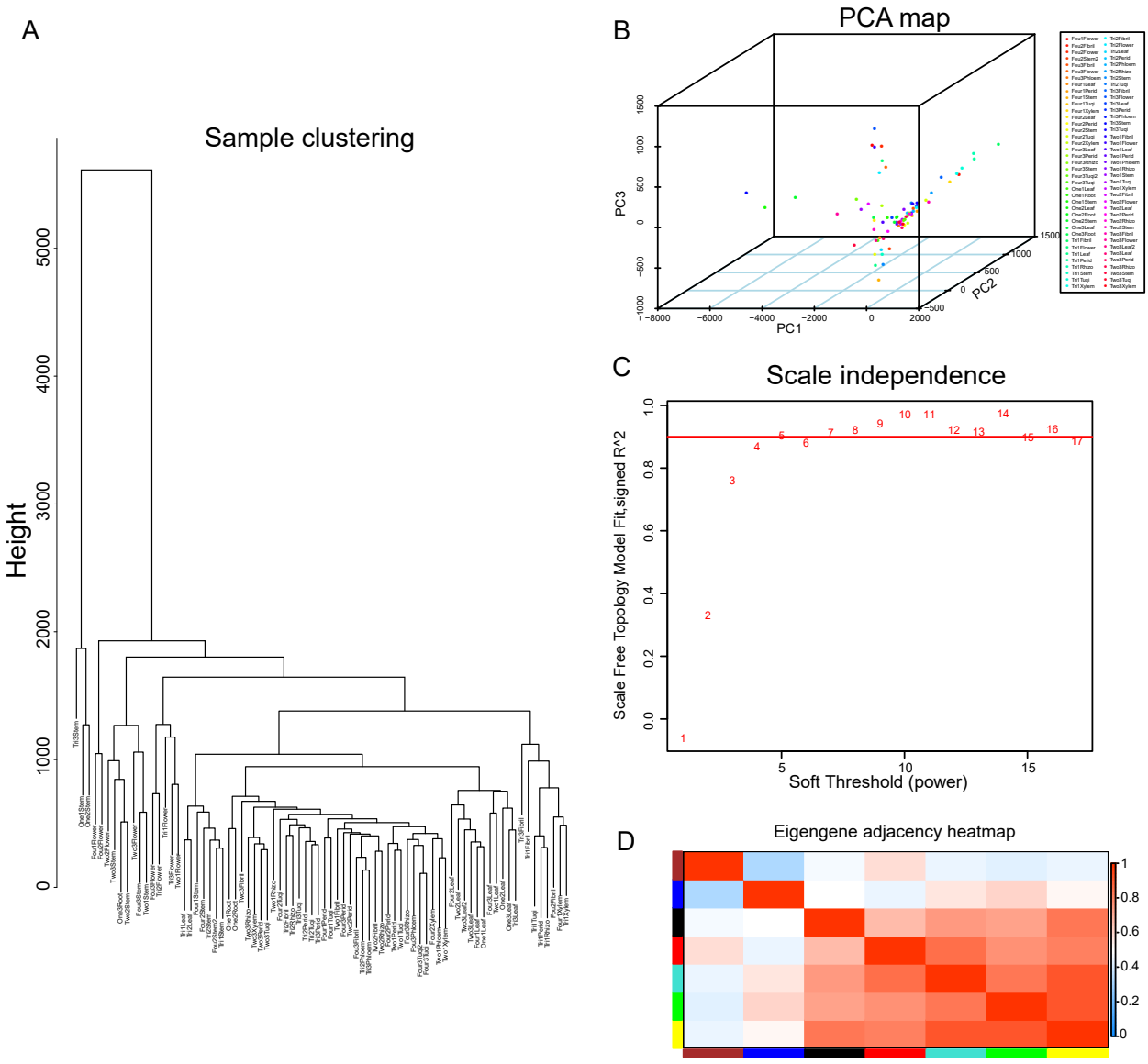

Supplemental Figure 33. WGCAN analysis and characterization of corresponding data.
(A) Construction of the sample clustering evolutionary tree of transcriptome to screen out outliers. **(B)** Construction the PCA map of transcriptome samples. **(C)** Analysis of network topology for various soft-thresholding powers. When we set R^2=0.9, the optimal candidate threshold to reach this height is 10. **(D)** Visualization of the eigengene network representing the relationships among the modules. The redder the color in the heat map, the stronger the correlation between the two modules.

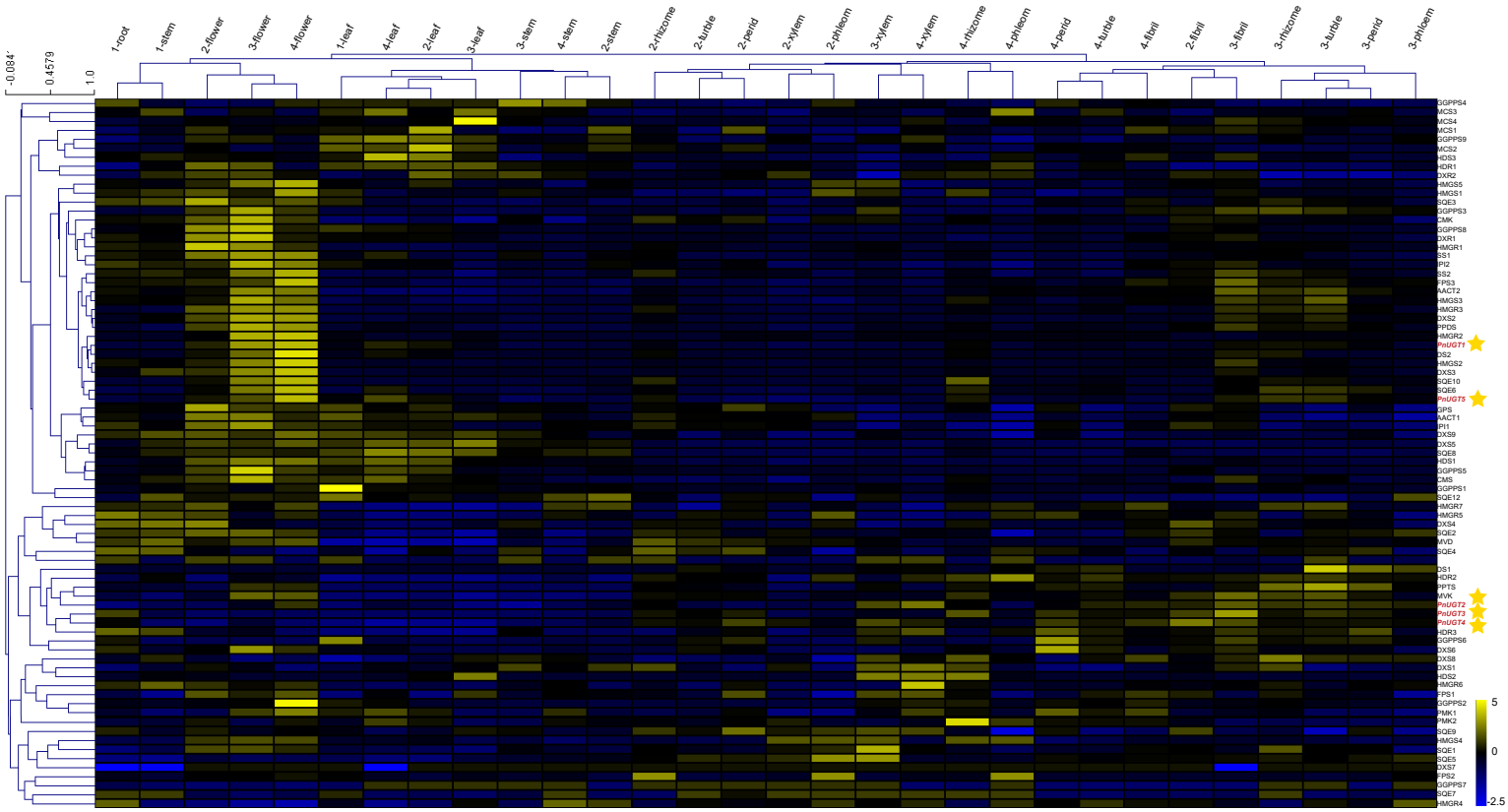

Supplemental Figure 34. Expression profile of key enzyme genes in saponin biosynthesis pathway. The right side of the heatmap shows the evolutionary tree of genes, and genes with similar expression patterns are clustered into one group.

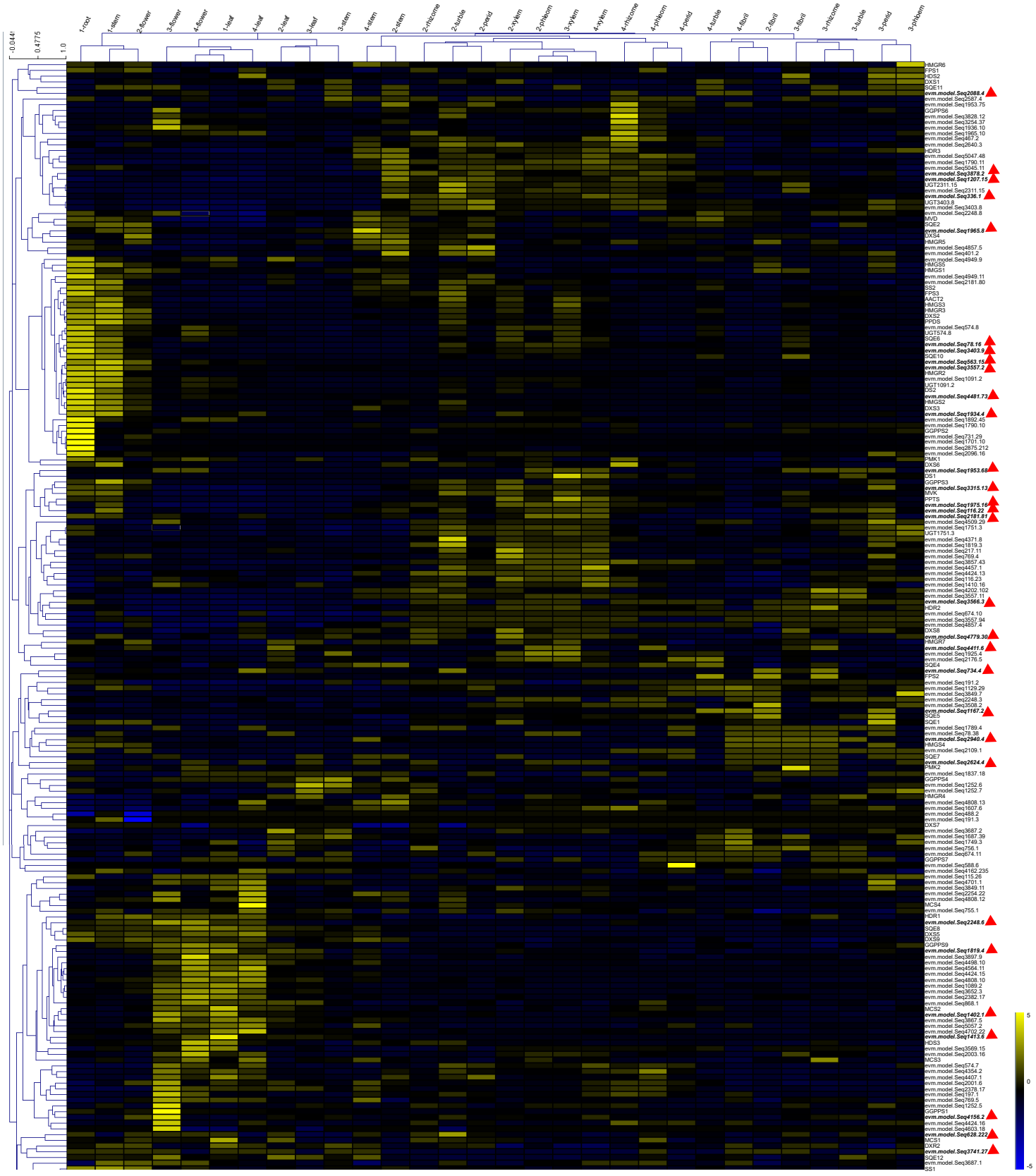

Supplemental Figure 35. Heat map of expression of UGT genes and genes in terpenoid biosynthesis pathway. The right side of the heatmap shows the evolutionary tree of genes, and genes with similar expression patterns are clustered into one group.

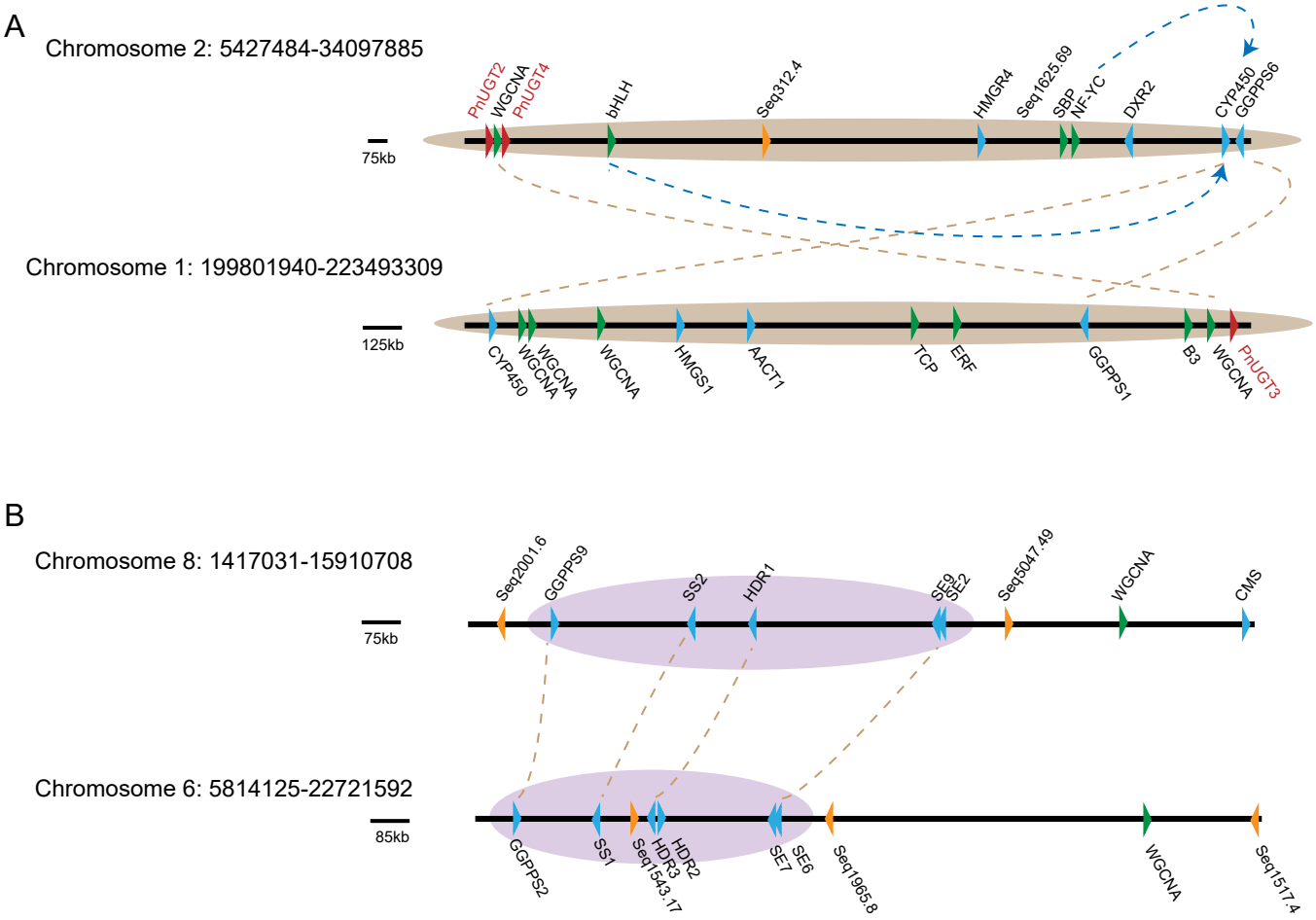

Supplemental Figure 36. Gene clusters involved in saponins biosynthesis found in *P. notoginseng* genome. (A) Gene clusters on chromosomes 1, 2 and their correspondence. **(B)** Gene clusters on chromosomes 6, 8 and their correspondence. Orange lines indicate copies of genes with the same function, and blue lines indicate the correlation between transcription factors and pathway genes.

Supplementary Tables

Supplementary Table 1. Estimation of genome size of *P. notoginseng* based on *K-mer* analysis.

Version	V1.0
Total base (Gb)	231.06
K	31
K-mer number	136,285,293,064
K-mer depth	58
Genome size (Gb)	2.38
Revised genome size (Gb)	2.35
Heterozygous ratio (%)	0.58
Repeat (%)	69.05

Supplementary Table 2. Sequencing data statistics of *P. notoginseng*.

Pair-end libraries	Insert size	Total data (Gb)	Reads length (bp)	Sequence coverage (X)
Illumina reads	350 bp	240.22	150	90.31
Pacbio reads	30 kb	284.07	-	106.79
Hi-C	-	340.83	150	128.13
Total	-	865.12	-	325.23

Supplementary Table 3. The Statistics of Pseudomolecule based on Hi-C technique.

Pseudomolecule	Contig Num	Length
chr1	528	295,554,597
chr2	567	268,893,176
chr3	412	240,203,249
chr4	406	234,363,521
chr5	550	229,146,523
chr6	584	216,472,261
chr7	383	216,178,389
chr8	462	203,820,015
chr9	500	199,351,208
chr10	340	194,535,185
chr11	305	179,501,441
chr12	279	176,575,628
Total anchored	5316	2,654,595,193
Unanchored	44	2,772,262

Supplementary Table 4. Statistic of DNA base composition in the *P. notoginseng* genome.

Iterms	Number(bp)	Percent (%)
A	871,740,949	32.76
T	871,858,137	32.77
C	457,971,493	17.21
G	458,576,639	17.24
N	530,400	0.02
GC	916,548,132	34.45
Total	2,660,147,218	100

Supplementary Table 5. Statistics of consistency assessment of the *P. notoginseng* genome.

Sample	PNCCMU201908
Clean Reads	668,000,000
Clean Bases	100,200,000,000
Mapped Reads	666,778,003
Mapped Reads Rate (%)	99.82
Mapped Bases	99,793,880,477
Mapped Bases Rate (%)	99.59
Mean Depth	37.87
Coverage Rate (%)	97.97

Supplementary Table 6. Assessment the gene coverage rate using BUSCO.

Iterms	Number	Percent (%)
Complete BUSCOs (C)	2,049	96.6
Complete and single-copy BUSCOs (S)	1,495	70.5
Complete and duplicated BUSCOs (D)	554	26.1
Fragmented BUSCOs (F)	23	1.1
Missing BUSCOs (M)	49	2.3
Total BUSCO groups searched	2,121	100

Supplementary Table 7. Annotation of repetitive sequences in the *P. notoginseng* genome.

Type	Repeat length (bp)	% of genome
RepeatMasker	482,030,502	18.12
ProteinMask	597,728,373	22.47
Denovo	2,228,207,907	83.76
TRF	145,037,356	5.45
Total	2,283,667,181	85.85

Supplementary Table 8. Summary of repetitive sequences in the *P. notoginseng* genome.

Class	RepeatMasker TEs		RepeatProteinMasker TEs		RepeatModeler TEs		Combined TEs	
Type	**Length(bp)**	**% in genome**	**Length(bp)**	**% in genome**	**Length(bp)**	**% in genome**	**Length(bp)**	**% in genome**
DNA RT	16,404,105	0.62	6,987,822	0.26	28,157,924	1.06	38,999,478	1.47
LINE	2,256,979	0.08	998,015	0.04	3,718,106	0.14	6,035,132	0.23
SINE	3,185	0	0	0	0	0	3,185	0
LTR RT	463,294,570	17.42	525,365,110	19.75	1,533,286,234	57.64	1,566,296,092	58.88
Unknown	41,143	0	0	0	725,955,721	27.29	725,996,018	27.29
Other	1,185,919	0.07	65,048,999	2.45	7,539,129	0.28	71,825,002	2.7
Total	482,030,502	18.12	597,728,373	22.47	2,228,207,907	83.76	2,271,609,517	85.39

DNA RT：DNA retrotransposons; LINE：long interspersed nuclear elements; SINE：short interspersed nuclear elements; LTR RT：long terminal repeat retrotransposons; Unknown：which have been included in the database, but not classified; Other：Which can be classified by RepeatMasker, but don’t belong to the above categories

Supplementary Table 9. Basic statistical results of gene structure prediction of *P. notoginseng* genome.

Gene set		Number of proteins	Average gene length (bp)	Average CDS length (bp)	Average exon per gene	Average exon length (bp)	Average intron length (bp)
De novo	Augustus	49,549	4,535.36	1,043.08	4.38	238.04	1,033.62
	Genebank	55,883	4,452.17	1,119.06	5.1	219.37	813.69
Homolog	*A. thaliana*	28,931	4379.27	1069.89	4.77	224.13	878.00
	D. carota	32,038	4905.04	1074.87	4.74	226.99	1026.40
	P. ginseng	43,292	4653.92	1000.35	4.51	222.00	1043.04
	P. notoginseng-pub	41238	3031.43	960.98	3.76	255.82	752.13
RNA-seq	cDNA	58,196	5,834.68	925.12	5.09	351.88	990.1
EVM		37,606	5059.63	1202.85	5.21	231.00	917.71

Supplementary Table 10. Basic statistical results of gene structure prediction of *P. notoginseng* and relative species.

Species	Number of proteins	Average gene length (bp)	Average CDS length (bp)	Average exon per gene	Average exon length (bp)	Average intron length (bp)
P. notoginseng	37,606	5059.63	1202.85	5.21	231.00	917.71
P. ginseng	59,352	4213.49	1120.12	5.01	223.53	772.23
D. carota	32,112	3104.08	1187.75	5.01	237.23	479.28
A. thaliana	27,416	1855.01	1209.65	5.08	238.02	159.09
P. notoginseng-pub	34,369	2705	957	3.80	251.39	622.24

Supplementary Table 11. Statistical results of gene function annotation of *P. notoginseng* genome.

Database	Count	Percentage (%)
BLASTP	29,662	78.88
BLASTX	29,510	78.47
GO	29,931	79.59
KO	11,657	31.00
Map	7,459	19.83
NR	35,926	95.53
NT	26,037	69.24
PFAM	28,457	75.67
eggNOG	25,058	66.63
Total_anno	36,154	96.14
Total_unigene	37,606	100

Supplementary Table 12. Statistical results of non-coding RNA of *P. notoginseng* genome.

Class	Type	Copy	Average length (bp)	Total length (bp)	% of genome
miRNA	miRNA	14430	235.19	3393818	0.12758
tRNA	tRNA	1513	73.99	111954	0.00421
rRNA	18S	165	867.15	143079	0.00538
	28S	314	136.11	42737	0.00161
	5.8S	80	148.46	11877	0.00045
	5S	2459	118.23	290726	0.01093
snRNA	CD-box	7216	105.46	760992	0.02861
	HACA-box	272	146.74	39913	0.0015
	splicing	686	154.29	105842	0.00398

Supplementary Table 13. The Statistics of gene clustering to gene families in various species.

Species	Genes number	Genes in families	Unclustered genes	Family number	Unique families	Average genes per family
P. ginseng	59,352	45,808	13,544	17,112	1,658	2.68
D. carota	32,113	26,151	5,962	13,697	972	1.91
V. vinifera	31,845	23,639	8,206	13,987	936	1.69
C. annuum	35,884	28,781	7,103	13,172	1,243	2.19
G. uralensis	34,445	23,729	10,716	13,597	1,029	1.75
A. thaliana	27,416	23,374	4,042	12,739	777	1.83
O. sativa	42,189	30,038	12,151	13,183	2,239	2.28
P. notoginseng	37,525	30,874	6,651	15,655	1,059	1.97

Supplementary Table 14. Enriched GO terms of genes in *P. notoginseng*-specific families.

Accession	Ontology	Term name	p-value	FDR
GO:0042256	BP	mature ribosome assembly	8.69E-12	6.55E-09
GO:1901566	BP	organonitrogen compound biosynthetic process	8.65E-12	6.55E-09
GO:0034622	BP	cellular macromolecular complex assembly	3.60E-12	6.55E-09
GO:0065003	BP	macromolecular complex assembly	3.02E-11	1.71E-08
GO:0009260	BP	ribonucleotide biosynthetic process	8.70E-11	2.81E-08
GO:0009156	BP	ribonucleoside monophosphate biosynthetic process	6.66E-11	2.81E-08
GO:0046390	BP	ribose phosphate biosynthetic process	8.70E-11	2.81E-08
GO:0042255	BP	ribosome assembly	1.15E-10	3.26E-08
GO:0009124	BP	nucleoside monophosphate biosynthetic process	1.35E-10	3.39E-08
GO:0043933	BP	macromolecular complex subunit organization	1.78E-10	4.03E-08
GO:0044445	CC	cytosolic part	4.10E-12	1.66E-09
GO:0022626	CC	cytosolic ribosome	1.56E-10	3.16E-08
GO:0044391	CC	ribosomal subunit	4.19E-10	5.66E-08
GO:0022625	CC	cytosolic large ribosomal subunit	8.47E-10	8.58E-08
GO:0005829	CC	cytosol	2.56E-09	2.08E-07
GO:0032991	CC	macromolecular complex	9.62E-09	6.49E-07
GO:0005774	CC	vacuolar membrane	1.40E-08	8.11E-07
GO:0044437	CC	vacuolar part	2.61E-08	1.32E-06
GO:0098805	CC	whole membrane	6.13E-08	2.76E-06
GO:1990904	CC	ribonucleoprotein complex	3.78E-07	1.39E-05
GO:0036094	MF	small molecule binding	1.97E-13	1.15E-10
GO:0000166	MF	nucleotide binding	9.22E-13	1.15E-10
GO:0032559	MF	adenyl ribonucleotide binding	5.37E-13	1.15E-10
GO:0043168	MF	anion binding	2.64E-13	1.15E-10
GO:0005524	MF	ATP binding	4.75E-13	1.15E-10
GO:0032553	MF	ribonucleotide binding	1.11E-12	1.15E-10
GO:0008144	MF	drug binding	1.03E-12	1.15E-10
GO:0030554	MF	adenyl nucleotide binding	6.48E-13	1.15E-10
GO:0097367	MF	carbohydrate derivative binding	1.21E-12	1.15E-10
GO:1901265	MF	nucleoside phosphate binding	9.22E-13	1.15E-10

Supplementary Table 15. Enriched GO terms of genes in expanded gene families.

Accession	Ontology	Term name	FDR
GO:0006313	BP	transposition, DNA-mediated	1.32E-60
GO:0032196	BP	transposition	8.91E-49
GO:0006636	BP	unsaturated fatty acid biosynthetic process	1.41E-45
GO:0033559	BP	unsaturated fatty acid metabolic process	5.30E-45
GO:0006310	BP	DNA recombination	1.96E-18
GO:0022900	BP	electron transport chain	7.47E-12
GO:0006633	BP	fatty acid biosynthetic process	8.70E-12
GO:0019684	BP	photosynthesis, light reaction	1.62E-09
GO:0072330	BP	monocarboxylic acid biosynthetic process	5.02E-09
GO:0042773	BP	ATP synthesis coupled electron transport	1.57E-08
GO:0070469	CC	respiratory chain	1.53E-10
GO:0031224	CC	intrinsic component of membrane	1.56E-06
GO:0016021	CC	integral component of membrane	1.61E-06
GO:0031966	CC	mitochondrial membrane	2.59E-06
GO:0031897	CC	Tic complex	2.72E-05
GO:0005743	CC	mitochondrial inner membrane	3.62E-05
GO:0019822	CC	P4 peroxisome	9.83E-05
GO:0044425	CC	membrane part	0.000117
GO:0005739	CC	mitochondrion	0.000153
GO:0000799	CC	nuclear condensin complex	0.000217
GO:0004803	MF	transposase activity	4.81E-61
GO:0016717	MF	oxidoreductase activity, acting on paired donors, with oxidation of a pair of donors resulting in the reduction of molecular oxygen to two molecules of water	1.29E-51
GO:0102985	MF	Delta12-fatty-acid desaturase activity	1.08E-40
GO:0008234	MF	cysteine-type peptidase activity	8.78E-27
GO:0008270	MF	zinc ion binding	9.82E-23
GO:0019863	MF	IgE binding	3.20E-18
GO:0019865	MF	immunoglobulin binding	3.20E-18
GO:0140097	MF	catalytic activity, acting on DNA	2.89E-15
GO:0008483	MF	transaminase activity	1.96E-13
GO:0016769	MF	transferase activity, transferring nitrogenous groups	1.96E-13

Supplementary Table 16. Enriched GO terms of genes in contracted gene families.

Accession	Ontology	Term name	FDR
GO:0006468	BP	protein phosphorylation	2.63404E-66
GO:0016310	BP	phosphorylation	1.3388E-65
GO:0006796	BP	phosphate-containing compound metabolic process	5.17223E-36
GO:0006793	BP	phosphorus metabolic process	6.21129E-36
GO:0006464	BP	cellular protein modification process	1.40587E-24
GO:0036211	BP	protein modification process	1.40587E-24
GO:0005975	BP	carbohydrate metabolic process	6.30804E-24
GO:0051274	BP	beta-glucan biosynthetic process	3.40873E-23
GO:0051273	BP	beta-glucan metabolic process	9.58801E-23
GO:0048544	BP	recognition of pollen	7.66426E-21
GO:0005886	CC	plasma membrane	1.35E-59
GO:0031224	CC	intrinsic component of membrane	2.26E-36
GO:0016021	CC	integral component of membrane	2.27E-36
GO:0016020	CC	membrane	5.87E-33
GO:0044425	CC	membrane part	2.47E-28
GO:0009341	CC	beta-galactosidase complex	8.93E-13
GO:0005576	CC	extracellular region	3.69E-11
GO:0016459	CC	myosin complex	3.69E-11
GO:0044459	CC	plasma membrane part	6.17481E-10
GO:0000148	CC	1,3-beta-D-glucan synthase complex	1.82574E-08
GO:0017076	MF	purine nucleotide binding	7.86457E-88
GO:0032555	MF	purine ribonucleotide binding	7.86457E-88
GO:0035639	MF	purine ribonucleoside triphosphate binding	9.1967E-88
GO:0032553	MF	ribonucleotide binding	4.82089E-87
GO:0008144	MF	drug binding	5.31098E-86
GO:0097367	MF	carbohydrate derivative binding	4.96901E-85
GO:0032559	MF	adenyl ribonucleotide binding	4.96901E-85
GO:0030554	MF	adenyl nucleotide binding	8.50134E-85
GO:0005524	MF	ATP binding	1.24308E-84
GO:0043168	MF	anion binding	8.90045E-80

Supplementary Table 17. Copy number variation of genes involved in the ginsenoside biosynthesis in the *P. notoginseng* and seven other plant species.

Gene	PN	PG	DC	CA	VV	GU	AT	OS
AACT	2	4	2	2	2	3	2	2
HMGS	5	8	1	6	7	3	1	3
HMGR	7	17	3	10	3	4	2	3
MVK	1	2	1	1	1	1	1	1
PMK	2	4	2	0	1	2	0	1
MVD	1	2	1	2	1	1	2	2
DXS	9	13	5	3	8	5	3	3
DXR	2	4	1	1	1	3	1	1
CMS	1	2	2	1	1	1	1	1
CMK	1	2	1	1	1	1	1	1
MCS	4	4	1	1	1	1	1	1
HDS	3	4	2	1	1	1	1	1
HDR	3	6	3	3	1	1	1	2
IDI	2	3	1	3	2	0	2	2
GPS	1	2	1	1	1	2	1	2
FPS	3	5	1	2	1	1	2	5
GGPS	9	16	7	5	3	3	12	3
SS	2	4	1	2	1	2	2	2
SQE	12	25	7	7	8	8	9	4
DS	2	4	1	1	2	1	1	1
CYP450	336	482	311	480	410	257	248	360
GT	158	222	117	4	228	91	112	193
Total	566	835	472	537	685	392	406	594

PN: *P. notoginseng*; PG: *P. ginseng*; DC: *D. carota*; CA: *C. annuum*; VV: *V. vinifera*; GU: *G. uralensis*; AT: *A. thaliana*; OS: *O. sativa*

Supplementary Table 18. *Ks* values and duplication times of genes involved in ginsenoside biosynthesis in *P. notoginseng*.

GENE	Paralog1	Paralog2	*Ka*	*Ks*	MYA
AACT	Seq3227.16	Seq4366.20	0.1	1.4065	108.2
DS	Seq60.43	Seq2181.91	0.1218	0.608	46.8
DXR	Seq3336.90	Seq4886.4	0.0477	0.3082	23.7
DXS	Seq1892.29	Seq3392.7	0.1258	0.4184	32.2
DXS	Seq125.2	Seq2176.8	2.0513	0.4374	33.6
DXS	Seq125.2	Seq2599.2	2.0513	0.4374	33.6
DXS	Seq4710.4	Seq4702.20	0.0005	0.464	35.7
DXS	Seq1892.29	Seq3331.15	0.0541	0.5084	39.1
FPS	Seq4090.9	Seq4036.46	0.2527	0.421	32.4
GGPPS	Seq3857.39	Seq1249.12	0.0964	0.402	30.9
GGPPS	Seq2027.16	Seq3857.39	0.1699	1.6357	125.8
HDR	Seq580.1	Seq1543.10	0.0722	0.4323	33.3
HDS	Seq1699.17	Seq3612.118	0.0246	0.2446	18.8
HMGR	Seq1207.10	Seq2093.13	0.0239	0.3989	30.7
HMGS	Seq1609.4	Seq2103.7	0.0185	0.3479	26.8
HMGS	Seq3714.31	Seq1609.4	0.0488	1.4359	110.5
IPI	Seq4782.43	Seq4782.31	0.0277	0.0417	3.2
MCS	Seq311.72	Seq527.2	0.0731	0.5548	42.7
PMK	Seq1071.3	Seq2875.187	0.2405	0.3632	27.9
SQE	Seq734.26	Seq2337.9	0.0447	0.5602	43.1
SQE	Seq734.26	Seq3238.6	0.1236	1.5512	119.3
SS	Seq1220.5	Seq5026.3	0.0469	0.197	15.2
UGT	Seq1751.3	Seq3403.8	0.0454	0.0872	6.7
UGT	Seq2311.15	Seq1091.2	0.064	0.1306	10

Supplementary Table 22. Representative genes which are highly expressed in tubercle group.

Gene ID	P value	Annotation description	GO terms
Seq1082.27	5.9E-06	carotenoid cleavage dioxygenase 7	GO:0016121|carotene catabolic process; GO:0010223|secondary shoot formation; GO:1901601|strigolactone biosynthetic process;
Seq4384.8	0.0002419	carotenoid cleavage dioxygenase 8	GO:0016121|carotene catabolic process; GO:0010223|secondary shoot formation; GO:1901601|strigolactone biosynthetic process;
Seq2249.10	0.013745	Cytokinin hydroxylase	GO:0033466|trans-zeatin biosynthetic process;
Seq2362.18	0.013745	Cytokinin dehydrogenase 6	GO:0009690|cytokinin metabolic process; GO:0010103|stomatal complex morphogenesis;
Seq4266.75	0.002591	Expansin-A4	GO:0009664|plant-type cell wall organization; GO:0006949|syncytium formation;
Seq1722.34	0.001241	Protein WALLS ARE THIN 1	GO:0009851|auxin biosynthetic process; GO:0010315|auxin efflux; GO:0009734|auxin-activated signaling pathway; GO:0071555|cell wall organization;

Supplementary Table 23. Statistics of transcription factors in *P. notoginseng* genome.

TF family	Gene copy number
bHLH	188
ERF	175
NAC	141
MYB	128
C2H2	114
MYB_related	105
bZIP	91
GRAS	91
WRKY	90
G2-like	72
HD-ZIP	71
C3H	57
LBD	57
Trihelix	57
FAR1	52
B3	49
AP2	40
Dof	40
ARF	34
GATA	33
SBP	33
TCP	33
M-type_MADS	28
HSF	25
TALE	25
NF-YB	21
HB-other	19
NF-YC	19
WOX	18
MIKC_MADS	17
Nin-like	17
GRF	15
NF-YA	15
ZF-HD	15
GeBP	14
BES1	13
DBB	13
E2F/DP	13
BBR-BPC	12
CO-like	12
CPP	12

CAMTA	11
ARR-B	10
YABBY	10
HRT-like	8
SRS	7
EIL	6
LSD	5
RAV	5
STAT	3
HB-PHD	2
LFY	2
NF-X1	2
S1Fa-like	2
Whirly	2
SAP	1
VOZ	1
Total	2150

Supplementary Table 25. The CYP450 genes used to construct phylogenetic tree in this research.

Subfamily	Gene name	Genbank number	Reference
CYP51	CYP51G1	DQ335779.1	(Li et al., 2007)
	CYP51H10	DQ680852.1	(Qi et al., 2006)
CYP710	CYP710A1	NM_129002.3	(Lin et al., 1999)
	CYP710A4	NM_128445.3	(Lin et al., 1999)
	CYP710A2	NM_129001.3	(Lin et al., 1999)
CYP711	MAX1(CYP711A1)	NM_179743.2	(Lin et al., 1999)
CYP74	CYP74A51	LC063857.1	unpublished
	CYP74B24	LC063856.1	unpublished
CYP97	CYP97A3	NM_102914.3	(Theologis et al., 2000)
	CYP97C11	EU849604.1	(Stigliani et al., 2011)
	CYP97B3	NM_117600.6	(Mayer et al., 1999)
CYP704	CYP704	AY779540.1	(Ro et al., 2005)
CYP94	CYP94B1	NM_125740.3	(Tabata et al., 2000)
	CYP94B2	NM_111056.3	(Salanoubat et al., 2000)
	CYP94B3	NM_114710.3	(Salanoubat et al., 2000)
	CYP94C1	NM_128328.3	(Lin et al., 1999)
	CYP94N1v2	KJ869255.1	(Augustin et al., 2015)
CYP86	CYP86A1	MF197861.1	(Shi et al., 2018)
	CYP86A2	NM_116260.4	(Mayer et al., 1999)
	CYP86B1	NM_122225.3	(Tabata et al., 2000)
	CYP86C1	NM_102298.3	(Theologis et al., 2000)
CYP96	CYP96A1	NM_127882.3	(Lin et al., 1999)
	CYP96C1	AJ238402.1	(Oudin et al., 1999)
	CYP96A2	NM_119369.4	(Mayer et al., 1999)
	CYP96A3	NM_105208.1	(Theologis et al., 2000)
CYP88	CYP88D6	MG888351.1	unpublished
	CYP88A3	NM_100394.4	(Theologis et al., 2000)
CYP716	CYP716A52v2	JX036032.1	(Han et al., 2012)
	CYP716A83	KU878849.1	unpublished
	CYP716A86	KU878848.1	unpublished
	CYP716A14v2	KF309251.1	unpublished
	CYP716A140	KU878853.1	unpublished
	CYP716A15	AB619802.1	(Fukushima et al., 2011)
	CYP716A179	LC157867.1	(Tamura et al., 2016)
	CYP716A113v1	KU878866.1	unpublished
	CYP716A111	KY047600.1	unpublished
	CYP716A1	NM_123002.2	(Tabata et al., 2000)
	CYP716A2	NM_123005.2	(Tabata et al., 2000)
	CYP716A141	KU878855.1	(Tamura et al., 2017)
	CYP716Y1	KC963423.1	(Moses et al., 2014)

	CYP716A53v2	JX036031.1	(Han et al., 2012)
	CYP716A47	JN604536.1	(Han et al., 2011)
	CYP716D58	LC209201.1	(Tamura et al., 2017)
	CYP90G1v3	KJ869260.1	(Augustin et al., 2015)
	CYP90B27v1	KJ869252.1	(Augustin et al., 2015)
CYP90	CYP90A1	GU326353.1	unpublished
	CYP90B1	KX168703.1	unpublished
	CYP90C1	NM_001342408.1	(Mayer et al., 1999)
	CYP90B3	AB244039.1	unpublished
	CYP707A1	AB122149.1	(Saito et al., 2004)
CYP707	CYP707A2	NM_128466.4	(Lin et al., 1999)
	CYP707A3	AB122150.1	(Saito et al., 2004)
	SmCYP85A1	KP337712.1	(Chen et al., 2014)
	CYP85A2	AB087801.1	(Nomura et al., 2005)
CYP85	CYP85A3	NM_001247591.1	(Nomura et al., 2005)
	NtCYP85A1	DQ649022.1	unpublished
	SlCYP85A1	NM_001329859.1	(Li et al., 2016)
CYP720	CYP720	KJ624415.1	(Pham et al., 2016)
CYP724	CYP724A1	NM_121444.4	(Tabata et al., 2000)
	CYP724B2	AB244038.1	(Aoki et al., 2010)
CYP87	CYP87D16	KF318735.1	unpublished
	CYP87A2	NM_001198045.1	(Theologis et al., 2000)
CYP722	CYP722A1	NM_101819.6	(Theologis et al., 2000)
CYP718	CYP718	NM_129846.3	(Lin et al., 1999)
CYP708	CYP708A2	NM_001344755.1	(Tabata et al., 2000)
	CYP72A63	AB558146.1	(Seki et al., 2011)
	CYP72A154	AB558153.1	(Seki et al., 2011)
	CYP72A15	NM_112330.4	(Salanoubat et al., 2000)
CYP72	CYP72A67	DQ335780.1	(Li et al., 2007)
	CYP72A68	DQ335782.1	(Li et al., 2007)
	CYP72C1	NM_001332275.1	(Theologis et al., 2000)
	CYP72A129	JN604542.1	(Han et al., 2011)
	CYP72B1	NM_128228.4	(Salanoubat et al., 2000)
CYP709	CYP709B1	NM_130264.2	(Lin et al., 1999)
	CYP709B2	MF463434.1	(Chen et al., 2018)
CYP735	CYP735A1	NM_123206.3	(Tabata et al., 2000)
	CYP735A2	NM_105381.5	(Theologis et al., 2000)
CYP734	CYP734A7	NM_001247011.2	(Ohnishi et al., 2006; Vasav and Barvkar, 2019)
	CYP734A8	NM_001247808.2	(Ohnishi et al., 2006)
CYP715	CYP715A1	NC_003076.8	(Tabata et al., 2000)
CYP721	CYP721A1	NM_106169.4	(Theologis et al., 2000)
CYP714	CYP714A1	NM_122400.3	(Tabata et al., 2000)
	CYP714A2	NM_122399.3	(Tabata et al., 2000)

CYP749	CYP749A20	JN604538.1	(Han et al., 2011)
CYP73	CYP73A19	NM_001279222.2	(Overkamp et al., 2000)
	CYP73A100	JN604543.1	(Han et al., 2011)
CYP98	SbCYP98A1	AF029856.1	(Bak et al., 1998)
	SbCYP98A12	AJ583532.1	(Morant et al., 2007)
CYP736	CYP736A12	JN604539.1	(Han et al., 2011)
CYP78	CYP78A5	NM_101240.4	(Theologis et al., 2000)
CYP703	CYP703A2	NM_100010.3	(Theologis et al., 2000)
CYP75	EoCYP75	HQ268505.1	unpublished
	EgCYP75	U72654.2	unpublished
CYP76	CYP76AH1	JX422213.1	(Guo et al., 2013)
	CYP76M6	Q6Z517	(International Rice Genome Sequencing, 2005)
	CYP76AH3	KR140168.1	(Guo et al., 2016a)
	CYP76AK1	KR140169.1	(Guo et al., 2016a)
	CYP76A26	KF591593.1	(Salim et al., 2014)
	CYP76C3	NM_130120.4	(Lin et al., 1999)
	CYP76A47	MH124060.1	(Wang et al., 2019)
CYP77	CYP77A4	NM_120548.3	(Tabata et al., 2000)
	CYP77B1	NM_101033.4	(Theologis et al., 2000)
CYP92	CYP92	KC841857.1	unpublished
CYP71	CYP71D353	KF460438.1	(Krokida et al., 2013)
	CYP71A16	NM_123623.5	(Tabata et al., 2000)
	CYP71AV9	KF752453.1	(Eljounaidi et al., 2014)
	CYP71E1	AF029858.1	(Kahn et al., 1997)
	CYP71D313	JN604541.1	(Han et al., 2011)
	CYP71D1V1	JN613015.1	(Huang et al., 2012)
	CYP71BE52	KT157042.1	(Trikka et al., 2015)
	CYP71Z18	NM_001147894.2	(Mao et al., 2016)
	CYP71B31	NM_115190.1	(Salanoubat et al., 2000)
CYP706	CYP706A1	NM_118395.3	(Mayer et al., 1999)
	CYP706A2	NM_118397.4	(Mayer et al., 1999)
CYP84	CYP84A4	NM_120515.3	(Weng et al., 2012)
CYP79	CYP79A118	KX931079.1	unpublished
CYP81	CYP81G1	NM_126131.4	(Tabata et al., 2000)
	CYP81D1	NM_123013.4	(Tabata et al., 2000)
	CYP81F2	NM_125104.3	(Tabata et al., 2000)
	CYP81E11	DQ340238.1	unpublished
	CYP81H1	NM_119895.4	(Mayer et al., 1999)
	CYP81K1	NM_121099.4	(Tabata et al., 2000)
	CYP81K2	NM_121098.3	(Tabata et al., 2000)
CYP89	CYP89A2	U61231.1	(Courtney et al., 1996)
	CYP89A3	NM_125525.1	(Tabata et al., 2000)

CYP93	CYP93E1	AF135485.1	(Steele et al., 1999)
	CYP93E2	DQ335790.1	(Li et al., 2007)
	CYP93E3	AB437320.1	(Seki et al., 2008)
	CYP93E4	KF906535.1	unpublished
CYP80	CYP80	U09610.1	(KRAUS and KUTCHAN, 1995)
CYP82	CYP82G1	NM_113423.4	(Mayer et al., 1999)
	CYP82A2	NM_001253148.1	(Schopfer and Ebel, 1998)
	CYP82C2	NM_119348.2	(Mayer et al., 1999)
	CYP82D47	JN604545.1	(Han et al., 2011)
CYP99	CYP99A3	Q0JF01.1	(Feng et al., 2002)
CYP712	CYP712A1	NM_129787.2	(Lin et al., 1999)
	CYP712A2	NM_147845.2	(Tabata et al., 2000)
CYP83	CYP83A1	KP693684.1	(Guo et al., 2016b)
	CYP83B1	KU559565.1	unpublished
	CYP83E8	DQ340234.1	unpublished
CYP705	CYP705A1	NM_117621.5	(Mayer et al., 1999)
	CYP705A5	NM_124173.3	(Tabata et al., 2000)

Supplementary Table 26. The UGT genes used to construct phylogenetic tree in this research.

Subfamily	Gene name	GenBank number	Reference
UGT79	GmUGT79B30	NM_001359019.1	(Shaokang Di, 2015)
	GmUGT79A6	NM_001288595.2	(Rojas Rodas et al., 2014)
	HvUGT13248	GU170355.1	(Wolfgang Schweiger, 2012)
	PhUGT79B31	LC387490.1	(Knoch et al., 2017)
UGT91	GmSGT2	NM_001317455.2	(Shibuya et al., 2010)
	GmSGT3	NM_001253928.2	(Shibuya et al., 2010)
	CaUGT91A1-like	XP_027076440.1	Bioproject: PRJNA506972
	ItUGT91A1-like	XP_031110113.1	Bioproject: PRJNA574454
	LsUGT91D1-like	XP_023735445.1	Bioproject: PRJNA432228
	HaUGT91D1-like	XP_022007978.1	Bioproject: PRJNA396063
	CcUGT91C1	XP_024970787.1	Bioproject: PRJNA453787
	ItUGT91C1	XP_031118563.1	Bioproject: PRJNA574454
UGT94	VpUGT94F1	AB514127.1	(Ono et al., 2010)
	SiUGT94-related	LC484019.1	unpublished
	SiUGT94-related-2	LC484018.1	unpublished
	PgUGT94Q2	JX898530.1	(Jung et al., 2014)
UGT89	NaUGT89A2-like	XM_019370589.1	(Chen and Li, 2017)
	AtUGT89B1	NM_106048.4	(Theologis et al., 2000)
	AtUGT89C1	Q9LNE6	(Yonekura-Sakakibara et al., 2007)
UGT90	HpUGT90A7	EU561019.1	(Witte et al., 2009)
	CtUGT90A14	MH013340.1	(Zhang et al., 2019)
UGT73	AtUGT73B1	NM_119576.4	(Lim et al., 2006)
	AtUGT73B2	AY339370.1	(Lim et al., 2006)
	AtUGT73B3	NM_119574.3	(Lim et al., 2006)
	AtUGT73B4	NM_001202600.1	(Mazel and Levine, 2002)
	AtUGT73B5	NM_127108.4	(Mazel and Levine, 2002)
	AtUGT73C1	NM_129230.3	(Hou et al., 2004)
	AtUGT73C2	NM_129231.3	(Lin et al., 1999)
	AtUGT73C5	NM_129235.4	(Hou et al., 2004)
UGT71	CtUGT71AE1	MH013341.1	(Zhang et al., 2019)
	AtUGT71D1	NM_128527.4	(Lin et al., 1999)
	AtUGT71C1	NM_128529.3	(Hansen et al., 2009; Lim

			et al., 2003)
	AtUGT71C2	NM_128528.4	(Hansen et al., 2009)
	AtUGT71C3	NM_100600.4	(Xie et al., 2012)
	AtUGT71B1	NM_113070.3	(Salanoubat et al., 2000)
	PgUGT71A27	AIZ00429.1	unpublished
	AtUGT71B6	NM_113073.3	(Priest et al., 2006)
	ITUGT71B2	MK704396.1	unpublished
	AtUGT71B5	NM_117616.2	(Mayer et al., 1999)
	RsUGT72B14	KX262844.1	(Yu et al., 2011)
	AtUGT72B1	NM_116337.3	(Brazier-Hicks and Edwards, 2005)
	AtUGT72B3	NM_001331274.1	(Lin et al., 2016)
UGT72	AlUGT72C1	NW_003302552.1	(Hu et al., 2011)
	AtUGT72E1	NM_114934.2	(Lim et al., 2005)
	AtUGT72E2	NM_126067.3	(Lanot et al., 2006; Lim et al., 2005)
	AtUGT72E3	NM_122532.3	(Lanot et al., 2008; Lim et al., 2005)
	AtUGT78D1	NM_102790.4	(Jones et al., 2003)
	AtUGT78D2	NM_121711.5	(Kim et al., 2012)
UGT78	AtUGT78D3	NM_121709.2	(Yonekura-Sakakibara et al., 2008)
	GmUGT78K1	GU434274.1	(Kovinich et al., 2010)
	AtUGT85A2	NM_102086.3	(Theologis et al., 2000)
	TcUGT85A2	EOX92065.1	(Motamayor et al., 2013)
UGT85	AtUGT85A3	NM_102088.3	(Theologis et al., 2000)
	AtUGT85A5	NM_202156.2	(Theologis et al., 2000)
	AtUGT85A7	NM_102085.3	(Theologis et al., 2000)
	AtUGT76C1	NM_120669.4	(Hou et al., 2004)
	TaUGT76C1	KY784575.1	unpublished
	SlUGT76E1	NM_001361347.1	(Sun et al., 2017)
	AtUGT76E1	NM_125350.3	(Tabata et al., 2000)
UGT76	AtUGT76E2	NM_125351.3	(Tabata et al., 2000)
	AtUGT76E11	NM_114534.3	(Li et al., 2018a; Salanoubat et al., 2000)
	AtUGT76E12	NM_114533.2	(Salanoubat et al., 2000)
	AtUGT76D1	NM_128205.3	(Lin et al., 1999)
	VrUGT87A2-like	XP_034687331.1	Bioproject: PRJNA636344
	VvUGT87A2	RVX23022.2	(Roach et al., 2018)
UGT87	CsUGT87A1-like	XP_028057899.1	Bioproject: PRJNA524157
	CaUGT87K1	AUR26629.1	unpublished
	CaUGT87K2	AUR26632.1	unpublished

UGT86	NtUGT86A1-like	XP_009610181.1	Bioproject: PRJNA257218
	CsUGT86A1-like	XP_028052942.1	Bioproject: PRJNA524157
UGT74	AtUGT74B1	NM_102256.3	(Theologis et al., 2000)
	AtUGT74F1	NM_129946.3	(Lin et al., 1999)
	AtUGT74F2	NM_129944.3	(Lin et al., 1999)
	PgUGTP74AE2	JX898529.1	(Jung et al., 2014)
	AtUGT74D1	NM_128733.5	(Tanaka et al., 2014)
	AtUGT74E2	NM_100448.4	(Theologis et al., 2000)
UGT75	SlUGT75C1	NM_001361345.1	(Aoki et al., 2010)
	AtUGT75B1	NM_100435.3	(Theologis et al., 2000)
	AtUGT75B2	NM_100432.2	(Theologis et al., 2000)
	AkUGT75W2	AWU66066.1	(Sun et al., 2018)
UGT84	AtUGT84A1	NM_117638.3	(Mayer et al., 1999)
	AtUGT84A2	NM_113051.3	(Salanoubat et al., 2000)
	AtUGT84B1	NM_127890.3	(Lin et al., 1999)
UGT709	CrUGT709C2	KF302068.1	(Miettinen et al., 2014)
	CaUGT709L1	AUR26631.1	unpublished
UGT95	PgUGT95B2	MH507175.1	(Wilson et al., 2019)
UGT708	CsUGT708C1-like	XP_028096648.1	Bioproject: PRJNA524157
	PpUGT708C1	XP_007216617.1	Bioproject: PRJNA241430
UGT80	LhUGT80A2	XM_031153760.1	unpublished
	AtUGT80B1	NM_001084205.2	(Theologis et al., 2000)
	AtUGT80	KJ396595.1	unpublished
	AtUGT80A2	NM_001337686.1	(Salanoubat et al., 2000)
P. ginseng	PgUGT1	KF377585.1	(Yan et al., 2014)
	PgUGT3	AIE12480.1	(Yan et al., 2014)
	PgUGT4	AIE12477.1	(Yan et al., 2014)
	PgUGT7	AIE12476.1	(Yan et al., 2014)
	PgUGT16	AIE12486.1	(Yan et al., 2014)
	PgUGT17	AKA44597.1	(Wang et al., 2015)
	PgUGT25	AKA44595.1	(Wang et al., 2015)
	PgUGT33	AKA44590.1	(Wang et al., 2015)
	PgUGT39	AKA44591.1	(Wang et al., 2015)
	PgUGT100	AKQ76388.1	(Wei et al., 2015)
	PgUGT101	KP795114.1	(Wei et al., 2015)
	PgUGT102	KP795115.1	(Wei et al., 2015)
	PgUGT103	KP795116.1	(Wei et al., 2015)
	PgUGTPg29	KM401911.1	(Wang et al., 2015)
	PgUGTPg45	KM401918.1	(Wang et al., 2015)
	PgUGT11	AIE12482.1	(Yan et al., 2014)

	PgUGT12	AIE12481.1	(Yan et al., 2014)
	PgUGTPg36	AKA44596.1	(Wang et al., 2015)
	PgUGTPg37	AKA44583.1	(Wang et al., 2015)
UGT83	VrUGT83A1-like	XP_034705962.1	Bioproject: PRJNA636344
	VvUGT83A1	RVW82717.1	(Roach et al., 2018)
	PtUGT83A1	XP_002306038.2	Bioproject: PRJNA17973
UGT82	VrUGT82A1	XP_034676882.1	Bioproject: PRJNA636344
	MrUGT82A1	KAB1210460.1	(Jia et al., 2019)
Others	Zj arabinosyltransferase RRA3-like	XP_015866879.1	Bioproject: PRJNA315994
	Cs arabinosyltransferase RRA3-like	XP_028093686.1	Bioproject: PRJNA524157
	To Nucleotide-diphospho-sugar transferase	PON84914.1	unpublished
	Ac Beta-1,4-xylosyltransferase	PSS36057.1	unpublished
	Cs Beta-1,4-xylosyltransferase IRX14	XP_028090508.1	Bioproject: PRJNA524157
	Cs UDP-glucosyltransferase	AYQ58374.1	unpublished
	Ac Zeatin O-glucosyltransferase	PSS15686.1	unpublished
	Ac Zeatin O-glucosyltransferase-2	PSS01783.1	unpublished
	Mc Glycosyl transferase	OVA05033.1	(Liu et al., 2017)
	Vr galacturonosyltransferase-like 3	XP_034701103.1	Bioproject: PRJNA636344
	Ac Beta-1,4-xylosyltransferase IRX9H	PSS01196.1	unpublished
	Jr galacturonosyltransferase 8-like	XP_018807381.1	Bioproject: PRJNA350852
	Cs galacturonosyltrans	XP_028115305.1	(Li et al., 2017)

	ferase 8-like		
	Ls beta-1,4-xylosyltransferase IRX10L	XP_023744067.1	Bioproject: PRJNA432228
	Cc xyloglucan 6-xylosyltransferase 2-like	XP_024996410.1	Bioproject: PRJNA453787
	Ls xyloglucan 6-xylosyltransferase 2-like	XP_023760243.1	Bioproject: PRJNA432228
	Vr UDP-rhamnose:rhamnosyltransferase 1	XP_034708582.1	Bioproject: PRJNA636344
	Vr UDP-rhamnose:rhamnosyltransferase 2	XP_034708677.1	Bioproject: PRJNA636344

1272

1273

1274 **Supplementary Table 27.** Primers for cloning UGT genes in *P. notoginseng* genome.
1275

Genes	Primers	Sequence (5' to 3')
PnUGT1	Seq1091.2-F	ATGAAGTCAGAATTGATATTCTTGC
	Seq1091.2-R	TTACATAATTTCCTCAAATAGCTTC
PnUGT2	Seq1751.3-F	ATGGATAACCAAAAAGGTAGAATCA
	Seq1751.3-R	CTATTGTGCATCTTTCTTCTTCTTA
PnUGT3	Seq2311.15-F	ATGAAGTCAGAATTGATATTCGTGC
	Seq2311.15-R	TCACATAATTTCCTCAAATAGTTTC
PnUGT4	Seq3403.8-F	ATGGATATCGAAAAAGGTAGAATCA
	Seq3403.8-R	TTAATATTGTGCGTCTTTCTTCATC
PnUGT5	Seq574.8-F	ATGTTGAGCAAAACTCACATTATGT
	Seq574.8-R	TCAGGAGGACACAAGCTTTGAAATG
PnUGT6	Seq1424.9-F	ATGGTTTCTATTCGGAGAACATTGT
	Seq1424.9-R	TCAAAAAATTGTGGTATGAGGAACA
PnUGT7	Seq1517.4-F	ATGCTGGAGCAGTGTTTGGGACAAC
	Seq1517.4-R	TTATACCTTGACGGCTTTAAATGCA
PnUGT8	Seq1543.17-F	ATGGCAGGTCGTAGTAGAGACGGTC
	Seq1543.17-R	TTACTGTTCTGAACCATCAGGGAAG
PnUGT9	Seq1607.6-F	ATGGACTCACAAGTCTCATCACGTC
	Seq1607.6-R	TTACTGATCTGATCGTTCCTCTCTC
PnUGT10	Seq1625.69-F	ATGAGGAACTGGAGTTGGGGTTTTG
	Seq1625.69-R	CTACCATGGTTTGAGGTCTCCCATG
PnUGT11	Seq1743.56-F	ATGGATACGACAAGGCGGAAGGCGG
	Seq1743.56-R	TCAAAAACAATACTGAATTAACTTT
PnUGT12	Seq1790.11-F	ATGGATGGCAAGAGCCTTCACATAG
	Seq1790.11-R	CTAGGAGGCTACGAGAAGGTCTTGC
PnUGT13	Seq1935.39-F	ATGAAGAAGCTGAAGAGCTTTTACA
	Seq1935.39-R	CTATTTGCACTGCATTGGTCGGAAC
PnUGT14	Seq1965.8-F	ATGGAGTCTCCGAATAGACCTCATG
	Seq1965.8-R	TTAAGGTTTGCTAATATTTTTTCCA
PnUGT15	Seq1975.16-F	ATGATCCCCCTCTCCGAAATCGCCC
	Seq1975.16-R	TTATGCTTTCTCCCTTTTCTCTCTG
PnUGT16	Seq2001.6-F	ATGGGTCAGCTTAATGTGTTCTTTT
	Seq2001.6-R	TCAAGAATGATTAGAACTCAATTCT
PnUGT17	Seq2096.16-F	ATGGCTATTCTCCAAACCCAAGACC
	Seq2096.16-R	TCATTTCAATTTCAGTTGTTCCACG
PnUGT18	Seq2308.20-F	ATGAAGCTCTCTGCGCTGCAGCAGA
	Seq2308.20-R	CTACTTCTTACTGGTATGGCTTGCA
PnUGT19	Seq312.4-F	ATGGCGAACACGACGACGTTTCGAA
	Seq312.4-R	TTAGAGACCAAAATTGCAGGCCTGG
PnUGT20	Seq3221.1-F	ATGCCACCAAAACTCCACCTCCCAA
	Seq3221.1-R	TCAGCTGTCAGAATACAAATATTCA
PnUGT21	Seq3651.4-F	ATGAAGAACTCAGAATTGGTATTCG

	Seq3651.4-R	TCACATGATCTCCTCAATTAGTTTC
PnUGT22	Seq3959.10-F	ATGAAGCTCTCTGCGCTACAGCAGA
	Seq3959.10-R	CTACTTCTCACTGGTATGGCTTGCA
PnUGT23	Seq4354.2-F	ATGGAAAATAACCACGTTCTTCATG
	Seq4354.2-R	TTAACTCATCAATTGGGATTTCCTC
PnUGT24	Seq4407.1-F	ATGGCTCAACAAACAATCCCACCTC
	Seq4407.1-R	CTAGGGTGTGATGCCACCCAAAGTC
PnUGT25	Seq4424.12-F	ATGCCAACACAGAAATACTCAACCC
	Seq4424.12-R	TTATTGTTTAGATTTCACACCCATT
PnUGT26	Seq4424.13-F	ATGGAGAAAAAGGACTCAACTCGAC
	Seq4424.13-R	TCATCTCTCCACACCCATCAATTTA
PnUGT27	Seq4424.15-F	ATGGCTGAACAAACAATCCCACCTC
	Seq4424.15-R	CTAGGCTCTGATGCCACCCACAGTC
PnUGT28	Seq4424.16-F	ATGGATCAACCAGCAGCCGAACCTC
	Seq4424.16-R	TTAGCTACGCAAAACTACAGCCATC
PnUGT29	Seq4481.73-F	ATGGCAACTGAAGACCCTAAACTCC
	Seq4481.73-R	TTATCCATTTTTTGATTTCTCAAAA
PnUGT30	Seq4702.22-F	ATGGAGATTAACCGGCATAGGAAGC
	Seq4702.22-R	TTATTTTGTATGATTTTCAAGATAC
PnUGT31	Seq5047.49-F	ATGGGCTCCCTTCCTAAAGTAACTA
	Seq5047.49-R	CTACTTTGCTAACAACACCTGATCC
PnUGT32	Seq5124.21-F	ATGGTGGGTCGTAAAGAGAAGAGCA
	Seq5124.21-R	TTATTGCGTATTTGTTTGCCAGTCA

1276